Synthetic Models for Heme−Copper Oxidases

Eunsuk Kim, Eduardo E. Chufán, Kaliappan Kamaraj, and Kenneth D. Karlin*

Department of Chemistry, Johns Hopkins University, Charles and 34th Streets, Baltimore, Maryland 21218

Received September 16, 2003

Contents

1. Introduction

Cytochrome *c* oxidases, or more generally heme−copper oxidases (see section 2), have for a considerable time attracted the interest of modeling chemists. This is due to the importance of these enzymes in biological respiration and the dioxygen "activation" chemistry that occurs here and the presence of redox-active iron (heme) and copper centers. The metal ion properties are of particular interest to inorganic chemists, especially because they possess exceptionally interesting physical properties or spectroscopic features, in fact, due to their novel coordination environments.

For synthetic bioinorganic chemists, the metal center that has attracted the most attention is the heme−copper binuclear site (discussed below), where a heme and a proximate (∼4.4−5.3 Å, sections 2 and 4.1) copper ion center effect dioxygen binding and O−O reductive cleavage. Whereas the earliest and most common biomimetic efforts focused on the oxidized or "resting state" form of this center possessing a porphyrinate−iron(III) and copper(II), more recent efforts have been directed at modeling the reduced state and carrying out relevant reaction chemistry; the porphyrinate−iron(II) with copper(I) binds carbon monoxide (as dioxygen surrogate) and initiates O_2 chemistry. The so-called Cu_A center, now known to be a thiolate-bridged dicopper site that can readily exist in a delocalized mixed-valent state (section 6.1), effects electron transfer (ultimately) to the heme−Cu active site; this dicopper complex has also been of interest to synthetic modelers. This was originally thought to be a modified type 1 "blue" mononuclear copper electron-transfer center, with its known thiolate $Cu^{I,II}$ ligation. Thus, in fact, it is "modified" and is binuclear with an additional copper ion.

The late Nobu Kitajima reviewed the modeling of cytochrome *c* oxidase in 1992,[1] when essentially only models for oxidized enzyme forms were known and discussed. Collman and co-workers[2] have recently reviewed the area, including considerable coverage of dioxygen reactivity studies, either in electrochemical functional modeling efforts or with investigations focusing on isolation and characterization of meta-

10.1021/cr0206162 CCC: $48.50
Published on Web 01/28/2004

Eunsuk Kim, a native of Korea, received her B.S. in chemistry from Sangmyung University in 1994. She then obtained a M.S. degree in inorganic chemistry at Korea University under the supervision of Professor Ho Gyeom Jang in 1996, where she was first exposed to bioinorganic chemistry doing synthetic modeling studies of non-heme diiron enzymes. She is currently working toward her Ph.D. at Johns Hopkins University in the research group of Professor Kenneth D. Karlin, focusing on the reactions of dioxygen with synthetic heme–copper complexes. After completing her doctoral research in 2004, she will be pursing postdoctoral studies in the laboratory of Professor Bruce Demple in the Department of Genetics and Complex Diseases at the Harvard University School of Public Health.

Eduardo E. Chufán was born in San Juan, Argentina, in 1967. He graduated in biochemistry in 1993, and in 1999 he received his Ph.D. degree from the National University of San Luis (Argentina) under the direction of Professor José C. Pedregosa working on metal–drug complexes. He then collaborated with Professor Joaquín Borrás at the University of Valencia (Spain). Also, he was an inorganic chemistry lecturer at the University of San Luis for 10 years. In 2000, he was awarded a CONICET (Research Council of Argentina Government) postdoctoral fellowship to join the research group of Professor Kenneth D. Karlin at Johns Hopkins University to work in the field of synthetic model compounds for the active site of heme–copper oxidases.

stable O_2 adducts in heme−copper synthetic assemblies. The present review is updated and offers a different perspective, also with some different and new material covered, but also placed in the context of this *Chemical Reviews* thematic issue on bioinorganic modeling. Included are summaries of the relevant biochemistry, that is, structural, reactivity, and spectroscopic. Modeling efforts discussed include O_2 and CO chemistry of reduced heme−copper assemblies (section 3) and synthetic complexes mimicking or attempting to model aspects of the oxidized enzyme resting state of the heme−Cu center (section 4); discussions are also included of the novel and important histidine−tyrosine cross-link found as a

Kaliappan Kamaraj was born in Thiruthangal, Tamil Nadu, India, in 1968. He received his bachelor's and master's degrees in chemistry from Madurai Kamaraj University, India, in 1990 and 1992, respectively. He obtained his Ph.D degree in 1999 from the Indian Institute of Technology, New Delhi, India, under the guidance of Professor Debkumar Bandyopadhyay working on metal–carbon-bonded organometallic probes for the identification of biologically relevant high-valent metal–oxo intermediates. In June 1999, he joined the research group of Professor Kenneth D. Karlin at Johns Hopkins University to work on the development of active site synthetic models of heme–copper oxidases.

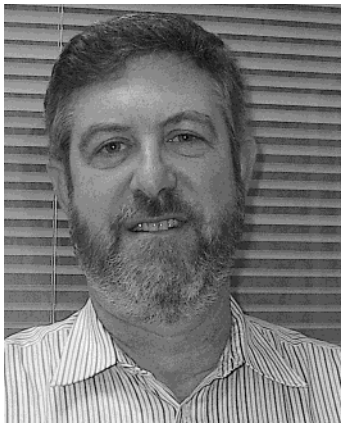

Kenneth D. Karlin received his B.S. in chemistry from Stanford University (1970) and his Ph.D. in 1975 at Columbia University while working with Prof. S. J. Lippard. After organometallic chemistry postdoctoral work with Professor Lord Jack Lewis and (now) Professor Brian F. G. Johnson at Cambridge, England, he joined the faculty at the State University of New York (SUNY) at Albany in 1977 as assistant professor. In 1990, he moved to Johns Hopkins University as professor, where he now holds the Ira Remsen Chair in Chemistry. He is a recipient of the 1991 Buck–Whitney Award for Research (ACS Eastern New York Section) and was elected as a Fellow of the American Association for the Advancement of Science. His research interests are in bioinorganic chemistry and synthetic modeling, emphasizing elucidation of fundamental aspects of the structure, spectroscopy, and reaction mechanisms relevant to copper and heme enzyme active sites that process molecular oxygen or nitrogen oxide species. Other research activities include environmental inorganic chemistry and organohalide transformations and metal–complex interactions with DNA and proteins/peptides.

Cu_B ligand (at the heme−copper active site) and recent efforts in modeling both the organic and inorganic aspects of this cofactor (section 5) and models for Cu_A (section 6).

The chemistry of metal ion sites in proteins cannot be separated from the inherent fundamental chemistry of the particular metal. Thus, the study of small molecule well-defined and characterized active-site synthetic models is useful.[3] Because models cannot by definition ever produce ultimate conclusions about

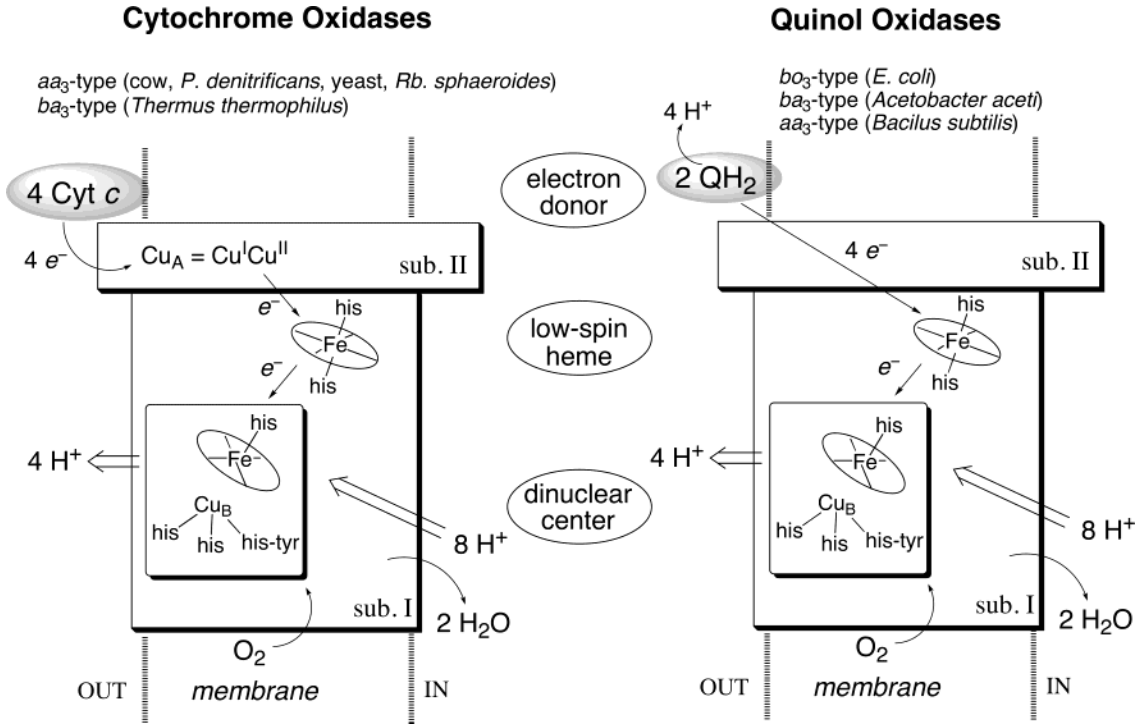

Figure 1. Schematic representation of subunits I and II of the two major classes of the heme–copper oxidase superfamily, indicating the important metal centers, the general pathway for electron transfer, and the reactions' stoichiometry and proton translocation chemistry.

an enzyme mechanism (only enzyme studies can do that), the purpose of models is not necessarily to duplicate natural properties or reactivity. Rather, biomimetic model investigations serve to sharpen or focus relevant questions. The goal is to elucidate fundamental aspects of structure, spectroscopy, magnetic and electronic structure, reactivity (e.g., plausibility of metal-based reactive intermediates and their kinetic competency), and thus chemical mechanism. A synergistic approach to the study of metalloenzymes can yield crucial information, because the synthetic analogue approach can be used to investigate the effects of systematic variations in coordination geometry, ligation, local environment, and other factors, often providing insights that cannot be easily deduced from protein studies. For example, although heme–O_2[4,5] and copper–dioxygen[6–9] chemistries are separately now reasonably well studied, the reactivity of O_2 in a heme *and* copper environment is just now rapidly developing (section 3); fundamental advances in heme/Cu/O_2 reaction dynamics, structure, spectroscopy, and O_2 reduction and O–O cleavage chemistry are sorely needed.

2. Overview of Heme–Copper Oxidases

Heme–copper oxidases (HCOs)[10,11] are the terminal respiratory enzymes that catalyze the reduction of dioxygen to water without the release of superoxide or peroxide. This exergonic reaction is coupled to proton translocation across the mitochondrial or the cytoplasmic membrane (Figure 1). During the O_2 reduction reaction, a total of eight protons are taken up from the inner side of the membrane. Four of these are utilized to form the water molecules, and the remaining four protons are released to the outer side. The resulting electrochemical proton gradient is subsequently used by ATP synthase, leading to the conversion of ADP and inorganic phosphate to ATP. Thus, in the larger framework, HCOs facilitate the generation of ATP as a chemical energy source (i.e., via ATP hydrolysis), by transduction of the energy available from O_2 reduction to water.

$$8H^+_{in} + 4e^- + O_2 \rightarrow 4H^+_{out} + 2H_2O$$

Most respiratory oxidases are members of the heme–copper oxidase superfamily, defined by two criteria:[12,13] (1) a high degree of amino acid sequence similarity in the largest subunit (subunit I) and (2) a unique bimetallic center composed of a high-spin heme and a copper. The superfamily can be divided into cytochrome *c* oxidases and quinol oxidases, on the basis of the identities of the electron donors utilized (see Figure 1). As indicated from their names, the former obtain reducing equivalents from cytochrome *c* as substrate, whereas the latter use quinol molecules (ubiquinol or menaquinol) as their electron source. Cytochrome *c* oxidases are found in the mitochondria of all eukaryotes and in many aerobic bacteria, whereas ubiquinol oxidases are found only in some prokaryotes. These two main branches can be further divided into several subclasses, depending on the presence and the types of heme groups associated with the enzymes. Three different hemes (heme B, heme O, and heme A, see Figure 2) are found among members of the HCO superfamily, with the oxidase subclass names originating from these.[13] A subscript 3 is also used in their nomenclature to indicate the O_2-binding heme site. For example, the ba_3-type C*c*O from *Thermus thermophilus* has two

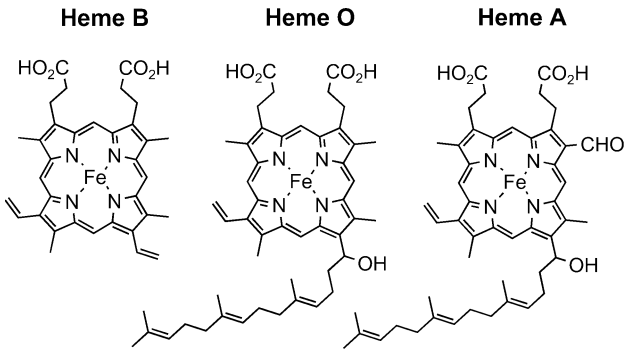

Figure 2. Structures of heme B, heme O, and heme A.

heme groups, a heme *b* and a heme *a*, indicating that the B heme occupies the low-spin site and the A heme is found at the binuclear center for O_2 binding (note that lower case letters are used for the protein-bound heme species).

In the absence of protein X-ray structural information, a considerable body of biochemical and biophysical research was directed to try to elucidate the structure and spectroscopic properties of the metal ion centers.[14] Such work in fact prompted synthetic modeling efforts to mimic or shed light on the spectroscopically more accessible fully oxidized ("resting") heme−copper binuclear center (see section 4). In the same week in the summer of 1995, significant breakthroughs occurred, with reports of the X-ray crystal structures of the oxidized cytochrome *c* oxidases from *Paracoccus denitrificans*[15] and bovine heart.[16] These were soon followed by improved higher resolution or further refined structures, as well as fully reduced, CO-bound, and various oxidized derivatives.[17−20] Surprisingly, the structures from bacterial and mammalian systems have essentially identical metal centers and three-dimensional structures of the common subunits (subunits I, II, and III). The structure of the 13 subunit bovine cytochrome *c* oxidase and the redox active metal centers are shown in Figure 3. A copper ion and two heme groups are located in subunit I. The two hemes (heme *a* and heme a_3) are "connected" through their axial histidine ligands (His-Phe-His linker), having a heme−heme interplanar angle of 104° and an Fe···Fe distance of 13.4 Å. Heme *a* is a low-spin heme with two axial histidine ligands, whereas heme a_3 is high-spin heme bound by one histidine, found in close proximity to Cu_B, thus comprising a binuclear site for O_2 binding and reduction. Cu_B has a tridentate chelation with three histidine ligands; one of these is linked to a tyrosine via a covalent bond between the $N_{\epsilon 2}$ of His^{240} and the $C_{\epsilon 2}$ of Tyr^{244} (see section 5). The origin and function of this modified tyrosine has provoked considerable interest; it has been proposed to provide an additional site for electron/proton transfer during the O_2 reduction catalytic cycle[21−23] (see sections 3 and 5). The Fe···Cu distances vary in the range of 4.9−5.3 Å, depending on the redox states and protein derivative (see further discussions in section 4).

Another redox active copper center (Cu_A) is found in subunit II (Figure 3). It has two copper atoms bridged by two thiolate ligands with a $Cu^{I}\cdots Cu^{I}$ distance of 2.58 Å in this fully reduced structure. This

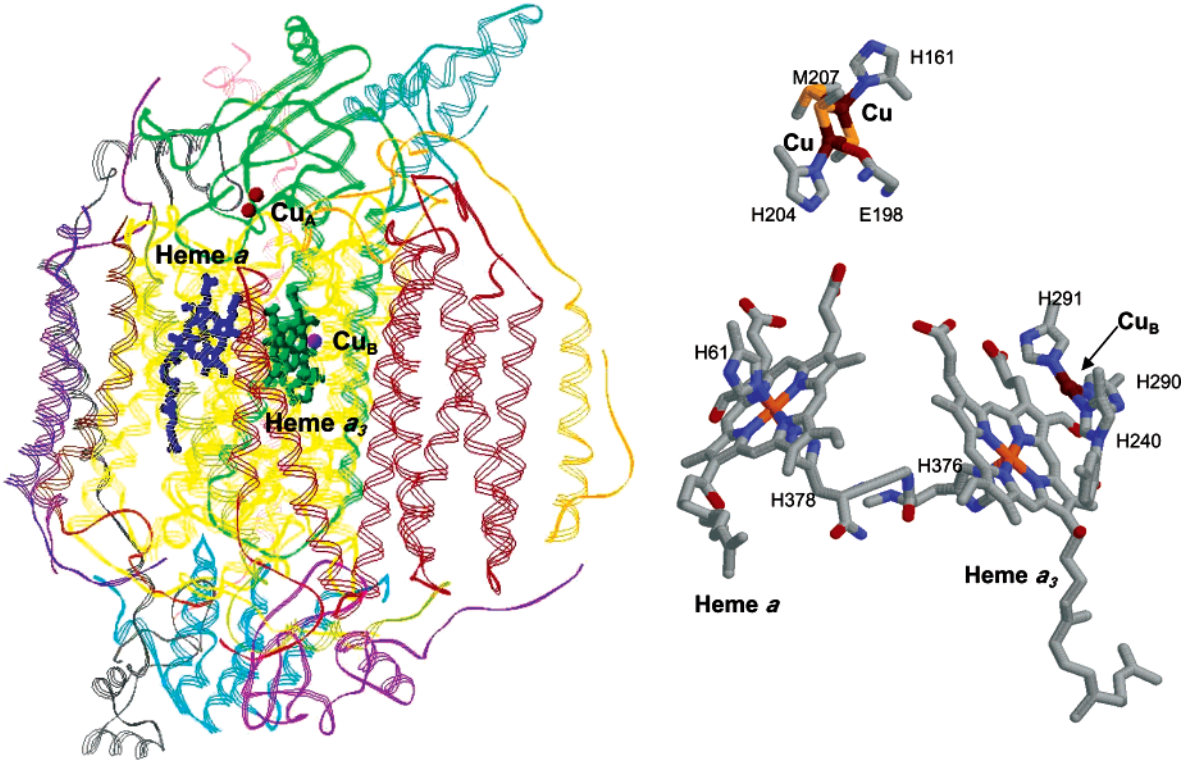

Figure 3. (Left) Overall structure of cytochrome *c* oxidase from bovine heart, where the 13 subunits are shown in different colors. Heme *a* (blue), heme a_3 (light green), and Cu_B (purple) are located in subunit I (yellow), whereas Cu_A (red) is positioned in subunit II (green). The binding site for the cytochrome *c* substrate is also located in subunit II (green) relatively close to Cu_A. (Right) Expanded view of the redox active metal centers. $Cu_A\cdots Fe_a = 20.6$ Å; $Cu_A\cdots Fe_{a3} = 23.2$ Å; $Fe_a\cdots Fe_{a3} = 13.4$ Å; $Cu_B\cdots Fe_{a3} = 5.2$ Å. Figures were generated from PDB ID 10CR coordinates using Rasmol and Swiss-PdbViewer.

center acts as a one-electron redox center, and the oxidized form is a fully delocalized mixed-valent $Cu^{I}\cdots Cu^{II} \leftrightarrow Cu^{II}\cdots Cu^{I}$ site. Each copper ion is essentially three-coordinate, with two bridging cysteines and one histidine. A further weakly bound (with a long Cu−ligand distance) methionine and carbonyl oxygen (from the backbone of a glutamate residue) are present (see also section 6). Cu_A is about 20.6 Å away from heme *a* and 23.2 Å away from heme a_3. It is generally accepted that Cu_A is the initial electron acceptor from cytochrome *c*,[24−26] the latter binding relatively nearby[27,28] (Figure 3). From Cu_A, an electron is transferred to heme *a* and subsequently passed on to heme a_3 at the binuclear site for O_2 reduction.[29] Thus, the electron "flow" is

$$\text{cyt } c \rightarrow Cu_A \rightarrow \text{heme } a \rightarrow \{\text{heme } a_3{-}Cu_B\}$$

After the reports on *P. denitrificans* and bovine heart enzymes, three additional oxidized heme−copper oxidases structures have been described. These are the ba_3-cytochrome *c* oxidase from *T. thermophilus*,[30] the aa_3-cytochrome *c* oxidase from *Rhodobacter sphaeroides*,[31] and the ubiquinol oxidase from *Escherichia coli*,[32] which were determined at 2.4, 2.3/2.8, and 3.5 Å resolutions, respectively. The ba_3-oxidase from *T. thermophilus* shows a clear but distant homology to other members of the superfamily, where a direct electron-transfer pathway from Cu_A to Cu_B was suggested.[30] The structures of a wild-type and an EQ(subunit I-286) mutant cytochrome *c* oxidase from *R. sphaeroides* show a conformational change and relocation of a water molecule upon mutation, indicating that structural rearrangement around E(I-286) could play an important role in the proton-transfer machinery of the enzyme. Cytochrome bo_3 oxidase from *E. coli* is the first structure of a ubiquinol oxidase. It is overall quite similar to what it is for cytochrome *c* oxidases, but it has a unique subunit I quinone binding site that is not present in cytochrome *c* oxidases. The similarities and differences found in the binuclear site of these various heme−copper oxidases will be discussed in section 4.

3. Reduced Heme–Copper Complexes and Reactivity

3.1. Dioxygen Reactivity of the Enzyme: O_2 Reduction Mechanism

A variety of biochemical and spectroscopic methods have been applied to study the O_2 reduction chemistry of cytochrome *c* oxidase (C*c*O), which occurs at the heme $a_3{-}Cu_B$ binuclear center[10,11,33] (Figure 4). Reduced heme a_3 has a structure very reminiscent of that of deoxymyoglobin or deoxyhemoglobin, with an open distal O_2-binding site, but which also is adjacent to Cu_B (Figure 4).

Typically, three different redox states (fully reduced, mixed-valence, and fully oxidized) of the enzyme are employed for investigation of O_2 reactivity. The fully reduced enzyme (FR) has four more electrons than the fully oxidized enzyme, and the

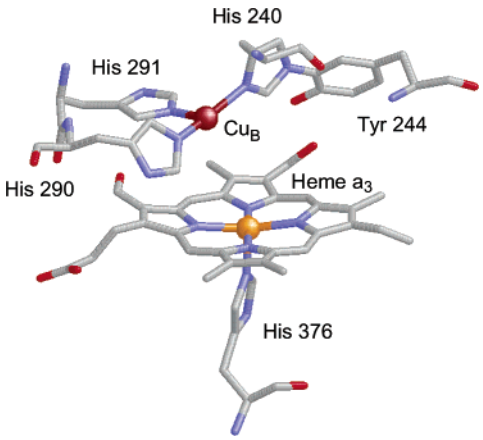

Figure 4. Structure of the fully reduced ($Fe^{II}\cdots Cu^{I}$) bovine cytochrome *c* oxidase structure; $Cu\cdots Fe = 5.19$ Å.

mixed-valence (MV) C*c*O is a two-electron reduced form in which the reducing equivalents are localized at the heme $a_3{-}Cu_B$ binuclear center. The fully reduced ($\{Cu^{I}Cu^{I}\}_A$, Fe_a^{II}, Fe_{a3}^{II}, Cu_B^{I}) and the mixed-valence ($\{Cu^{I}Cu^{II}\}_A$, Fe_a^{III}, Fe_{a3}^{II}, Cu_B^{I}) enzymes have been used for dioxygen reactivity studies, whereas the fully oxidized form ($\{Cu^{I}Cu^{II}\}_A$, Fe_a^{III}, Fe_{a3}^{III}, Cu_B^{II}) is employed for probing reactions with hydrogen peroxide. Because MV−C*c*O stores only half of the required electrons for the complete reduction of dioxygen to water, it carries out the O_2 reduction reaction only to the intermediate "**P**" (i.e., with only two electrons provided by the metal sites), halfway through the catalytic cycle, in the absence of external electrons (Figure 5). Thus, it provides rather convenient experimental conditions for enzyme mechanistic studies.

The reactions of MV or fully reduced enzymes with dioxygen are so fast that these processes require study by the flow-flash technique in which the O_2 reacts with the reduced heme $a_3{-}CO$. The heme/Cu_B site is initiated by CO photodissociation from the enzyme in the presence of O_2.[35−37] A more recent alternative approach developed by Einarsdóttir and co-workers avoids any presence of CO in the system, by employing the FR enzyme and obtaining dioxygen by its photodissociation from a dicobalt−O_2 adduct.[38]

Reactions of either the mixed-valence[39] or the fully reduced[40] proteins with O_2 produce an oxy intermediate **A** with 595 nm absorption, with a rate constant $k = 1 \times 10^5$ s^{-1} (Figure 5). Time-resolved resonance Raman spectroscopy identifies this intermediate as a "ferrous-oxy" species, revealing an Fe−O_2 stretching vibration at 571 cm^{-1},[41−44] where the O_2 binds to the iron in an end-on configuration, like that in myoglobin or hemoglobin.[45] Transient absorption visible region spectroscopic changes observed on a faster time scale lead to the suggestion that there is a prior (to the formation of **A**) interaction of dioxygen with Cu_B, $k = 3.7 \times 10^8$ M^{-1} s^{-1}.[46−48]

The second intermediate found in the catalytic cycle has been the subject of intensive discussions. It is generated from a MV−C*c*O/O_2 reaction ($\mathbf{P_M}$, see Figure 5) and has an absorption at 607 nm that was initially thought of as a heme-bound "peroxo" species $Fe_{a3}^{III}{-}O_2^{2-}$, thus designated **P**.[14,39,49,50] However, more recent investigations have shown that the O−O

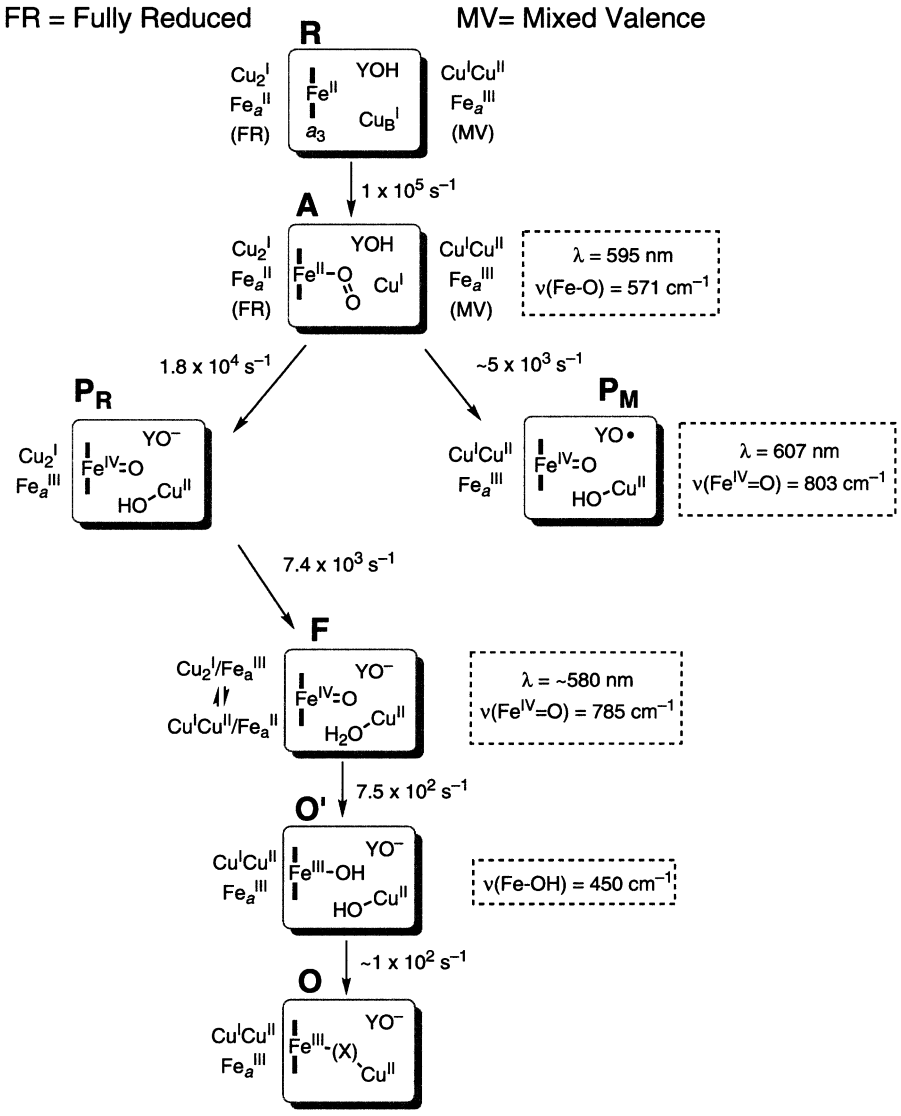

Figure 5. Schematic diagram showing one of the proposed O_2 reduction mechanisms for cytochrome *c* oxidase. The rate constants for each step are from a reaction with *R. sphaeroides* enzyme.[34] Proton uptake and translocation are not shown in the scheme. The exact identity of the bridging ligand (if any) in the oxidized enzyme (**O**) is not known. See text for further discussion.

bond is already broken at this stage.[21,51−55] Intermediate $\mathbf{P_M}$ has an isotope-sensitive Raman band at 804 cm^{-1}, assigned as a $\nu(Fe^{IV}{=}O)$ vibration.[21] Independent mass spectroscopic studies show that only one oxygen atom (from $Cu_B^{II}-OH$ or $Cu_B^{II}-OH_2$) per equivalent of $\mathbf{P_M}$ is exchangeable with solvent water, supporting the assignment of $\mathbf{P_M}$ as a O−O bond-cleaved species.[54] Because four electrons are required to break an O−O bond and only three electrons are readily available from the binuclear site (two from iron, $Fe^{II} \rightarrow Fe^{IV}$, and one from copper, $Cu^{I} \rightarrow Cu^{II}$), it is suggested that the tyrosine cross-linked to the Cu_B imidazole ligand is the source of the fourth electron for the reductive O_2-bond cleavage, leaving a tyrosyl radical (Figure 5; see also section 5).[21−23] Tryptophan 236 (in bovine C*c*O) has also been considered as another source of the fourth electron.[56] It is a highly conserved HCO residue, and it π-stacks with one of the Cu_B histidine ligands.[56]

When the starting point is the fully reduced enzyme, dioxygen binding (**A**) is followed by fast formation of a transient intermediate $\mathbf{P_R}$ (Figure 5).[57−60] By comparison, generation of $\mathbf{P_R}$ occurs ∼5−6 times faster than that of $\mathbf{P_M}$.[61] The optical absorption spectra indicate that $\mathbf{P_R}$ also has a ferryl−oxo ($Fe^{IV}{=}O$) moiety, as found in $\mathbf{P_M}$,[62] but the fourth electron for generation of $\mathbf{P_R}$ is suggested to come from the heme *a* site, not from the His−Tyr tyrosine residue (Figure 5). Both Raman[58] and optical[24,50,62] spectroscopies support this idea, indicating that the decay of oxy (**A**) corresponds to the oxidation of the low-spin heme *a* center. The structure of the heme a_3-Cu_B binuclear site in $\mathbf{P_R}$ is believed to be the same as that of $\mathbf{P_M}$,[62] but the exact nature of $\mathbf{P_R}$ is not fully understood.

In studies employing the fully reduced enzyme, it has been shown that $\mathbf{P_R}$ decays to produce another ferryl−oxo intermediate **F** (see Figure 5). The reducing equivalent required for this conversion does not derive from the binuclear center, but rather partial electron transfer from Cu_A to heme *a* occurs, resulting in an equilibrium mixture of two redox states of heme *a* and Cu_A sites (see Figure 5).[50,63,64] Intermediate **F** has a broad absorption at ∼580 nm, and it also

contains a well-established $\nu(Fe^{IV}{=}O)$ stretching vibration at 785 cm^{-1}.[45,65] Compared to $\mathbf{P_R}$, the binuclear center in **F** is suggested to have an additional proton with a hydrogen-bonded ferryl−oxo moiety ($Fe^{IV}{=}O$).[21] However, the exact site for this protonation (e.g., tyrosinate, OH^- bound to Cu_B, or other residues) is not known. The rates of both the $\mathbf{P_R} \rightarrow \mathbf{F}$ transition and the $Cu_A \rightarrow$ heme *a* electron transfer are pH dependent,[66,67] and this transition is accompanied by proton translocation (proton pumping).[68−70]

The final ferric hydroxide intermediate (**O′**) forms as the fourth electron enters the binuclear center. It is characterized by time-resolved resonance Raman spectroscopy showing a $\nu(Fe^{III}{-}OH)$ stretching mode at 450 cm^{-1}.[45,48,71−73] Hydroxide is presumably bound at both the heme a_3 and Cu_B centers (Figure 5). One of them is released with a rate of $\sim 1 \times 10^2$ s^{-1} to yield the fully oxidized enzyme (**O**).[66,74,75] Wikström and co-workers suggest that **O′** is relevant to the catalytic cycle but that **O** is not.[68] There are several possibilities [e.g., $H_2O{\cdots}OH^-$, μ-O_2^{2-}, μ-O^{2-}, μ-$(OH)^-$, etc.] for the bridging ligand of the fully oxidized enzyme, if there is one, but the precise identity of the bridging group(s) needs to be resolved (see further discussions, section 4). The formation of intermediate **O′** is pH dependent, and the transition of $\mathbf{F} \rightarrow \mathbf{O'}$ is also coupled to proton pumping.[68−70]

Hydrogen Peroxide Reactions. Investigations employing hydrogen peroxide (H_2O_2) and its reactions with the oxidized (i.e., $Fe_{a3}^{3+}{-}Cu_B^{2+}$) C*c*O support the general picture and have been useful in a variety of studies.[21,51−53,76] In fact, the pioneering optical and resonance Raman investigations revealing the O−O bond cleavage in the **P** intermediate were originally carried out in this manner.[51−53] Later, resonance Raman[21] and optical absorption[55] spectroscopic studies of the reduced enzymes with dioxygen confirmed that the intermediate generated from the reaction of oxidized C*c*O/H_2O_2 is indeed identical with $\mathbf{P_M}$ from the MV−C*c*O/O_2 reaction.

Theoretical studies on O_2 intermediates or the O−O cleavage process are ongoing, especially focused on the dramatic transition, the **A** to $\mathbf{P_M}$ conversion.[56,77−79] They generally propose that the O−O cleavage is facilitated by protons (or water) through hydrogen-bonding networks (see section 5).

Although significant advances have been made in detecting and identifying the O_2 intermediates of the C*c*O catalytic cycle, further details are needed. Proposed reaction schemes continue to evolve, and especially the relationship of O_2 intermediates to the proton-pumping process still requires considerable insight.

3.2. Dioxygen Reactivity in Heme–Copper Assemblies

3.2.1. Synthetic Fe^{II}–Cu^{I} Complexes and O_2 Reactions

In this section we summarize the chemistry advanced with respect to heme−copper/dioxygen reactions employing synthetically derived binucleating ligands, or even mononuclear components, leading to heme−Cu/superoxo, heme−Cu/peroxo, or O−O cleaved products of relevance to the chemistry involved. The ligand complexes employed are summarized in Figure 6, and data pertaining to spectroscopic or structural characterization of O_2-derived adducts are provided in Table 1. To help the reader, we state here our compound numbering method: Each ligand−metal(s) complex, in order of its discussion in the text, is given an Arabic number assignment, **1**, **2**, **3**, etc. A suffix **a**, **b**, **c**, etc. (e.g., **2a**, **4c**), then refers to other derivatives of the ligand−metal(s) complex that are discussed, such as the reduced heme−copper complex, an O_2 adduct, etc.

In most cases, the dioxygen intermediates turn out to be bridged heme−peroxo−copper complexes; such a peroxo moiety was originally suggested for the intermediate **P** in the enzyme catalytic cycle (**P** is now generally accepted as an O−O bond cleaved $Fe^{IV}{=}O$ species, see section 3.1). Although an Fe−O_2−Cu bridged intermediate is not observed or established in the enzyme, it is suggested to exist in a protein X-ray crystal structure (see below),[18] and it cannot yet be ruled out. A bonded peroxo species (Fe−O−O−Cu) or one weakly interacting with Cu_B (Fe−O−O···Cu) may be an important transient species in the O_2 reduction chemistry of heme−copper oxidases, and its significance has been discussed in theoretical studies (see also section 5.1.4).

Systems Employing Tetradentate Chelates for Copper. The earliest observations of dioxygen reactivity with a synthetic Fe^{II}/Cu^{I} complex were made in the early 1980s by the research groups of Gunter and Murray.[88] They prepared a binuclear heme−copper complex (compound **1a**, Figure 6), adapting the concept of the "picket-fence" porphyrin (from the group of J. P. Collman)[89] in their ligand design. In the presence or absence of an axial ligand (Me_2SO or 1-methylimidazole) at ambient temperature, the binuclear complex $[(P)Fe^{II}Cu^{I}(N_4)]^+$ (**1a**) and the copper-free complex $[(P)Fe^{II}(N_4)]^+$ (**1b**) react with dioxygen to yield oxidized compounds (Scheme 1). The reactions were monitored by UV−vis and EPR spectroscopies and magnetic moment measurements, and the final products were determined to be a terminal hydroxy $[(P)Fe^{III}{-}OH(N_4)]$ and a bridging hydroxy $[(P)Fe^{III}{-}OH{-}Cu^{II}(N_4)]^{2+}$ (**1c**) complex (Scheme 1). No electronic/magnetic interaction between iron and copper was observed in **1c**. Although the researchers did not observe any significant role of copper ion complex in the reaction of **1a**/O_2 compared to the **1b**/O_2 system, this was important pioneering work that examined the reaction chemistry of the reduced Fe^{II}/Cu^{II} complex with dioxygen.

Major advances in the understanding of the heme/Cu/O_2 chemistry have been made over the past few years through the isolation and characterization of the O_2 intermediates, especially from the research groups of Collman, Karlin, Naruta, and Boitrel. Collman, Boitrel, and their co-workers especially have emphasized electrocatalytic studies, and these are reviewed in detail in another paper authored by Collman, Boulatov, Sunderland, and Fu, in this issue.[90]

The focus of Karlin's research group has been to elucidate fundamental aspects of the O_2 interactions

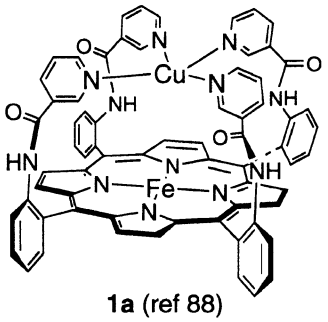

1a (ref 88)

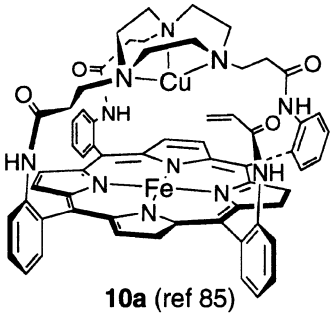

10a (ref 85)

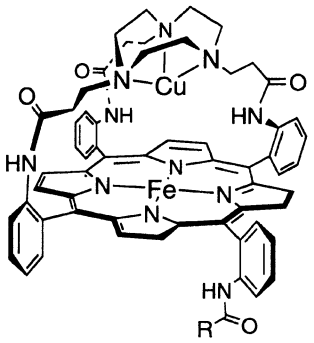

11a, 12a, 13a (ref 106,107)

R = 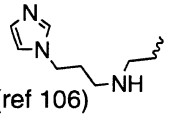

11a (ref 106)

R = 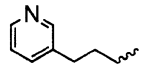

12a (ref 107)

R = 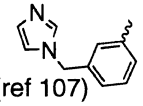

13a (ref 107)

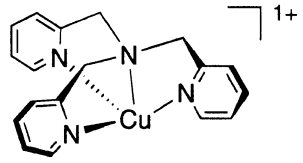

2a (ref 80)

+

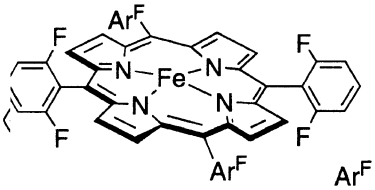

3a (ref 80)

Ar^F = 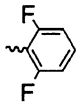

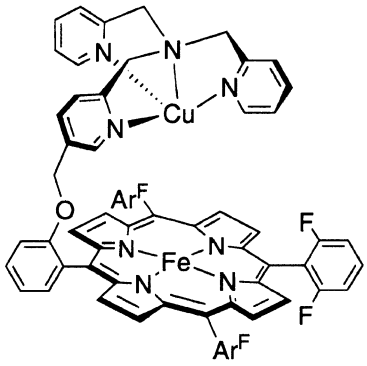

5a (ref 81)

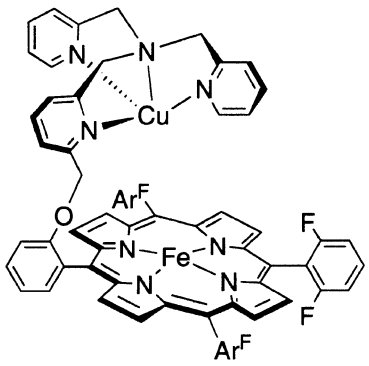

6a (ref 81)

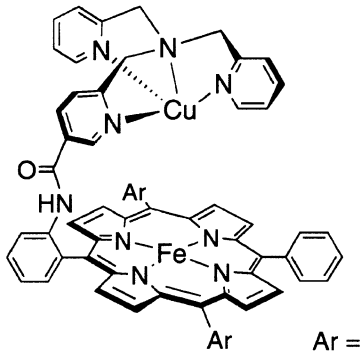

7a (ref 82)

Ar = 

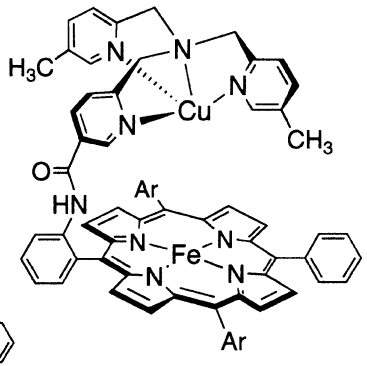

8a (ref 83)

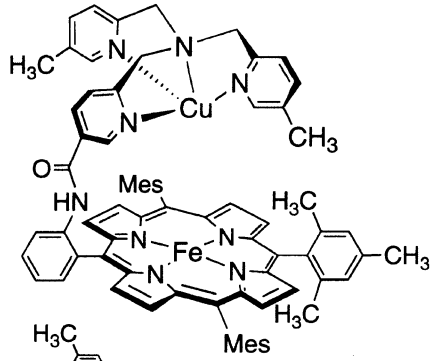

Mes = 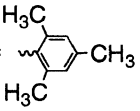

9a (ref 84)

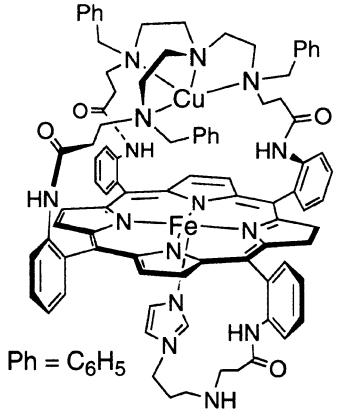

Ph = C_6H_5

14a (ref 106)

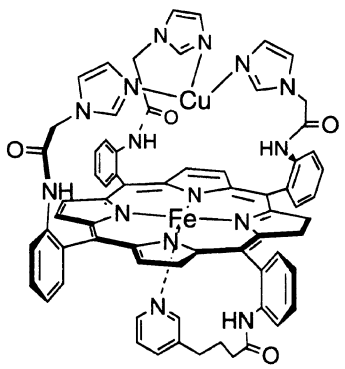

15a (ref 108)

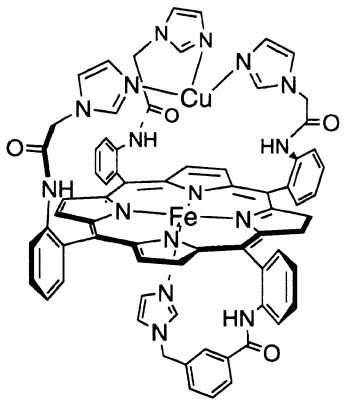

16a (ref 109)

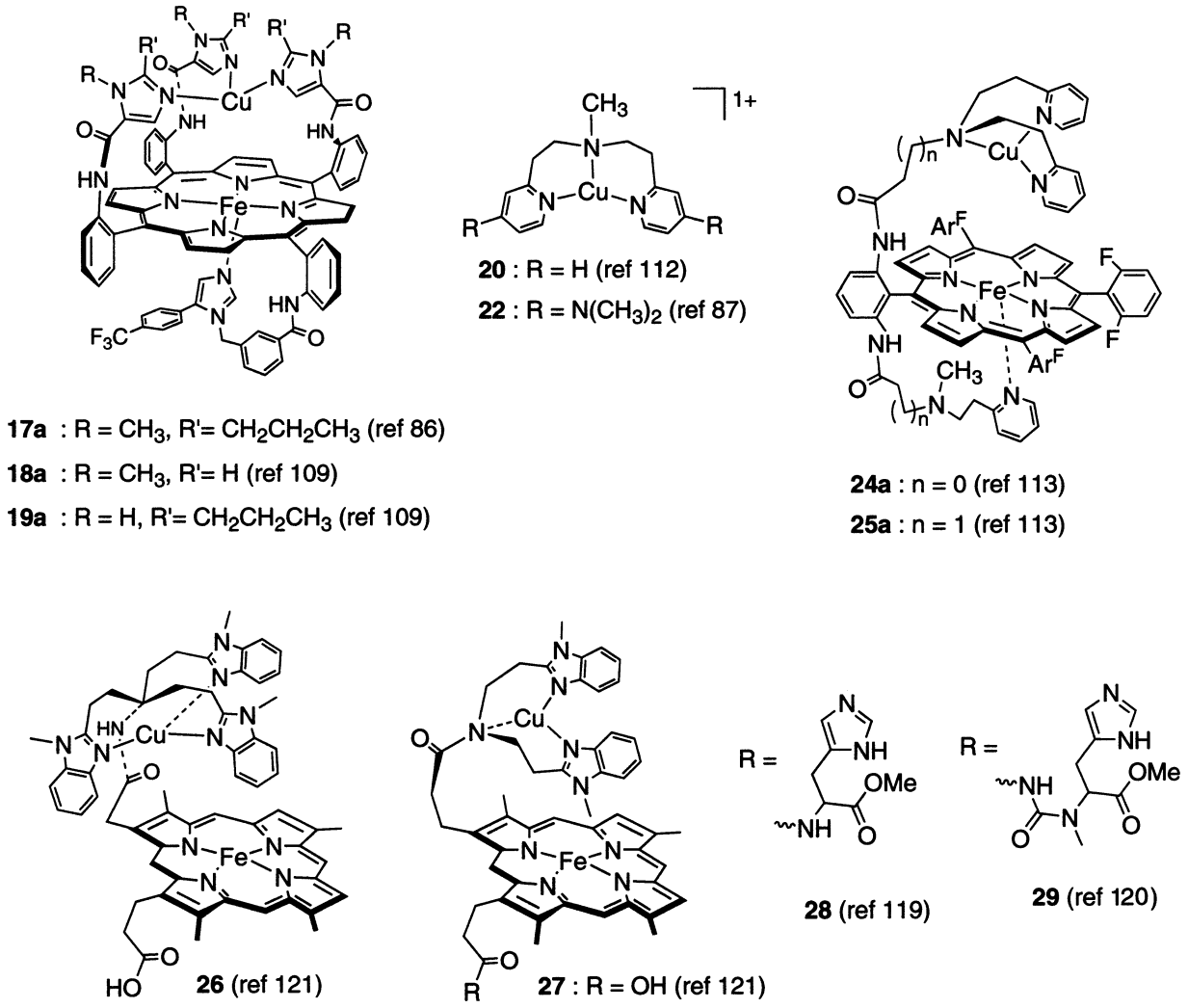

Figure 6. Synthetically derived heme–Cu assemblies possessing reduced iron(II) and copper(I) metal ions. The diagrams are meant to clearly depict the ligand structures, and overall complex charge is not indicated. The formulations for binuclear complexes are $[(\text{ligand})Fe^{II}Cu^{I}]^{+}$.

Table 1. Physical Properties of the Dioxygen Adducts of Heme–Copper Model Complexes

compound	λ_{max}, nm	ν(O–O) ($\Delta^{18}O_2$), cm^{-1}	magnetism	ref
$[(F_8TPP)Fe^{III}-(O_2^{2-})-Cu^{II}(TMPA)]^{+}$ (**4a**)	412, 558	808 (−46)	$S = 2$ ($\mu_{eff} = 5.1\ \mu_B$)[a]	80
$[(^5L)Fe^{III}-(O_2^{2-})-Cu^{II}]^{+}$ (**5b**)	NA[b]	809 (−53)	diamagnetic	81
$[(^6L)Fe^{III}-(O_2^{2-})-Cu^{II}]^{+}$ (**6b**)	418, 561, 632	787 (−43)	$S = 2$	81
$[tpaCu^{II}-(O_2^{2-})-TPPFe^{III}]^{+}$ (**7b**)	419, 560	803 (−44)	EPR silent	82
$[5\text{-}MetpaCu^{II}-(O_2^{2-})-TPPFe^{III}]^{+}$ (**8b**)	NA	793 (−42)	NA	83
$[(TMP)Fe^{III}-(O_2^{2-})-(5MeTPA)Cu^{II}]^{+}$ (**9b**)	420, 557, 612	790 (−44)	$S = 2$ ($\mu_{eff} = 4.65\ \mu_B$)[c]	84
$[(DHIm)(\alpha_3TACN\alpha Acr)Fe^{III}-(O_2^{2-})-Cu^{II}]^{+}$ (**10b**)	428	758 (−18)	diamagnetic	85
$[(\alpha_3NMePr\beta Im_{PhF})Fe^{III}-(O_2^{-})\cdots Cu^{I}]^{+}$ (**18b**)	422, 542	NA[d]	diamagentic	86
$[(F_8TPP)Fe^{II}-(O_2^{2-})-Cu^{II}(L^{Me2N})]^{+}$ (**23a**)	420, 540, 567	767 (−41), 752 (−45)	$S = 2$	87

[a] Solution Evans method. [b] NA = not available. [c] Magnetic susceptibility measurement from solid. [d] Iron–oxygen vibrational data are available, exhibiting $\nu(Fe-O) = 570\ cm^{-1}$ ($\Delta^{18}O_2 = -26\ cm^{-1}$).

with heme–copper centers. Much of their efforts have been directed to understanding the influence of Cu ion on the heme/O_2 chemistry and/or the effects of hemes on the Cu/O_2 reactivity, employing the systems in which the dioxygen chemistry of the individual heme and copper components are well understood or being simultaneously studied.

In their initial attempts to mimic the O_2 reduction chemistry of C*c*O, Karlin and co-workers utilized TMPA–copper complexes, where TMPA = tris(2-pyridylmethyl)amine.[91,92] They observed that an oxo-bridged heme–copper complex $[(F_8TPP)Fe^{III}-(O^{2-})-Cu^{II}(TMPA)]^{+}$ (**4b**) could be generated from the O_2 reaction with an equimolar mixture of $[(TMPA)Cu^{I}(RCN)]^{+}$ (**2a**) and $(F_8TPP)Fe^{II}$ (**3a**) [or an analogue with axial piperidine ligands, where F_8TPP = tetrakis(2,6-difluorophenyl)porphyrin] (Scheme 2). Labeling experiments indicate that the O-bridging atom in **4b** is derived from dioxygen.

Upon further investigation of this reaction, they found a heme–peroxo–Cu complex as a low-temperature stable O_2 intermediate.[80] Remarkably, mixing

Scheme 1

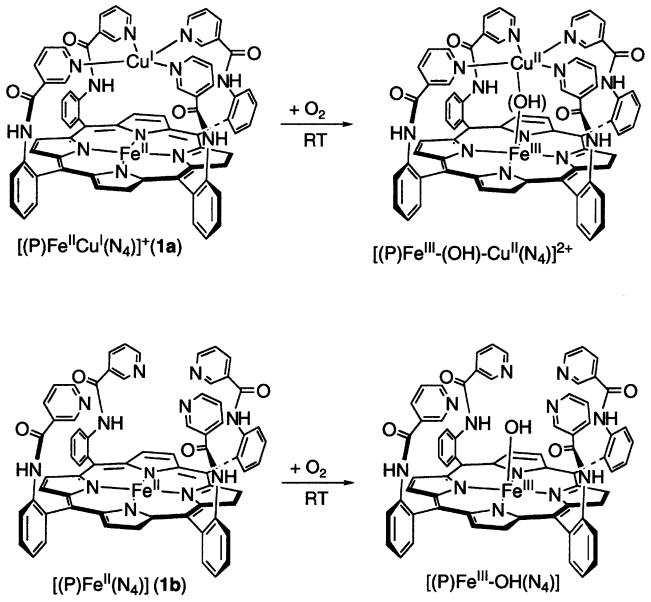

Scheme 2

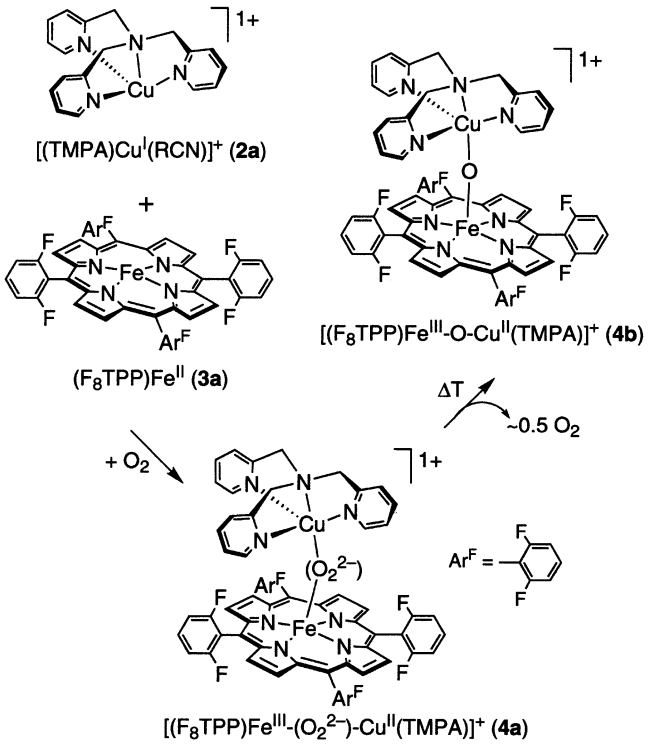

of dioxygen with Fe and Cu mononuclear components led to the heteronuclear peroxo complex $[(F_8TPP)Fe^{III}-(O_2^{2-})-Cu^{II}(TMPA)]^+$ (**4a**) (Scheme 2), in preference to the homonuclear μ-peroxo heme-only or copper-only products. The formulation of **4a** is supported by various spectroscopic methods. Dioxygen uptake measurements (through spectrophotometric titration) and MALDI-TOF-MS reveal that **4a** is a dioxygen adduct with a stoichiometry of **2a**:**3a**:O_2 = 1:1:1. Resonance Raman spectroscopy further supports the peroxo formulation, exhibiting a ν(O−O) stretching vibration at 808 cm^{-1} ($\Delta^{18}O_2 = -46$ cm^{-1}, $\Delta^{16/18}O_2 = -23$ cm^{-1}). Solution magnetic moment measurements and ^1H NMR investigations indicate that **4a** has an $S = 2$ spin state ($\mu_{eff} = 5.1\mu_B$, −40 °C), arising from the antiferromagnetic coupling between the high-spin iron(III) and the copper(II) centers. Mössbauer spectroscopy reveals that ΔE_Q = 1.14 mm/s and $\delta = 0.57$ mm/s (4.2 K, zero field); thus, the high-spin ferric ion possesses an electron-rich peroxide ligand. Formation of **4a** has been studied by stopped-flow UV−vis spectroscopy in the temperature range of −94 to −75 °C in acetone as solvent. It reveals that a heme−superoxide intermediate (S)-$(F_8TPP)Fe^{III}-(O_2^-)$ (**3b**) (λ_{max} = 537 nm, S = solvent) is generated within the mixing time (~1 ms) prior to reaction with the copper complex and formation of $[(F_8TPP)Fe^{III}-(O_2^{2-})-Cu^{II}(TMPA)]^+$ (**4a**) (λ_{max} = 556 nm). This transformation of **3b** to **4a** can be described by a first-order rate constant with $\Delta H^{\ddagger} = 45 \pm 1$ kJ/mol, $\Delta S^{\ddagger} = -19 \pm 6$ J/mol·K, and $k = 0.007$ s^{-1} (at −90 °C).

Scheme 3

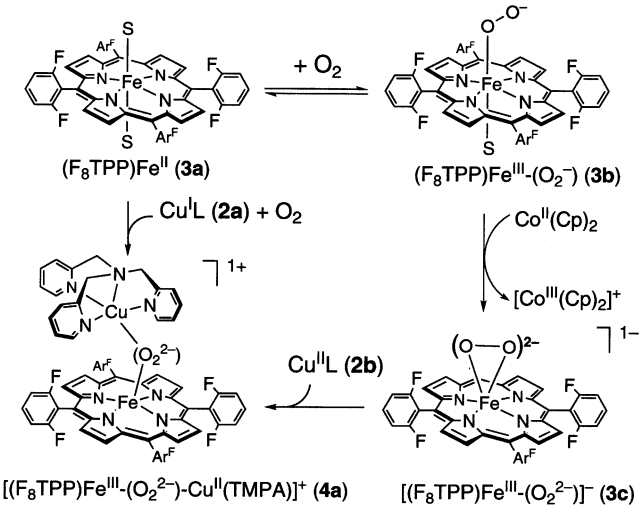

As implied by the earlier observations,[91,92] the μ-peroxo complex **4a** thermally transforms to the μ-oxo complex **4b** in a slow reaction ($t_{1/2}$ = 1015 ± 20 s, room temperature). Separate measurements indicate that ~0.5 equiv of dioxygen is released during the μ-peroxo to μ-oxo conversion, indicating this process involves a disproportionation reaction, **2** $[(F_8TPP)Fe^{III}-(O_2^{2-})-Cu^{II}(TMPA)]^+$ (**4a**) → **2** $[(F_8TPP)Fe^{III}-(O^{2-})-Cu^{II}(TMPA)]^+$ (**4b**) + O_2. Such chemistry has also been observed in non-heme diiron(II) reactions with O_2,[93] where peroxo complexes form as low-temperature-stabilized species, which then thermally transform to μ-oxo diiron(III) products. The mechanism of the heme−peroxo−copper disproportionation chemistry is as yet not understood, but is of future interest, because O−O bond-breaking reactions (which are of fundamental interest) occur.

The Karlin group has also described an alternative way to generate the heme−peroxo−Cu intermediate $[(F_8TPP)Fe^{III}-(O_2^{2-})-Cu^{II}(TMPA)]^+$ (**4a**), utilizing a ferric−peroxo complex $[(F_8TPP)Fe^{III}-(O_2^{2-})]^{1-}$ (**3c**) and a copper(II) compound $[Cu^{II}(TMPA)(MeCN)]^{2+}$ (**2b**) (Scheme 3).[94] They have developed a new method to synthesize the key heme−peroxo component $[(F_8TPP)Fe^{III}-(O_2^{2-})]^{1-}$ (**3c**), by reduction of a heme−superoxide complex $(S)(F_8TPP)Fe^{III}-(O_2^-)$ (**3b**) [S = tetrahydrofuran (THF) or acetonitrile solvent, acting as heme axial ligand] with the one-electron reductant

Scheme 4

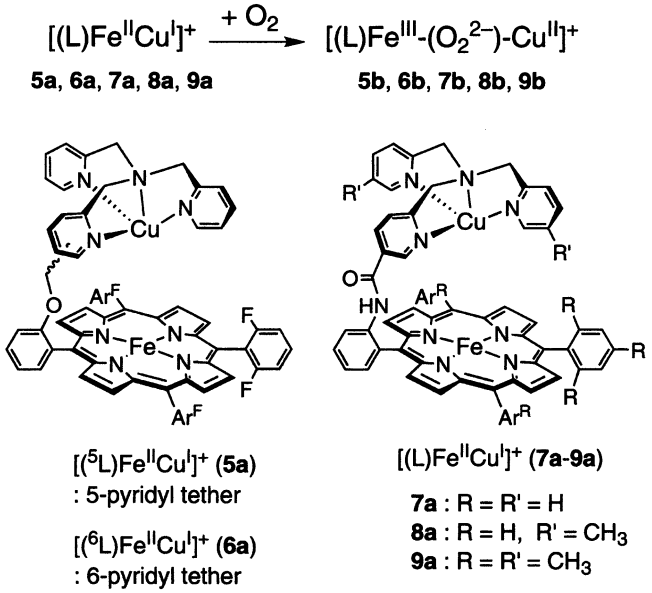

cobaltocene ($CoCp_2$). Similar ferric–peroxo complexes were previously prepared and characterized by Valentine and co-workers[95] through a different synthetic approach, reaction of porphyrinate–Fe^{III}–Cl complexes with 2 equiv of potassium superoxide. Such complexes are known to be nucleophilic and to possess a side-on (η^2-mode) peroxide ligand bound to a high-spin iron(III) atom, as depicted in Scheme 3. The formulation [(F_8TPP)Fe^{III}–(O_2^{2-})]$^{1-}$ (**3c**) has been confirmed by observation of characteristic UV–vis, ^{1}H NMR, and EPR spectroscopic parameters. Upon addition of a copper complex **2b** to a solution of **3c** at −95 °C, formation of [(F_8TPP)Fe^{III}–(O_2^{2-})–Cu^{II}-(TMPA)]$^+$ (**4a**) occurs immediately (Scheme 3), and the complex generated in this manner could be isolated as a solid. A notable difference occurs when the reactivity of the strong reductant $CoCp_2$ with [(F_8TPP)Fe^{III}–(O_2^{2-})–Cu^{II}(TMPA)]$^+$ (**4a**) is compared with that of [(F_8TPP)Fe^{III}–(O_2^{2-})]$^{1-}$ (**3c**). Excess $CoCp_2$ does not react with **3c**, but it does reduce heme–Cu complex **4a** to yield the μ-oxo species [(F_8TPP)Fe^{III}–(O^{2-})–Cu^{II}(TMPA)]$^+$ (**4b**) (Scheme 2). This implies that peroxo coordination to copper(II) plays a significant role in facilitating the reductive O–O bond cleavage reaction.

Another system that provides insights into heme-containing Fe^{II}/Cu^{I}/O_2 reactions is a group of binuclear complexes, in which a Cu–TMPA moiety is tethered to a (TPP)Fe^{II}-derivatized porphyrin (TPP = tetraphenylporphyrinate; compounds **5a**, **6a**, **7a**, **8a**, and **9a**, Figure 6, Scheme 4).[81–84,96] The research groups of Karlin and Naruta have independently studied these rather similar complexes using a variety of spectroscopic techniques. As expected from their ligand architectures (Scheme 4), the majority of these complexes show very similar O_2 reactivities and spectroscopic features. Upon oxygenation, all of them form low-temperature-stable high-spin "heme–peroxo–copper" complexes possessing strong magnetic coupling between iron and copper.

As an analogue of the [(TMPA)Cu^{I}(RCN)]$^+$/(F_8-TPP)Fe^{II} (**2a**/**3a**) system (Scheme 2), Karlin and co-workers have developed binuclear complexes in which a Cu–TMPA moiety is covalently attached to the periphery of the porphyrin through either the 5-position (^{5}L) (reduced Fe^{II}Cu^{I} compound **5a**, Figure 6) or the 6-position (^{6}L) (reduced Fe^{II}Cu^{I} compound **6a**, Figure 6) of the pyridine arm.[81,96] When [(^{6}L)Fe^{II}Cu^{I}]$^+$ (**6a**) reacts with O_2 in MeCN solvent, the 1:1 dioxygen adduct [(^{6}L)Fe^{III}–(O_2^{2-})–Cu^{II}]$^+$ (**6b**) forms, as determined by spectrophotometric titration and MALDI-TOF-MS. This dioxygen adduct shows significant thermal stability in MeCN or acetone ($t_{1/2}$ = ∼60 min, room temperature). The resonance Raman spectrum of **6b** reveals a peroxide O–O stretching vibration at 787 cm^{-1} ($\Delta^{18}O_2$ = −43 cm^{-1}). ^{1}H and ^{2}H NMR and EPR spectra of **6b** indicate that it is a high-spin (S_{total} = 2) heme–copper dioxygen adduct, where a high-spin Fe (S = $^5/_2$) and Cu (S = $^1/_2$) are antiferromagnetically coupled. Stopped-flow kinetic studies of the [(^{6}L)Fe^{II}Cu^{I}]$^+$ (**6a**)/O_2 reaction reveal that a new short-lived intermediate (λ_{max} = 538 nm, thought to be a superoxo species [(^{6}L)Fe^{III}(O_2^-)···Cu^{I}]$^+$ and/or a bis adduct [(^{6}L)Fe^{III}(O_2^-)···Cu^{II}(O_2^-)]$^+$), plus the peroxo complex **6b** (λ_{max} = 561 nm), are independently produced within a mixing time (∼1 ms), and the ratio of these two species is dependent on temperature and O_2 concentration. The 538 nm intermediate is favored at low temperatures, and it converts to the peroxo complex **6b** in a first-order reaction (−94 to −60 °C), where $\Delta H^{\ddagger}$ = 37.4 ± 0.4 kJ/mol and $\Delta S^{\ddagger}$ = −28.7 ± 2.3 J/mol·K.

Complex [(^{5}L)Fe^{II}Cu^{I}]$^+$ (**5a**), a constitutional isomer of **6a**, also reacts with O_2 to form a peroxo intermediate (**5b**) with ν(O–O) stretching vibration at 809 cm^{-1} ($\Delta^{18}O_2$ = −53 cm^{-1}). However, this reaction shows a significantly different behavior from **6a**/O_2. ^{1}H NMR spectroscopy indicates that **5b** is a diamagnetic compound, and further spectrophotometric titration experiments reveal that the stoichiometry of the reaction is **5a**:O_2 = 2:1. The nature of **5b** is not understood, but the contrasting features between **5b** and **6b** are believed to originate from the differences in their ligand architecture.[97] Such ligand influences are also seen in their μ-oxo structures and acid–base chemistry (see section 4.2.1 for further discussion).

Independently, Naruta and co-workers have been carrying out studies using an approach very similar to that of Karlin and co-workers. They have emphasized the synthesis and characterization of heme–copper complexes and their O_2 reactivity, using a series of binuclear complexes where a Cu–TMPA moiety is attached to an iron porphyrin through a 5-pyridyl amide linkage (compounds **7a**, **8a**, and **9a**, Figure 6, Scheme 4).[82–84] All three reduced heme–copper complexes react with O_2 and give very stable μ-peroxo intermediates (**7b**, **8b**, and **9b**).

The formulation of [tpaCu^{II}–O_2–TPPFe^{III}]$^+$ (**7b**) (Scheme 4) is supported by various spectroscopic evidence.[82,83] Electrospray ionization mass spectroscopic (ESI-MS) data generated for **7b** with $^{16}O_2$ and $^{18}O_2$ confirm this product forms by addition of 1 mol of O_2 per complex, where the magnetically coupled bridging heme–peroxo–Cu moiety is further confirmed by resonance Raman and EPR spectroscopy (Table 1). Formation of **7b** from [tpaCu^{I}–TPPFe^{II}]$^+$/

O_2 (**7a**/O_2) (tpa ≡ TMPA) studied by benchtop UV−vis spectroscopic monitoring can be analyzed as a pseudo-first-order reaction (i.e., excess dioxygen), where $\Delta H^{\ddagger} = 12.8 \pm 0.3$ kJ/mol, $\Delta S^{\ddagger} = -220 \pm 2$ J/mol·K, and $k = 2.73 \times 10^{-3}$ s^{-1} (at −90 °C, toluene). These parameters have been compared with those of the known $[(TMPA)Cu^{I}(RCN)]^{+}$ (**2a**)/O_2 reaction (EtCN solvent: $[(TMPA)Cu^{I}(RCN)]^{+}$ (**2a**) + $O_2 \rightarrow [(TMPA)Cu^{II}(O_2^{-})]^{+}$ + RCN),[98] in which $\Delta H^{\ddagger} = 32.4 \pm 4$ kJ/mol, $\Delta S^{\ddagger} = 14 \pm 18$ J/mol·K, and $k = 2 \times 10^{4}$ M^{-1} s^{-1} (−90 °C). On the basis of the observed slow **7a**/O_2 reaction rate (compared to **2a**/O_2) and the observed large negative $\Delta S^{\ddagger}$ value, the researchers suggest that the rate-limiting step for the formation of $[tpaCu^{II}-(O_2^{2-})-TPPFe^{III}]^{+}$ (**7b**) is the *intra*molecular coupling between the covalently linked $[(TMPA)Cu^{II}(O_2^{-})]^{+}$ and $(TPP)Fe^{II}$ components.

A related complex with 5-methyl substituents on the TMPA tether, $[5\text{-}MetpaCu^{I}-TPPFe^{II}]^{+}$ (**8a**) (Figure 6 and Scheme 4), exhibits similar O_2 reactivity as is observed for **7a**, yielding a heme−peroxo−copper complex $[5\text{-}MetpaCu^{II}-(O_2^{2-})-TPPFe^{III}]^{+}$ (**8b**) (Table 1). The reduced ν(O−O) value of **8b** (compared to that of **7b**) has been explained by the electron donation effect from methyl substituents of the ligand. However, other spectroscopic features (i.e., UV−vis, ESI-MS, NMR) of **8b** are not yet described, and the exact nature of **8b** is unclear.

In the complex $[(TMP)Fe^{II}-(5MeTPA)Cu^{I}]^{+}$ (**9a**) (Figure 6 and Scheme 4), four mesityl (≡ 2,4,6-trimethylphenyl) groups are introduced to the porphyrin ring, in addition to the methyl substituents on the TMPA ligand.[84] Dioxygen reaction yields $[(TMP)Fe^{III}-(O_2^{2-})-(5MeTPA)Cu^{II}]BPh_4$ (**9b**). The multiple methyl group steric effects increase the thermal stability of **9b** compared to **7b** or **8b**. Complex **9b** has been fully characterized (Table 1), including its Mössbauer properties [$\Delta E_Q = 1.17$ mm/s, $\delta = 0.56$ mm/s, which are very similar to those for $[(F_8TPP)Fe^{III}-(O_2^{2-})-Cu^{II}(TMPA)]^{+}$ (**4a**) described above]. Thus, **9b** is an $S = 2$ spin state system with strong antiferromagnetic coupling between a high-spin iron(III) and copper(II) atoms through the bridging peroxide ligand.

One of the most remarkable recent achievements in heme/Cu/O_2 chemistry and elucidation of dioxygen reduced metal-bound products comes from a Naruta and co-worker's X-ray crystal structure determination of the complex described above, $[(TMP)Fe^{III}-(O_2^{2-})-(5MeTPA)Cu^{II}]^{+}$ (**9b**) (Figure 7).[84] The bridging peroxide ligand is coordinated to the iron(III) and copper(II) ions in an asymmetric μ-η^2:η^1 fashion. In this mode, both oxygen atoms are ligated to Fe, whereas only one oxygen atom [O(2) in Figure 7] is bound to Cu. The O−O bond length is 1.460(6) Å, exactly in the range expected for a peroxide O−O bond distance. The iron atom is 0.595(10) Å out of the porphyrin plane (least-squares plane based on the pyrrole nitrogen atoms) toward the peroxide ligand. One of the iron−oxygen bonds [Fe−O(2), 2.031(4) Å] is significantly longer than the other [Fe−O(1), 1.890(6) Å]. The Fe(1)−O(2)−Cu(1) bond angle is 166.0(3)°, similar to that of a related μ-oxo complex $[(^6L)Fe^{III}-O-Cu^{II}]^{+}$ [Fe−O−Cu = 171.1(3)°,[96] see

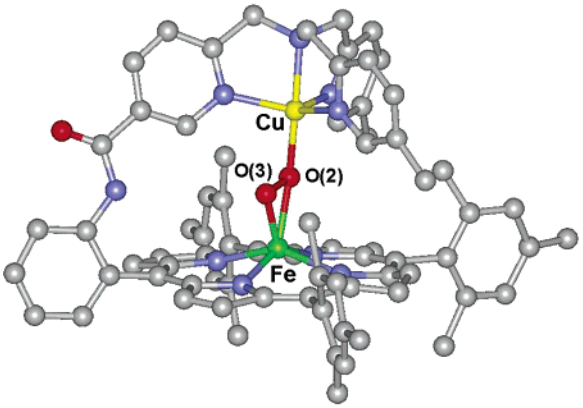

Figure 7. X-ray crystal structure of **9b**, the O_2 adduct of **9a**. Selected interatomic distances (angstroms) and bond angles (degrees); Fe···Cu, 3.92, O(2)−O(3), 1.460(6); Cu−O(2), 1.915(5); Cu−O(3), 2.657(7); Fe−O(2), 2.031(4); Fe−O(3), 1.890(6); Cu−O(2)−Fe, 166.0(3); Cu−O(2)−O(3), 103.0(4).[84]

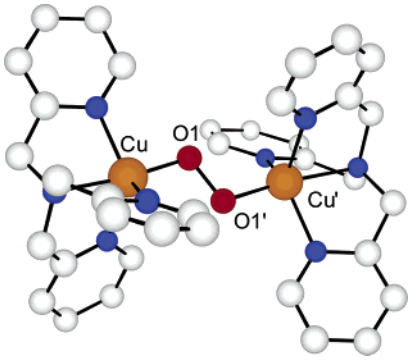

Figure 8. Chem 3D representation of the dioxygen complex $[\{Cu(TMPA)\}_2(O_2)]^{2+}$.[99,100] Selected bond distances (angstroms) and angles (degrees): Cu···Cu′, 4.369(1); O1−O1′; 1.432(6); Cu−O1, 1.852(5); Cu−O1−O1′, 107.7(2).

section 4.2.1]. The structure of the Cu−O−O unit in **9b** is similar to that of $[\{(TMPA)Cu^{II}\}_2(O_2)]^{2+}$, a *trans*-($\mu$-1,2-peroxo)dicopper(II) complex whose structure has also been determined through X-ray crystallography by Karlin and co-workers,[99,100] where the copper ion has a distorted trigonal−bipyramidal geometry having three pyridyl nitrogens at the equatorial positions (Figure 8).

The μ-η^2:η^1 structure observed for the Naruta complex **9b** makes it likely that the same or similar (porphyrinate)Fe^{III}−peroxo−Cu^{II}(ligand) structure, or perhaps an end-on Fe−O−O−Cu μ-1,2 connectivity, is present in Karlin's analogues, $[(F_8TPP)Fe^{III}-(O_2^{2-})-Cu^{II}(TMPA)]^{+}$ (**4a**) and $[(^6L)Fe^{III}-(O_2^{2-})-Cu^{II}]^{+}$ (**6b**) (see above).

Analysis/Discussion of the Bovine Peroxo C*c*O Structure. In the X-ray crystallographic studies of oxidized ("resting" state) bovine C*c*O, a μ-peroxide ligand giving a heme $a_3-O_2-Cu_B$ structure is suggested to be present (Figure 9).[18] The researchers have also tested the possibility of a water−hydroxide bridge ($H_2O\cdots OH^{-}$) instead of O_2^{2-} in their refinement of data, but the bridging peroxide model is found to give significantly better fits. Such a bridged peroxo species has not as yet been seen in other heme−copper oxidases (see section 4.1), and, more importantly, there is no supporting spectroscopic evidence for such a peroxo species.

Table 2. Core Structures of Oxidized Bovine C*c*O and *μ*-Peroxo Complexes

	O_2-binding mode	Fe···Cu, Å	O–O, Å	Fe–O, Å	Cu–O, Å	ref
heme a_3–O_2–Cu_B[a] (Figure 9)	*trans*-*μ*-1,2	4.91	1.63	2.52	2.16	18
$[(TMP)Fe^{III}–(O_2^{2-})–(5MeTPA)Cu^{II}]^+$ (**9b**) (Figure 7)	μ-η^2:η^1	3.92	1.460(6)	2.031(4) 1.890(6)	1.915(5)	84
$[\{Cu(TMPA)\}_2(O_2)]^{2+}$ (Figure 8)	*trans*-*μ*-1,2	4.359(1)[b]	1.432(6)		1.852(5)	99, 100
$[Fe_2(O_2)(O_2CCH_2Ph)_2\{HB(pz')_3\}_2]$	*trans*-*μ*-1,2	4.004[b]	1.408(9)	1.885(12)		101

[a] The structure is determined at 2.3 Å resolution. [b] Metal···metal distance.

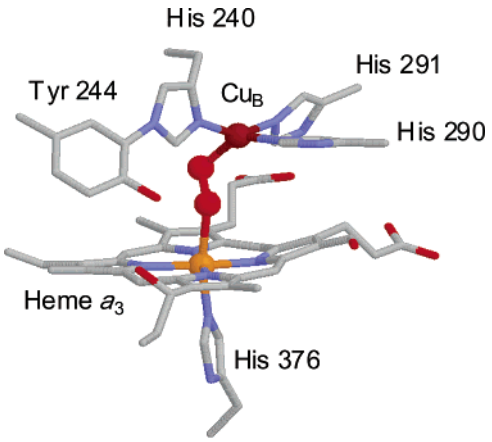

Figure 9. Crystal structure of heme a_3–Cu_B site of the fully oxidized bovine cytochrome *c* oxidase.[18] Coordinates were taken from the Protein Data Bank (PDB 20CC) and displayed using the program Rasmol. See text for further discussions about the nature of this putative peroxo-bridged heme–Cu structure.

Furthermore, a detailed examination of structural data known for coordination complexes brings insights that would seem to make the bovine enzyme peroxo formulation unlikely. Table 2 shows comparisons of the core structures for the oxidized bovine heme a_3–Cu_B center and *μ*-peroxo-bridged binuclear coordination complexes. $[(TMP)Fe^{III}–(O_2^{2-})–(5MeTPA)Cu^{II}]^+$ (**9b**), the only available crystal structure for synthetic heme–peroxo–copper species, has a different O_2-binding mode from that claimed for the enzyme, making a direct comparison between **9b** and the heme a_3/Cu_B site difficult. However, the combined structural information obtained from **9b** and other complementary *trans*-*μ*-peroxo dicopper(II)[99,100] and diiron(III)[101] complexes provides ranges for the expected metal–metal and metal–oxygen and O–O distances in a bridging-peroxo situation. Synthetic compound peroxide O–O bond distances are all almost identical with the expected value, varying between 1.4 and 1.5 Å (Table 2); however, the O–O separation in bovine C*c*O is 1.63 Å (Table 2). The synthetic complex Fe–O and Cu–O distances are also within the tight range of 1.8–2.0 Å. However, the metal–O distances in bovine C*c*O are significantly longer. *Thus, it is unlikely that the heme a_3 and Cu_B are bridged through a peroxide ligand.*

Of course, the resolution of the protein X-ray structure has to be carefully considered to make such conclusions. However, the observed Fe···Cu distance at the binuclear site, which can be measured relatively accurately, is also significantly longer than those found in any synthetic peroxo-bridged model complexes. On the other hand, the oxygen atoms (assigned as peroxide in the protein X-ray structure) are still at a metal–O distance (2.52 to Fe and 2.16 Å to Cu_B, Table 2), which can be considered as possessing a weak interaction with the heme–iron and Cu_B metal ions. In conclusion, other possibilities for a bridging ligand, including water and/or hydroxide, or even dioxygen, need to be reconsidered in an assignment of the ligation/coordination at the binuclear site in this oxidized bovine C*c*O X-ray structure. [Note: In a copper amine oxidase X-ray structure, a diatomic species is observed; it is noted as a dioxygen molecule but further described as a peroxide (product).[102,103]]

Scheme 5

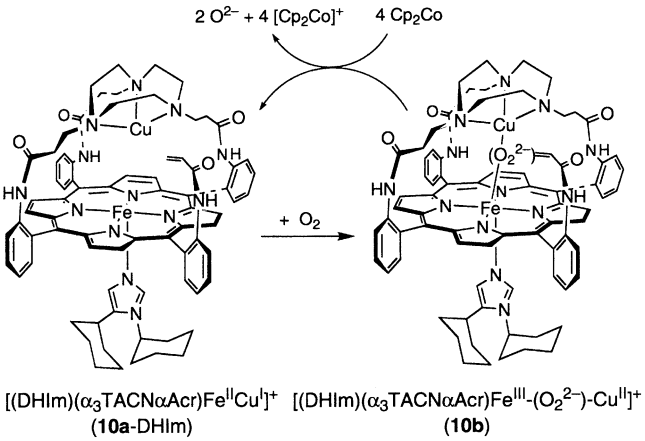

Systems Employing Tridentate Chelates for Copper. As will be shown, tridentate nitrogen ligands chelating copper ions in heme/Cu assemblies show interesting and potentially important differences in some properties of their O_2 chemistry and derived products (i.e., O_2 adducts).

Collman's research group reported the first example of a well-characterized discrete dioxygen adduct in a heme/Cu assembly using a sophisticated superstructured "capped" porphyrin with appended triazacyclononane (TACN) tridentate ligand for copper.[85,104] When a solution of $[(\alpha_3TACN\alpha Acr)Fe^{II}Cu^{I}]^+$ (**10a**) is mixed with 500 equiv of 1,5-dicyclohexylimidazole (DHIm) and subsequently exposed to dioxygen, rapid and irreversible formation of a dioxygen adduct $[(DHIm)(\alpha_3TACN\alpha Acr)Fe^{III}–(O_2^{2-})$-$Cu^{II}]^+$ (**10b**) occurs (Scheme 5). In contrast, the analogous Fe-only complex, $[(\alpha_3TACN\alpha Acr)Fe^{II}]^+$, binds O_2 reversibly under the same conditions, implying that copper plays a fundamental role in dioxygen binding. The formulation of **10b** comes from various spectroscopic techniques. Electrospray mass spectrometry supports **10b** as being a 1:1 adduct of **10a** and dioxygen. Resonance Raman spectroscopy confirms the peroxo formulation, with a ν(O–O) stretching vibration at 758 cm^{-1}, which gives an isotope shift of −18 cm^{-1}

Scheme 6

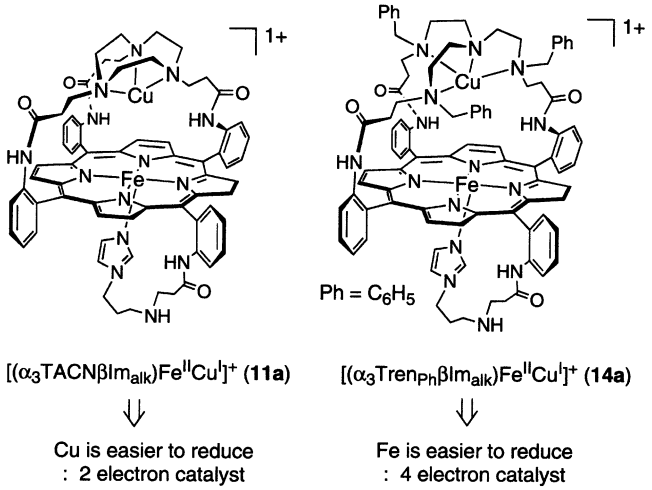

upon $^{18}O_2$ substitution (Table 1). Although this isotope shift is not in the expected range for a typical peroxide, further studies on **10b** generated from $^{17}O_2$ reveal the presence of vibronic coupling that can account for this abnormal behavior.[104] Furthermore, the diamagnetic features in ^{1}H NMR spectroscopy suggest the presence of an antiferromagnetic coupling between the low-spin Fe(III) and the Cu(II) center through a peroxide bridge. A similar diamagnetic intermediate, [(pyridine)(α_3TACNαAcr)Fe^{III}−(O_2^{2-})-$Cu^{II}]^+$, can also be generated from **10a**/O_2 reaction in pyridine-d_5 solvent. A redox titration of [(DHIm)-(α_3TACNαAcr)Fe^{III}−(O_2^{2-})−$Cu^{II}]^+$ (**10b**) with cobaltocene ($CoCp_2$), a one-electron reductant, reveals that 4 equiv of $CoCp_2$ (four electrons) are required for the complete reduction of **10b** to generate [(α_3TACNαAcr)-$Fe^{II}Cu^{I}]^+$ (**10a**). The gas titration also shows that the fully reduced complex **10a** consumes 1 equiv of O_2 to regenerate **10b**. The cycle of redox titration and O_2 binding could be repeated several times (Scheme 5).

The Collman group has further developed a series of capped porphyrin complexes, in which an imidazole or pyridine axial base is covalently bound to one side of a porphyrin, whereas a TACN or *N*,*N*′,*N*″-tribenzyltris(aminoethyl)amine (TBTren) copper ligand is attached to the opposite side (**11a**, **12a**, **13a**, and **14a** in Figure 6, Scheme 6).[105−107] All of these Fe^{II}/Cu^{I} complexes irreversibly bind O_2 to form a bridging peroxo intermediate, Fe^{III}−(O_2^{2-})−Cu^{II}, with diamagnetic ^{1}H NMR spectra supporting the formulation; more detailed characterization has not been described. Most of these complexes demonstrate an efficient four-electron, four-proton electrocatalytic reduction of O_2 to H_2O at physiological pH. However, depending upon the ligand environments of the metal centers, they exhibit different chemical reactivity. For example, when the peroxo complexes [(α_3TACNβIm_{alk})-Fe^{III}−(O_2^{2-})−$Cu^{II}]^+$ (**11b**) and [($\alpha_3Tren_{Ph}\beta Im_{alk}$)$Fe^{III}$−($O_2^{2-}$)−$Cu^{II}]^+$ (**14b**) are titrated with Cp_2Co, **11b** requires only 2 equivalent of Cp_2Co to regenerate **11a**, whereas **14b** needs 4 equiv to form **14a**.[104,106] Differences in behavior between **11a** and **14a** are also observed in electrocatalytic reactivities, carried out through the use of rotating ring-disk voltammetry (Scheme 6). Complex **14a** catalyzes the 4e$^-$ reduction of O_2 to H_2O, whereas **11a** predominantly catalyzes

Scheme 7

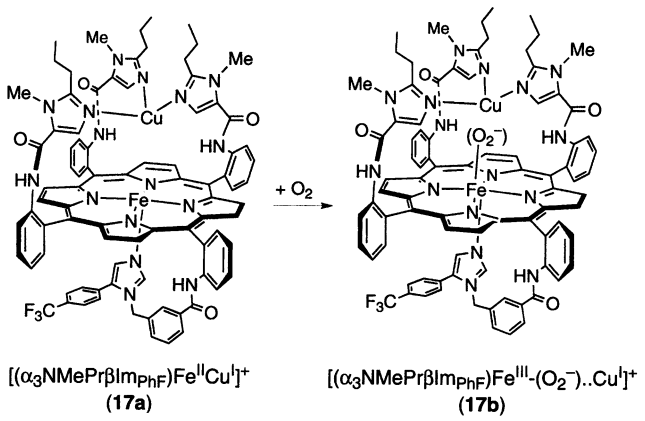

the 2e$^-$ reduction of O_2 to H_2O_2. Interestingly, a cobalt analogue of **11a**, [(α_3TACNβIm_{alk})$Co^{II}Cu^{I}]^+$ (**11c**), catalyzes the 4e$^-$ reduction of O_2 with very little H_2O_2 leakage.[105] Such observed differences can be attributed to their redox behavior. Cyclic voltammograms of **11c** and **14a** show that $Co^{III/II}$ or $Fe^{III/II}$ redox potentials are higher (more positive, i.e., easier to reduce) than $Cu^{II/I}$ potentials. In contrast, a more positive $Cu^{II/I}$ potential (as compared to $Fe^{III/II}$) is observed for **11a**, allowing Cu to be reduced before Fe in the electrocatalytic cycle. The researchers suggest[104] that prior O_2 binding to copper(I) [rather than iron(II)] could lead to a Cu−O_2 moiety which resides nearer the outside of the porphyrin−macrocycle cavity, resulting in a 2e$^-$ reduction pathway in which only Cu is involved. On the other hand, in complexes **11c** or **14a**, prior reduction of the Co or Fe center would direct the O_2-binding site inside the bimetallic cavity (because the other side of the porphyrin is blocked by an axial ligand), and it could further react with Cu as the copper center is (electrochemically) reduced. Studies of this series of complexes suggest that both copper and a heme-axial base are important in the 4e$^-$ reduction of O_2 and that the catalytic properties of these complexes can be fine-tuned through small structural ligand modifications.

In more recent investigations from the Collman group,[86,108,109] the copper ion is bound by three imidazole ligands instead of a TACN or TBTren moiety (compounds **15a**, **16a**, **17a**, **18a**, and **19a**, Figure 6); the authors suggest this is more biomimetic, as imidazole donors are employed, and there are only three N-ligands for copper, as in the enzymes. Similar to previous models, these complexes are also found to be very efficient 4e$^-$ catalysts, but they show rather different O_2 reactivities. One of the intriguing findings is the observation of a room temperature stable "heme−superoxide/Cu^{I} intermediate" from the $Fe^{II}/Cu^{I}/O_2$ reaction (Scheme 7; Table 1).[86] Thus, when [(α_3NMePrβIm_{PhF})$Fe^{II}Cu^{I}]^+$ (**17a**) is exposed to dioxygen, a fast formation of a 1:1 ratio of the complex/dioxygen intermediate occurs. This dioxygen adduct is diamagnetic, as shown by NMR and EPR spectroscopies. Resonance Raman spectroscopy fails to detect a ν(O−O) vibration, but the oxygen isotope sensitive ν(Fe−O) vibration is observed at 570 cm^{-1} ($\Delta^{18}O_2$ = −26 cm^{-1}). This ν(Fe−O) value is well-

matched with those of other known heme−superoxide complexes, suggesting that the intermediate is indeed an iron−superoxo species [(α_3NMePrβIm$_{PhF}$)Fe^{III}−(O_2^-)···Cu^I]$^+$ (**17b**) (Scheme 7; Table 1), rather than a μ-peroxo heme−Cu complex. This formulation is further supported by the oxygen reactivities of a cobalt analogue [(α_3NMePrβIm$_{PhF}$)Co^{II}Cu^I]$^+$ (**17c**) and the iron-only complex (α_3NMePrβIm$_{PhF}$)Fe^{II} (**17d**), in which they unambiguously form superoxo intermediates upon oxygenation. Dioxygen adduct **17b** is claimed to resemble intermediate **A**, the first O_2-derived heme−copper oxidase enzyme intermediate. Even though the copper ion in **17b** does not seem to have any redox activity, there is a clear difference in the dioxygen affinity between [(α_3NMePrβIm$_{PhF}$)Fe^{II}-Cu^I]$^+$ (**17a**) and iron-only analogue (α_3NMePrβIm$_{PhF}$)-Fe^{II} (**17d**). In fact, Cu^I in the distal site strongly enhances dioxygen binding to iron and makes the Fe/Cu−superoxide species more stable than a "Cu-free" iron−superoxide in this particular ligand framework. Interestingly, complexes **15a** and **16a**, which also contain three imidazole copper ligands (Figure 6), yield a "short-lived" peroxo Fe^{III}−(O_2^{2-})−Cu^{II} species rather than a superoxo species from the Fe^{II}/Cu^I/O_2 reaction.[108] Much of the research on complexes **15a**, **16a**, **18a**, and **19a** is at this time limited to electrocatalytic studies, and the exact nature of dioxygen intermediate(s) that may form in these reactions of reduced Fe^{II}···Cu^I complexes with O_2 is not fully understood.

Karlin and co-workers also expanded their studies with tridentate ligands, to compare and contrast the chemistry with that for systems possessing tetradentate TMPA-containing ligands. Extensive previous (and ongoing) Cu^I/O_2 chemical investigations have shown that even subtle differences in ligand/denticity can dramatically change the nature of the copper−dioxygen adduct and its reactivity toward substrates.[7,110,111] Tetradentate ligands, such as TMPA, induce formation of end-on (μ-1,2) peroxo dicopper(II) structures (Figure 8), whereas tridentate ligands generate side-on (μ-η^2:η^2) peroxo dicopper(II) species, which can be in equilibrium with bis-μ-oxo dicopper(III) isomers (see also articles by T. D. P. Stack and colleagues in this issue).[6] In their initial O_2 reactivity studies of a heme/tridentate−Cu system, Karlin and co-workers have utilized a PY2 moiety for a copper ligand, where PY2 = *N*,*N*-bis[2-(2-pyridyl)ethyl]-amine (**20**, **22**, **24a**, and **25a**, Figure 6).[87,112,113] The Cu^I/O_2 reactivity with this particular chelate, including variants with substituents and binuclear analogues, had been separately studied.

Preliminary stopped-flow kinetic studies[112] on the dioxygen reaction of 1:1 mixture of (F$_8$TPP)Fe^{II} (**3a**) and [(MePY2)Cu^I(MeCN)]$^+$ (**20**), where MePY2 = *N*,*N*-bis[2-(2-pyridyl)ethyl]methylamine (Figure 6), have shown that dioxygen reacts with iron first to form the heme−superoxo complex (S)(F$_8$TPP)Fe^{III}−(O_2^-) (**3b**) (S = acetone or THF), which subsequently reacts with copper chelate **20** to generate a presumed bridging peroxo intermediate [(F$_8$TPP)Fe^{III}−(O_2^{2-})−Cu^{II}(MePY2)]$^+$ (**21a**). However, complex **21a**, or other intermediates whose presence was indicated by stopped-flow spectroscopy, are not stable even at low temperatures, precluding further investigations in this system. The mixture of **3a**/**20**/O_2 eventually transforms to an isolable and characterizable μ-oxo complex [(F$_8$TPP)Fe^{III}−(O^{2-})−Cu^{II}(MePY2)]$^+$ (**21b**) (see section 4.2.1).

Scheme 8

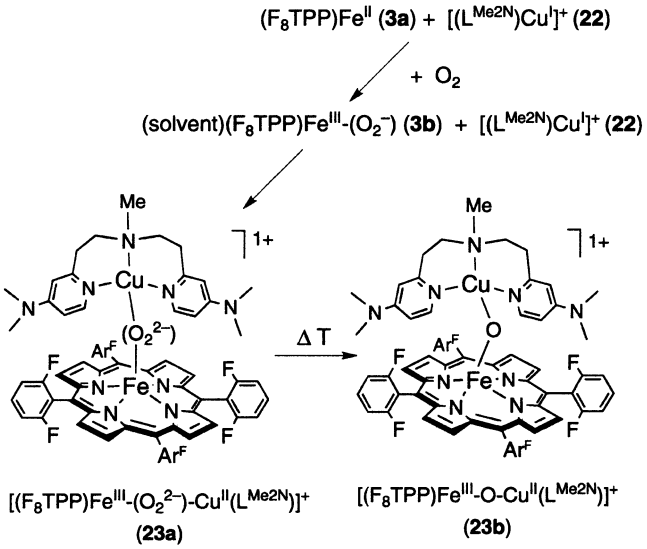

Further insights into O_2 reactivity with a heme/tridentate Cu system come from the study of the (F$_8$TPP)Fe^{II} (**3a**)/[(L^{Me2N})Cu^I]$^+$ (**22**)/O_2 reaction, where L^{Me2N} is an MePY2 analogue that has dimethylamino substituents on the para positions of the pyridine groups (Figure 6 and Scheme 8).[87] Spectroscopic investigations reveal that low-temperature oxygenation of **3a** and **22** in CH_2Cl_2/6% EtCN or THF/6% EtCN leads to rapid formation of a "short-lived" heme−superoxo species (S)(F$_8$TPP)Fe^{III}−(O_2^-) (**3b**) (S = THF or propionitrile), which subsequently reacts with **22** to form a bridging peroxo intermediate [(F$_8$TPP)Fe^{III}−(O_2^{2-})−Cu^{II}(L^{Me2N})]$^+$ (**23a**) (Scheme 8). From other studies, it is known that the presence of the nitrile (from solvent) in the system precludes independent O_2 reaction with [(L^{Me2N})Cu^I]$^+$ (**22**) or other closely related pyridyl-alkylamine-containing tridentate Cu^I−ligand complexes. To assist the assignment of the short-lived species, the researchers have separately prepared (S)(F$_8$TPP)Fe^{III}−(O_2^-) (**3b**) from iron-only reactions, **3a**/O_2. The formulation of **3b** is supported by resonance Raman spectroscopy, revealing ν(O−O) = 1178 cm^{-1} ($\Delta^{18}O_2$ = −64 cm^{-1}) and ν(Fe−O) = 568 cm^{-1} ($\Delta^{18}O_2$ = −24 cm^{-1}) for this low-spin six-coordinate heme−superoxo moiety, consistent with other chemical and spectroscopic studies.[114] Formation of **3b** in the presence or absence of copper complex **22** has been analyzed through stopped-flow kinetic studies. The rate constants and activation parameters for (S)(F$_8$TPP)Fe^{III}−(O_2^-) (**3b**) formation obtained show that the presence of **22** has essentially no effect. [In THF/6% EtCN: **3a**/**22**/O_2, $\Delta H^‡$ = 20 ± 1 kJ/mol, $\Delta S^‡$ = −25 ± 6 J/mol·K, k = 3.05 ± 0.14 × 10^5 M^{-1} s^{-1} (−90 °C); **3a**/O_2, $\Delta H^‡$ = 21.0 ± 0.6 kJ/mol, $\Delta S^‡$ = −19 ± 4 J/mol·K, k = 4.21 ± 0.08 × 10^5 M^{-1} s^{-1} (−90 °C).] However, in the presence of copper, the iron−superoxo complex **3b** is short-lived because it reacts further to give μ-peroxo

Scheme 9

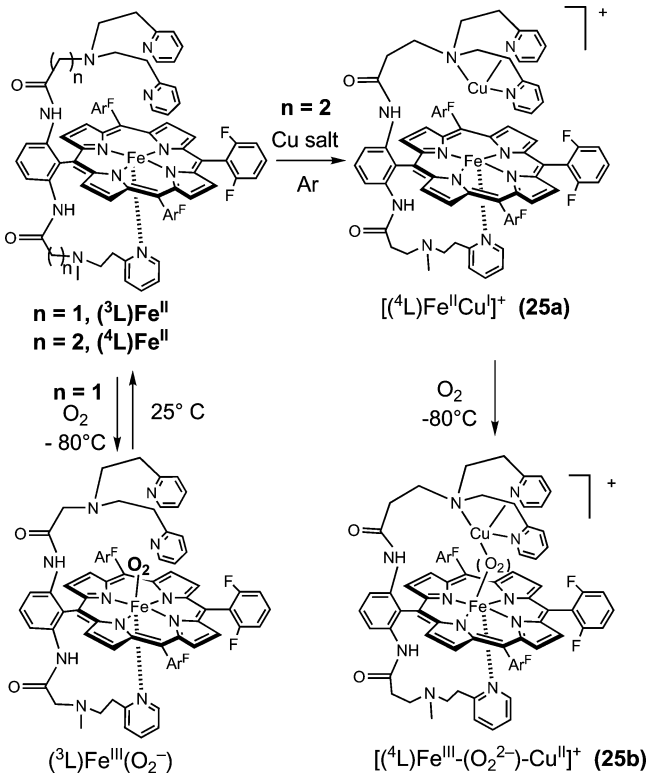

species $[(F_8TPP)Fe^{III}-(O_2^{2-})-Cu^{II}(L^{Me2N})]^+$ (**23a**) (Scheme 8).

The μ-peroxo formulation for **23a** is supported by ^2H and ^1H NMR spectroscopic properties, whose characteristic hydrogen resonance patterns are consistent with those for an antiferromagnetically coupled $S = 2$ system, arising from the bridged high-spin Fe(III) and Cu(II) centers. Direct evidence for the peroxo ligand in **23a** is provided by resonance Raman spectroscopy. Two distinct peroxo species (suggested as arising from isomer or conformer forms) are detected with ν(O−O) vibrations at 767 and 752 cm^{-1} ($\Delta^{18}O_2 = -41$ and -45 cm^{-1}, respectively). These ν(O−O) values are significantly lower than those observed for tetradentate systems (Table 1). Karlin and co-workers propose that the reduced ν(O−O) vibrations are attributable to the presence of a μ-η^2:η^2 side-on bound heme−peroxo−copper structure, induced by the structural preferences of the Cu−tridentate moiety in Cu−L^{Me2N} (see further discussion, below). Complex **23a** thermally converts to a μ-oxo complex $[(F_8TPP)Fe^{III}-O-Cu^{II}(L^{Me2N})]^+$ (**23b**) (Scheme 8), as seen for other related systems. However, **23b** contains a severely bent Fe−O−Cu core (compared to other tetradentate systems), and the differences observed in the metal core structures are also suggested to originate from copper ligand influences (see section 4.2.1).

Karlin and co-workers also have developed binuclear systems that possess a tridentate PY2 chelate for copper ion and a covalently linked pyridyl axial base for iron (**24a** and **25a** in Figure 6, Scheme 9).[113] Complexes $[(^3L)Fe^{II}Cu^I]^+$ (**24a)** and $[(^4L)Fe^{II}$-$Cu^I]^+$ (**25a)** have the same ligand donor sets, but they contain different linkers to the PY2 and heme axial base, and the effects of these subtle changes in the

Scheme 10

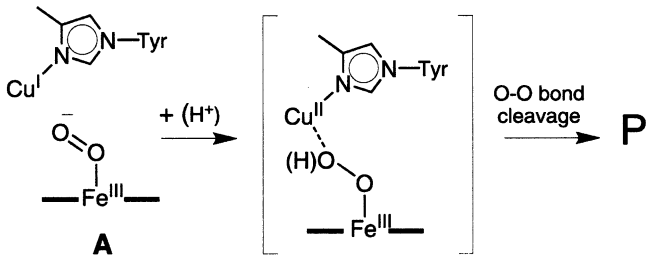

ligand superstructures are exhibited in their dioxygen reactivities. The iron-only complex $(^3L)Fe^{II}$ binds O_2 reversibly, whereas only irreversible O_2 binding is observed with $(^4L)Fe^{II}$ (Scheme 9). For the $Fe^{II}Cu^I$ complexes, both **24a** and **25a** react with O_2 irreversibly to form low-temperature stable dioxygen adducts (Scheme 9). The formulation of $[(^4L)Fe^{III}-(O_2^{2-})-Cu^{II}]^+$ (**25b**) is supported by a spectrophotometric titration (i.e., one O_2 per complex) and NMR and EPR spectroscopies. Complex **25b** is a magnetically coupled peroxo-bridged species, whose features are analogous to Collman's several low-spin peroxo complexes. Warming of the O_2 adducts **24b** and **25b** leads to different thermal products. For **25b**, the major thermal product (>70%) is the μ-oxo complex $[(^4L)Fe^{III}-O-Cu^{II}]^+$. In contrast, no μ-oxo final species has ever been observed from O_2 reaction of $[(^3L)Fe^{II}Cu^I]^+$ (**24a**), showing the importance of the ligand architecture on heme/O_2 and heme/Cu/O_2 chemistry.

Ligand Influences on the O−O Stretching Vibration in Heme−Peroxo−Cu Complexes. The presence of a μ-peroxo (porphyrinate)$Fe^{III}-(O_2^{2-})-Cu^{II}$ species has not been detected in the enzyme catalytic cycle. However, such a bridged μ-peroxo or (protonated) hydroperoxo heme−copper species has been suggested or even presumed by workers such as Babcock, Blomberg, Siegbahn, and Wikström,[21,56,77] as it may facilitate reductive O−O bond cleavage [Scheme 10 and Figure 21 (section 5.1.4)]. Labeling studies suggest that the hydroxide (or water) that ends up on Cu_B after O_2 reaction is derived from dioxygen, consistent with a Cu_B association with an O_2-derived moiety during the O−O cleavage process.[56,115] As (porphyrinate)$Fe^{III}-(O_2^{2-})-Cu^{II}$ complexes have now been characterized in just the past few years, one can discuss what trends thus far observed may contribute to eventual O−O bond cleavage. In fact, the research groups of both Karlin and Naruta observed that the O−O bond strengths in the heme−peroxo−copper complexes can be weakened by controlling the metal−ligand environments.

Karlin and co-workers have especially focused on the copper−ligand influences on heme/Cu/O_2 reactivities. As discussed above, the chemistry of the heme/Cu with tridentate ligands (Scheme 8) is similar to the μ-peroxo and μ-oxo chemistry with tetradentate CuL systems (Schemes 2 and 4). However, a striking decrease of >40 cm^{-1} in the μ-peroxo ν(O−O) stretching vibration is observed over the range of complexes **4a**, **5b**, **6b**, and **23a** (Table 1). The researchers have made an analogy of the observed differences in ν(O−O) vibrations with those known from Cu_2/O_2 chemistry, where μ-η^2:η^2 side-on peroxo (vs μ-1,2 end-on peroxo, Chart 1) ligation

Chart 1

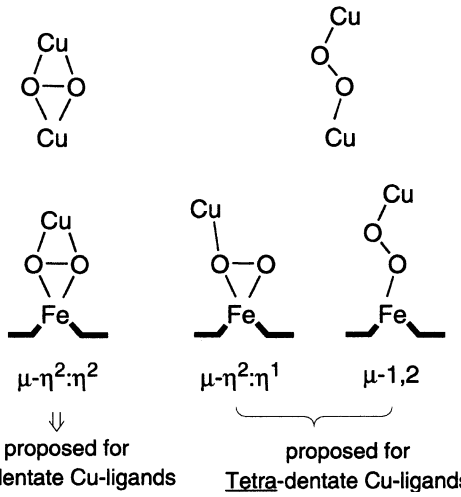

considerably reduces the ν(O−O) values (805−830 → 710−760 cm^{-1}).[111,116,117] With the data obtained and with the known preference in copper−dioxygen chemistry (vide supra), the authors favor the view that the tetradentate containing systems **4a**−**6b** (Schemes 2 and 4) possess either end-on Fe^{III}−(μ-1,2-peroxo)−Cu^{II} or Fe^{III}−(μ-η^2:η^1−peroxo)−Cu^{II} (i.e., like **9b**) structures, whereas the tridentate Cu−ligand containing systems such as **23a** (Scheme 8) possess side-on Fe^{III}−(μ-η^2:η^2−peroxo)−Cu^{II} structures. In a different approach, Naruta and co-workers[83] have also observed a decreased ν(O−O) stretching vibration (by 13 cm^{-1}) by introduction of electron-donating methyl groups into either the porphyrinate (mesityl instead of phenyl for the aryl group of a tetraarylporphyrin) or copper ligand (5-pyridyl substituents) complexes **7b**−**9b** (Table 1).

Several other factors may also contribute to the O−O bond weakening and eventual cleavage, such as the influence of axial heme ligands and/or hydrogen bonding networks. Babcock and co-workers[21] suggested that the basicity of the axial histidine ligand might change during the C*c*O catalytic cycle, yielding the different spectroscopic features observed in comparing the **P** and **F** intermediates. It seems highly likely that the heme axial base participates in tuning the C*c*O reactivity, but exactly how this occurs is not understood and represents an area in which model compound chemistry can contribute to our fundamental understanding.

In the Karlin and Naruta synthetic models, a weakly basic axial ligand (i.e., a nitrile or THF or acetone, but in concentrations as high as the solvent) is present, and Karlin's work shows that it promotes formation and stabilization of (solvent)(heme−Fe)−O_2 iron−superoxo species;[87] however, it is not bound to the heme upon further reaction with a copper complex, when a bridging peroxo complex forms (e.g., see Scheme 8).[80,81,84,87] Thus, even the presence of weak and untethered solvent ligands in these systems provides a "biomimetic" heme axial base, promoting strong O_2-to-iron(II) coordination, as in C*c*O intermediate **A** (Figure 5). It will be exciting to see future investigations in the Karlin and Naruta systems exposed to external donors (e.g., 1,5-dicyclohexylimidazole), to systematically study the effects of such a "strong" heme ligand on heme−peroxo−Cu structure and physical properties. This approach contrasts and will eventually nicely complement the systems from Collman and Boitrel, which possess covalently tethered pyridine or imidazole groups as heme axial donors (vide supra). Because the key step in heme−copper oxidase function and mechanism is the reductive O−O cleavage, the study of model systems in which this process can be investigated by examining the influences of Cu−ligand denticity, type of heme axial ligand, and presence of protons will be very pertinent.

3.2.2. Dioxygen Reactivity of Models Derived from Natural Hemes

As a different approach to mimicking the features of the dinuclear center in C*c*O, a few research groups have generated new model systems, in which natural heme groups are utilized for generating an analogue of a heme a_3 site. One such approach by Casella and co-workers[118−120] is the use of a "covalent peptide−porphyrin system". In the initial models, they have attached a polybenzimidazole as chelate for copper ion to a propionic acid side chain of deuteriohemin [(3,7,12,17-tetramethylporphyrin-2,18-dipropionate)-iron(III)] (Figure 6, compounds **26** and **27**).[121] Later, the system was modified, and a heme−axial base was attached to the second propionic acid chain of the porphyrin, using an L-histidine (Figure 6, compound **28**) or a glycyl-L-histidine residue (Figure 6, compound **29**).[119,120] For all of this series of the complexes, the redox potential of copper seems to be experimentally higher than that of heme center, allowing the researchers to generate a partially reduced $Fe^{III}Cu^{I}$ or a fully reduced $Fe^{II}Cu^{I}$ form by utilizing various reductants such as ascorbate or dithionite.

Upon exposure of the fully reduced heme−copper complexes **26**−**29** to dioxygen at −45 °C, direct oxidation occurs to give the fully oxidized $Fe^{III}Cu^{II}$ species without generating any O_2 intermediates, as determined by UV−vis spectroscopy.[118,119] No degradation of the porphyrin is involved in this oxidation process at −45 °C, but **26** and **27** show rather different O_2 reactivities at higher temperatures, where complete porphyrin degradation occurs, as monitored by loss of intensity of the strong Soret absorption. However, for **28** and **29**, which contain a heme−axial base, the room temperature oxygenation results in little or no porphyrin degradation. The researchers also have studied the O_2 reactivity of copper-free analogues of **27**−**29**, finding that oxygenation reactions for all three complexes lead to complete bleaching of the porphyrin. On the basis of all of these observations, the authors suggest[120] that formation of an intramolecular heme−peroxo−copper complex could play a role in preventing the porphyrin degradation chemistry otherwise observed.

Another new approach for the modeling C*c*O active site is through the use of "protein engineering", which also has been important in studies of the binuclear Cu_A electron-transfer site (see section 6). Several engineered proteins containing a model for the heme−copper oxidase heme a_3−Cu_B site start by employing cytochrome *c* peroxidase or myoglobin

Scheme 11

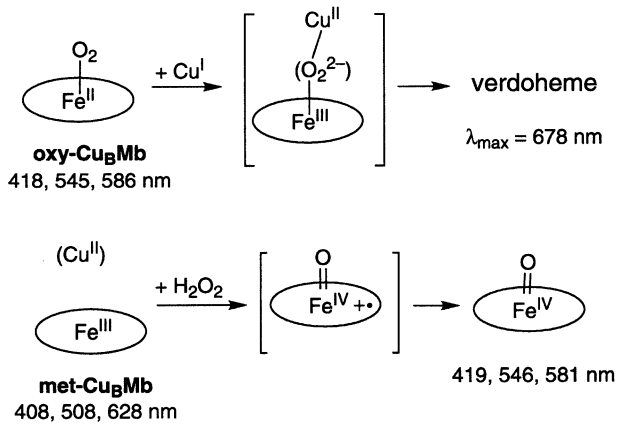

(Mb).[122−124] Lu and co-workers[124] have reported the first example of $Fe^{II}/Cu^{I}/O_2$ and $Fe^{III}/(Cu^{II})/H_2O_2$ reaction chemistry of such a protein-based model system. They have engineered a copper-binding site into a sperm whale myoglobin by utilizing the already present distal histidine and adding two more such residues by carrying out specific mutations, namely, Leu-29 → His and Phe-43 → His. This new protein is named Cu_BMb, which retains the heme iron and possesses a potential tridentate copper-binding site, but in fact it does not contain any copper ion. Upon exposure of O_2 to reduced Cu_BMb, formation of a heme-derived dioxygen adduct (oxy−Cu_BMb) occurs. The presence of the engineered copper-binding site, in the absence of a metal ion, decreases the O_2-binding affinity of the heme relative to that in wild-type (WT) Mb. However, addition of Ag(I), a redox inactive mimic of Cu(I), is found to enhance the O_2-binding affinity of Cu_BMb.

The researchers have further studied a reaction of oxy−Cu_BMb in the presence of added Cu(I) [in the form of 2 Cu(II) plus excess dithionite reductant, with added catalase to get rid of any hydrogen peroxide generated] (Scheme 11). Oxy−Cu_BMb (λ_{max} = 418, 545, 586 nm) plus Cu(I) ion results in a rapid change in UV−vis spectra, indicating the formation of the porphyrin oxygenated product verdoheme (λ_{max} = 678 nm), whose presence in the reaction mixture is also confirmed by electrospray mass spectrometry. Because this reaction product is similar to that generated by the heme oxygenase (HO) enzyme reaction, the researchers propose that the O_2 reduction in Cu^{I}/oxy−Cu_BMb proceeds through a heme−peroxy−copper intermediate, followed by porphyrin attack and heme degradation, as seen in the HO reaction pathway (Scheme 11). However, when H_2O_2 is reacted with Met−Cu_BMb, with or without Cu(II) present, a detectable ferryl−heme (λ_{max} = 419, 546, 581 nm) species is formed, instead of verdoheme (Scheme 11). The researchers explain this behavior by an effect of the hydrogen-bonding network in the distal pocket of the engineered heme protein. The reason that the putative heme−peroxo−Cu species in Cu_BMb undergoes heme degradation like that in HO, rather than ferryl−heme formation as in C*c*O, is that the engineered protein may not have the hydrogen-bonding network found in C*c*O to deliver extra protons to the peroxy species. When H_2O_2 is employed for the reaction, it itself carries protons to the active site, thus allowing Cu_BMb to switch from an HO reaction to a C*c*O-like pathway involving O−O cleavage and production of a high-valent ferryl species. On the basis of the observed different reactivities of O_2 and H_2O_2, the researchers propose that proton delivery would be critical in determining the reaction pathway of Cu_BMb with O_2, as is known with many other heme proteins. Further studies on this Mb mutant, which elucidate more detailed aspects of proton delievery in this system, would seem to be required.

3.3. Heme–Copper Carbon Monoxide (CO) Reactivity

As a structural or reactivity surrogate for dioxygen, generally stable carbon monoxide derivatives of O_2-binding heme proteins and heme copper oxidases have been extensively studied over the decades through various spectroscopic methods (optical, FTIR, resonance Raman, etc.).[11,35,125−141] The distinct spectral features of the CO adducts of iron and copper have been widely used to analyze structural information of the catalytic center in heme−copper oxidases and also to understand dynamic changes occurring in the heme periphery, such as effects on the proximal and distal side of the heme upon CO binding. In addition to gaining insight into the nature of the active site environment, CO photodissociation studies have been extremely useful in probing the dynamics and coordination chemistry of the heme−Cu_B binding pocket after CO photolysis.[129,134−136,138,140] Furthermore, time-resolved spectroscopic measurements on the photolysis of the CO inhibited enzyme have been utilized to measure electron-transfer between cytochrome *c* and the binuclear active site and within the heme−copper center.[140−142] Although a large amount of information is available for CO adducts of heme−copper oxidases[11,125−127,129−133,135−143] and the carbonmonoxy complexes of simple iron porphyrin synthetic complexes,[144,145] only a few recent papers describe studies on carbon monoxide adducts of heme−copper binuclear model compounds.[109,146,147] This may perhaps be due to the requirement of a suitably constructed porphyrin ligand for iron with a covalently appended tridentate or tetradentate chelate ligand for copper, to obtain binucleating heme−copper biomimics for these studies. The construction of such ligand systems involves considerable investment of effort, due to the multistep organic syntheses required.

3.3.1. Heme–Copper Enzyme CO Adducts

The preparation of carbon monoxide adducts of heme−copper oxidases, leading to histidine−heme-Fe^{II}−CO···Cu_B^{I} species, typically involves incubation of dithionite-reduced enzyme with CO. Carbon monoxide binds strongly to heme a_3 but transfers to Cu_B upon photolysis, as described in pioneering work of Woodruff, Einarsdóttir, and co-workers (Figure 10).[64,134,148] Thus, enzyme Cu_B−CO vibrational properties are determined from these dynamic photochemically initiated studies.[133−139,143,148] Dioxygen reactivity studies initiated in this way are mentioned in section 3.1.

Table 3. C–O Stretching Frequencies of the α, *β*, and *γ* Forms of the CO-Bound Heme–Copper Oxidases

	Fe			Cu		
type	α, cm^{-1}	*β*, cm^{-1}	*γ*, cm^{-1}	α, cm^{-1}	*β*, cm^{-1}	ref
aa_3						
bovine	1965	1952		2065	2043[a]	130, 134, 148, 157
R. sphaeroides	1966	1955		2064[a]	2039[a]	126
B. subtilis	1963		1975			128
P. denitrificans	1966	1956	1971[c]			132, 137
	1966[c]	1952[c]		2061	2038[c]	132
bo_3	1960			2065[b]		158
cbb_3		1956		2065		139
ba_3	1967	1973/1982	1975	2053		159
caa_3	1967	1958		2062		143

[a] Measurement at 10 K. [b] Measurement at 15 K. [c] Measurement at 84 K. All other values reported are from measurements at 300 K.

Table 4. Heme–Copper Oxidase Soret Absorption Maxima for Heme–CO Species and Vibrational Frequencies for Fe–His, Fe–CO, and Fe–C–O Moieties

type	Soret, nm	*ν*(Fe(II)–His), cm^{-1}	*ν*(Fe–CO), cm^{-1}	*δ*(Fe–C–O), cm^{-1}	ref
aa_3					
bovine	430	214	520	578	125
P. denitrificans	430	220	517	578	137
R. sphaeroides	430	~213	519/493	573	126
ba_3	429	193/209			160
bo_3	416	208	524	577	126, 161
aa_3-600		194/214	520	575	128, 162
cbb_3	415	235	495	574	126, 128, 163
caa_3	429	211			143

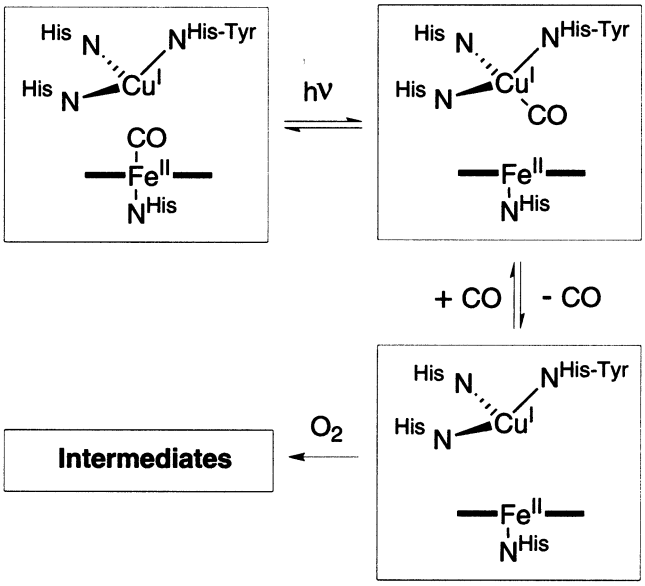

Figure 10. Photolability of CO in heme–copper oxidases and generation of Cu_B–CO adducts and O_2 reaction with fully reduced enzyme.

Values for *ν*(Fe–C–O) and *ν*(Cu–CO) are given in Table 3, as determined from a wide variety of heme–copper enzyme investigations. The *ν*(CO)Cu values observed are in fact very low by comparison to well-characterized copper(I)–carbonyl complexes derived from the synthetic (bio)inorganic literature.[149–153] This point is discussed further in section 3.3.2.

Heme–CO Properties and Implications for the Heme–Copper Active Site. The vibrational properties of the histidine–heme–Fe–CO···Cu_B unit of different types of heme–copper oxidases have been determined from the frequencies and intensities of the *ν*(Fe^{2+}–C–O) carbonyl stretch, the *ν*(Fe^{2+}–CO) iron–carbon stretch, the *δ*(Fe–C–O) bend, and iron–nitrogen(histidine) *ν*(Fe^{2+}–His) vibrational modes, as measured by FTIR or resonance Raman spectroscopy. The data are summarized in Tables 3 and 4. Mixtures of (major and minor) C–O stretching modes have been identified and assigned to arise from different conformations believed to occur at the active site. The two *major* conformers generally are found among heme–copper oxidases and are termed α- and *β*-forms.[129,136,137,143,154–156] The C–O stretching frequencies of both Fe–C–O and Cu_B–C–O in the α-form have been identified to have significantly higher values than those of their *β*-forms. In addition, two other very rare conformations (*δ*- and *γ*-forms) have also been identified in some oxidases under certain conditions.[137,156]

The functional significance for the presence of different conformations at physiological pH and the origin for the splitting of the C–O stretching frequency into distinct major and minor components are not fully understood. The special steric and/or electronic structures of the enzyme binuclear active site have been considered a possible cause for the unusual Fe–C–O modes observed in cytochrome *c* oxidase.[129,137,156]

The α-, *β*-, and *γ*-conformational states have been suggested to originate from the changes in the distances of the heme a_3 iron atom and Cu_B, which varies over a range of 4.4–5.3 Å in the different enzyme derivatives characterized by X-ray crystallography (see Table 5, section 4). The most stable conformer in many oxidases is the α-form.[126,128,129,132] Large steric factors and a restricted heme pocket are anticipated because of the reasonable proximity of Fe and Cu and the fact that ligands bound to either metal ion "face" each other. Thus, heme a_3 CO

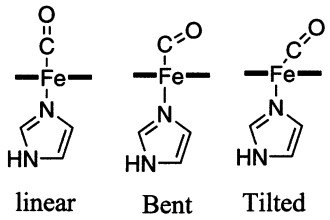

Figure 11. Some possible structures for heme−CO adducts.

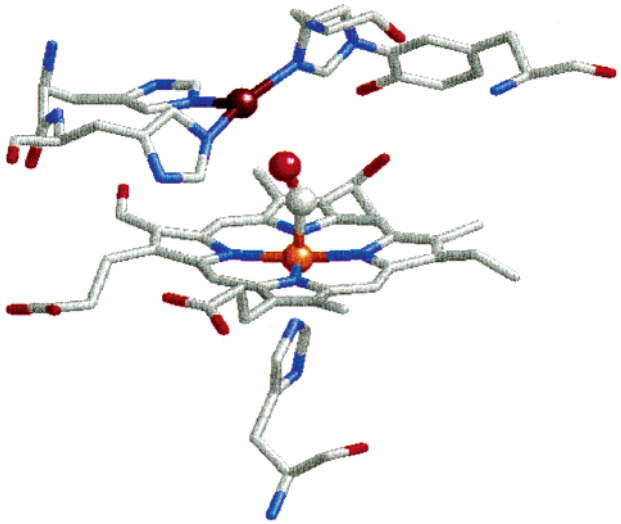

Figure 12. Crystal structure of the carbon monoxide adduct of cytochrome *c* oxidase from bovine heart.[18] Coordinates (1OCO) were taken from the Protein Data Bank (Brookhaven) and displayed using the program Rasmol.

coordination likely cannot occur without strong distal polar or steric interactions between CO and Cu_B. In the α-conformer, the Fe−C−O moiety might be significantly bent or tilted (Figure 11). However, as per recent discussions[144,145] updating and analyzing heme protein (and synthetic complex) Fe−CO structures and binding energetics, such severe distortions are unlikely, as the Fe−CO moiety should be nearly linear. In the alternate conformation (*β*-form), lower Fe−CO and Fe−C−O vibrational frequencies have been observed and attributed possibly to a less tightly structured binuclear center, that is, having an "open pocket". In this case, Cu_B (*β*-form) is moved a little further away than in the α-form.[137]

In 1998, Yoshikawa and co-workers reported the X-ray structure of a CO-bound form of the bovine enzyme (Figure 12 and Table 5). Here, the Fe−carbonyl unit is reported as being bent with ∠Fe−C−O = 146°. As mentioned above, this seems unlikely in terms of basic bonding considerations, and an alternative description of the structure should be considered. The heme a_3 iron and Cu_B distance is 5.3 Å in this fully reduced CO-bound state, and the CO oxygen atom is 2.5 Å away from Cu_B, therefore suggesting a weak interaction.[18] The authors do not mention possibly which form (α, *β* or other) this structure may represent.

Several factors may govern the modulation of the distance between the heme iron atom and Cu_B. Das et al.[129] have recently identified a pH-dependent mixture of α and *β* conformers in the aa_3 type oxidase from *R. sphaeroides*. It has been postulated that the different conformations may vary slightly in structure, from a change in the position of Cu_B with respect to the heme-bound CO. The modulation of the Fe_{a3}−Cu_B distance may arise from protonation/deprotonation of one or more ionizable residues close to the active site. This may be the covalently cross-linked tyrosine or one of the histidine ligands coordinated to Cu_B.[129] The involvement of His-290 (a Cu_B ligand) in the protonation/deprotonation events is also suggested from resonance Raman experiments in an aa_3 type quinol oxidase from *Acidophilic archaeon*.[164]

Das et al.[129] also carried out molecular simulation studies using the crystal structure parameters reported for the bovine oxidase, observing that as a result of varying the Fe···Cu distance from 4.7 to 6.0 Å, the Fe−C−O angle increases from 143° to an orientation nearly perpendicular (178°) to the heme. Thus, in the *β*-form the Fe−C−O bending angle has been suggested to be less than that of the α-form and therefore slightly lowers the vibrational frequency. In a similar study by Rousseau and co-workers with a CO complex of the cbb_3-type oxidase from *Rhodobacter capsulatus*, a proposed open structure exists lacking the distal interactions; thus, heme b_3 bound CO adopts a perpendicular conformation with respect to heme.[165]

Varotsis and co-workers[159] studied the CO adduct of the ba_3-type oxidase from *T. thermophilus* and noticed that the Cu_B−CO stretch is invariant in the pH range 5.5−9.7. It also remains unaffected by H/D exchange. On the basis of the argument that if one of the Cu_B−His ligands is capable of cycling through imidazolate (i.e., deprotonated), imidazole, and imidazolium (doubly protonated imidazole cation) states, then the *ν*(CO) frequency is expected to vary; however, this is not observed. Thus, they propose that the Cu_B−His environment is very rigid and not subject to conformational transitions associated with Cu_B−His ligand protonation/deprotonation events.[159] In a similar study on the CO adduct of aa_3-600 quinol oxidase, a single conformer has been detected, which is essentially the α-form, exhibiting *ν*(Fe−CO), *δ*(Fe−C−O) and *ν*(C−O) modes at 520, 575, and 1963 cm^{-1}, respectively. On the basis of this observation and the existence of an inverse correlation between the frequencies of the Fe−CO and Fe−His modes, they suggested that the effects exerted by Cu_B and the proximal His-376 (which is hydrogen-bonded to the peptidyl carbonyl of Gly-351) are the key determinants for the observed Fe−CO and C−O stretching modes in heme−copper oxidases. In a separate FTIR study on a CO adduct generated from a mixed-valent state of bovine C*c*O, $(Cu_AFe_a)^{5+}Fe_{a3}^{2+}Cu_B^{1+}$, a distinct Cu_B−C−O stretching band at 2040 cm^{-1} was noted, in addition to those corresponding to the α/*β*-forms (Table 3); it was assigned to the $(Cu_AFe_a)^{4+}Fe_{a3}^{3+}$-$Cu_B^{1+}$−CO species generated by back electron-transfer.[166]

As mentioned, photolysis of the reduced heme-bound CO of the enzyme at low temperatures results in the dissociation of iron-bound CO followed by binding to Cu_B (Figure 10). The formation of Cu_B−CO is completed within 1 ps,[135] and CO remains

bound only for ~1.5−2 μs and subsequently dissociates and either escapes (to solvent) or rebinds to the heme.[133,148,167] Transient binding of CO to Cu_B has also been reported to be dynamically linked to structural changes of carboxylic acid groups of amino acid residues nearby Cu_B in the binuclear active site.[129,138,166] For example, there are changes in the hydrogen bonding at the functionally important residue glutamic acid-286 [E(I-286)] of subunit I, positioned in the D-pathway for proton translocation, ~25 Å from the protein surface on the proton-input side [D(I-132)] and ~10 Å from the binuclear heme−Cu center.[138] In this way, a role for Cu_B in the proton translocation pathway can be implicated or tracked.[129,137,138,166]

In summary, investigations utilizing CO binding to heme−Cu enzymes have been and continue to be an incredibly useful tool and probe.

3.3.2. Heme–Copper CO Complexes

As described above (section 3.2) for O_2-reactivity studies, biomimetic approaches have utilized systems with 1:1 mixtures of porphyrin−iron(II) and L_n−copper(I) (where L_n = tridentate or tetradentate chelate ligands) and/or the employment of hemes with covalently appended chelates for copper, generating binuclear heme−copper systems. Because reduced dioxygen species such as peroxide (O_2^{2-} when deprotonated) are good bridging ligands, the use of mononuclear copper and porphyrinate iron components to generate heme−Cu assemblies is a reasonable strategy, and it has been successful (section 3.2). Heterobinucleating ligands for the generation of heme−Cu assemblies, however, would seem to be necessary for studies on heme−Cu carbon monoxide complexes, because CO is unlikely to be a bridging ligand from a porphyrinate−iron(II) to copper(I) complex; there are no such examples. Properly designed heme−Cu complex assemblies with bound CO may then possess iron−copper separations similar to that observed in the enzyme structures (~4−5 Å away) in order to study the influence of Cu_B in proximity to the heme-bound CO.

Carbon monoxide derivatives of heme−Cu complexes have in fact been only recently described.[109,147,168] Collman and co-workers[109] have studied the CO adducts of tris(imidazole) copper picket containing binucleating models (Scheme 12) and iron-only derivatives (i.e., without copper). The use of NMR spectroscopy on such diamagnetic derivatives, including in some cases zinc-containing analogues, has allowed for detailed structural and conformational comparisons of these superstructured compounds; valuable insights have been obtained. In the absence of copper bound within the tris(imidazole) picket, the $\nu(CO)_{Fe}$ of (α_3NMePrIMβIM$_{PhF}$)Fe^{II}−CO (**17f**) and that of (α_3NMeIMHβIM$_{PhF}$)Fe^{II}−CO (**18f**) are observed at 1978 and 1979 cm^{-1}, respectively, ~10 cm^{-1} higher in value than in a similar compound where the imidazole picket is replaced by acetyl amide groups. The high CO stretching frequency is postulated to arise from electrostatic interactions of the heme-bound CO with negative dipoles such as those of aromatic rings or lone pairs. With the addition of a copper(I) source into the distal imidazole picket, the iron-bound CO stretching frequencies decrease ~29 cm^{-1} compared to the iron-only analogues, suggesting that the positive charge of copper stabilizes backbonding to the CO ligand, which leads to weakening of the C−O bond. In addition, under an atmosphere of CO (α_3NMeHIMβIM$_{PhF}$)Fe^{II}−CO/Cu^{I} (**18c**), an additional carbonyl stretch is observed at 2085 cm^{-1}, which is in the range of CO bound to Cu^{I} in a variety of N_3−Cu coordination environments.[149−152,169,170] Thus, the large frequency shift ascribable to the presence of copper(I) (compared to iron-only carbonyl derivatives) suggests that in the heterobinuclear structure, the copper ion in the tris(imidazole) environment resides in close proximity, over the iron−CO moiety.[109] Similar frequency changes in addition to the substantial loss of copper were noted for an H333A mutant enzyme where one or more copper-binding His residues were modified.[171]

Karlin and co-workers[147] have also recently characterized carbonmonoxy adducts of reduced Fe^{II} heme and Fe^{II}Cu^{I} heme−copper binuclear complexes. UV−vis spectral changes that are analogous to those of other heme complexes and proteins are observed

Scheme 12

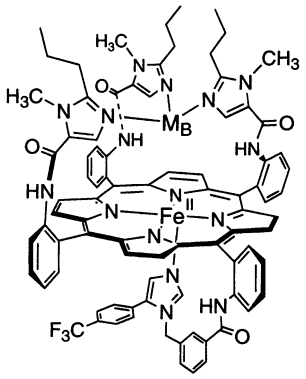

17a : M_B = Cu^{I}

17e : Fe^{II}-CO, M_B = Cu^{I}

17d : M_B = no metal ion

17f : Fe^{II}-CO, M_B = no metal ion

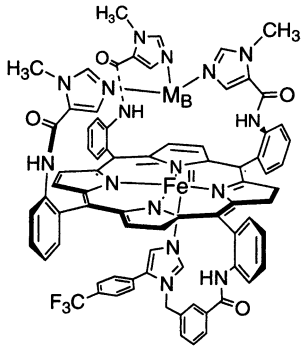

18a : M_B =Cu^{I}

18c : Fe^{II}-CO, M_B = Cu^{I}

18d : Fe^{II}-CO, M_B = Cu^{I}-CO

18e : M_B = no metal ion

18f : Fe^{II}-CO, M_B = no metal ion

Scheme 13

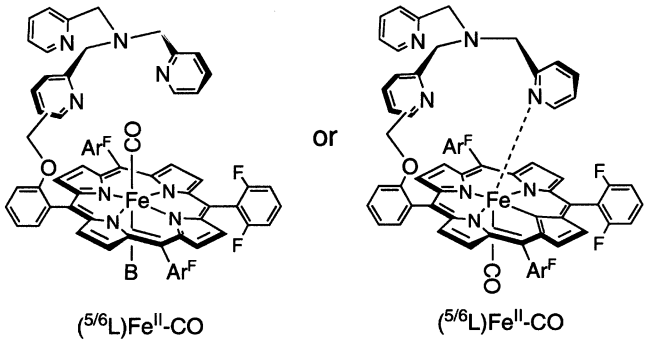

upon addition of CO to the reduced iron−porphyrin complex ($^{5/6}$L)Fe^{II}, lacking copper in the proximal chelate. Carbonylation produces a six-coordinate (low-spin) species ($^{5/6}$L)Fe^{II}−CO, with either a solvent molecule or a pyridine arm occupying the sixth coordination site (Scheme 13). The ν(CO)$_{Fe}$ stretching frequencies for ($^{5/6}$L)Fe^{II}−CO varied from 1968 to 1980 cm^{-1} as a function of solvent (such as THF, CH_2Cl_2, acetone, and toluene).

Additional studies on the products of carbonylation of [($^{5/6}$L)Fe^{II}Cu^{I}]$^+$ (**5a/6a**, Figure 6) identify both ν(CO)$_{Fe}$ and ν(CO)$_{Cu}$ vibrational frequencies. The latter occur in the range 2091−2094 cm^{-1}, which are typical of Cu−CO complexes, although these are ∼30 cm^{-1} higher in energy than those observed for Cu−CO moieties found in heme−copper oxidases (see Table 3). Interestingly, an additional shoulder at ∼2070 cm^{-1} is also observed in these [($^{5/6}$L)Fe^{II}−CO···Cu^{I}-CO]$^+$ (**5c/6c**) complexes. On the basis of the relative intensities of two Cu−CO (major and minor shoulder) infrared stretches and comparison of known Cu−CO stretching frequency values for close copper (only) complex analogues with either tetradentate or tridentate pyridylalkylamine ligand donors, it is postulated that the major isomer form [with higher 2090−2094 cm^{-1} ν(CO)$_{Cu}$ value] possesses a "dangling" pyridine arm and tridentate nitrogen coordination (Scheme 14). The minor product, with a ∼2070 cm^{-1} shoulder, perhaps involves an additional weak coordination of the third pyridyl arm (i.e., fourth nitrogen ligand) to the copper(I) ion (Scheme 14).[147]

Low ν(CO)$_{Cu}$ Values: Comparison to Other Copper Proteins and Synthetic Complexes. An examination of ν(CO)$_{Cu}$ values in heme−copper oxidases (Table 3) reveals that stretching frequencies observed (Table 3, 2038−2065 cm^{-1}) are comparable to or lower than those found for copper proteins such as hemocyanins (2043−2063 cm^{-1}),[172] amine oxidases (2064−2085 cm^{-1}),[173,174] peptidylglycine glycine monooxygenase (2033 cm^{-1}),[175] dopamine β-hydroxylase (2089 cm^{-1}),[176] and nitrite reductases (2041−2060 cm^{-1}).[177] These are strikingly low compared to well-characterized copper(I)−carbonyl complexes observed in the synthetic (bio)inorganic literature. N$_x$-Cu^{I}−CO complexes (N, a nitrogen donor ligand; x = 2−4) have been studied to model the poly(imidazole) binding sites of copper-containing proteins,[149−153,178] and they generally exhibit ν(CO)$_{Cu}$ values >2070 cm^{-1}, some even exhibiting stretching frequencies >2100 cm^{-1}, for example, ν(CO) = 2123 cm^{-1} for [Cu(CO)(pzs)]$^+$, where pzs is a thioether- and pyrazole-containing tridentate ligand.[169] Coordination complexes that possess unusually low ν(CO) values are a series with nonchelating imidazoles, such as [(1,2-dimethylimidazole)$_3$Cu(CO)]$^+$ (2062 cm^{-1}),[153] and those with anionic tris(pyrazolylborate) ligands, [(Tp^R)Cu^{I}−CO] (2059−2067 cm^{-1}),[149,150] at least somewhat comparable to heme−copper oxidase values (Table 3). Renaud and co-workers[179] have discussed the trends, indicating that ligand flexibility (in the nonchelating imidazole case) most likely allows metal−ligand geometries which maximize ligand overlap and donation to copper(I), lowering the carbonyl stretching frequency. The exceptionally low values found for certain heme−copper oxidase forms or derivatives are notable and certainly must indicate very unusual environments for Cu$^{I}_B$; implications for enzyme function are not clear and should be the subject of future investigations.

Scheme 14

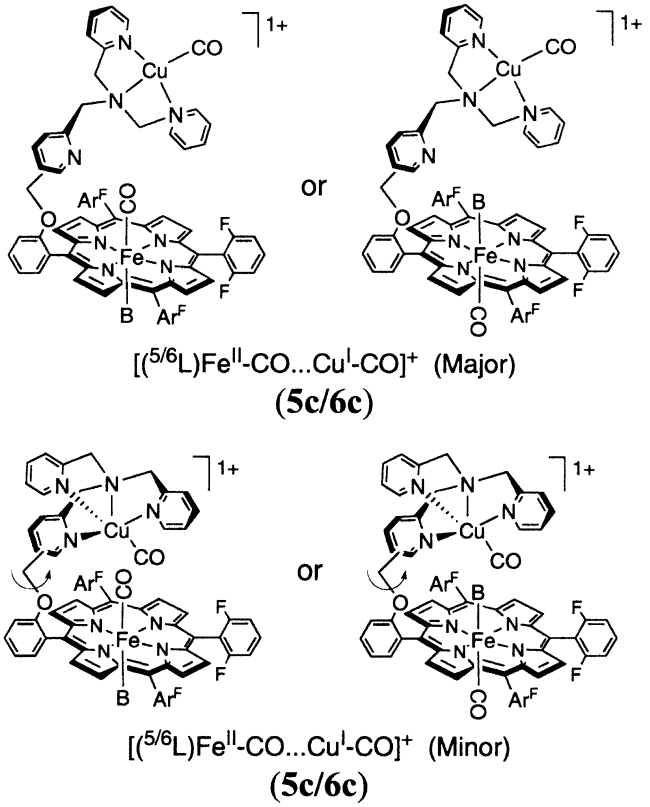

When **5c/6c** are bubbled with Ar at room temperature, carbon monoxide is lost from the copper ion, but not the heme, and complexes of the type [($^{5/6}$L)-Fe^{II}−CO···Cu^{I}]$^+$ (**5d/6d**) are generated (see following diagram). Thus, the Cu^{I}−CO moiety is more labile than the heme−CO group. Future studies comparing the thermodynamics of CO binding to the heme and Cu in such model systems will be of interest. In heme−copper oxidases, it is clear that the heme−CO is more thermodynamically stable, as indicated by the return of CO to the heme after it is photoejected and transfers to Cu$_B$ (see section 3.3.1). Collman and co-workers[168] have reported equilibrium constants for CO binding to **18c** and **18f** (with or without Cu), observing clear influences. In the study[109] involving CO binding to **17a**, steric effects limit CO binding to the copper ion (see Scheme 12).

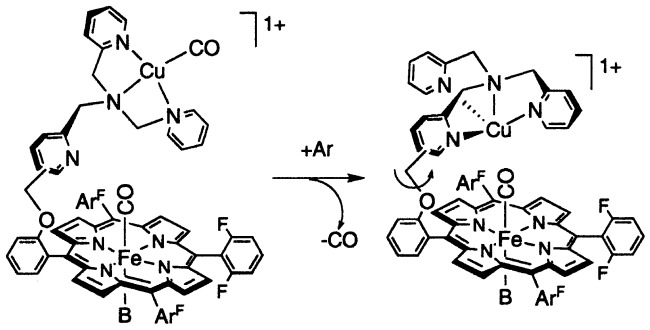

$[(^{5/6}L)Fe^{II}\text{-}CO...Cu^{I}\text{-}CO]^{+}$ **(5c/6c)**

$[(^{5/6}L)Fe^{II}\text{-}CO...Cu^{I}]^{+}$ **(5d/6d)**

The presence of copper(I), that is, in complexes **5d/6d**, does not shift $\nu(CO)_{Fe}$ values compared to those observed in the iron-only complexes $[(^{5/6}L)Fe^{II}-CO]^{+}$. Thus, in contrast to Collman's complexes (vide supra), there is little or no influence of copper(I) on CO bound to the heme. Karlin and co-workers suggest that either the Fe···Cu distance in these more flexible binucleating ligands (which have only a one-point attachment to the tethered chelate for copper) is much greater than in **17a** and **18a** (Scheme 12) or CO binding occurs on the heme face opposite the side where the copper-chelate resides (Scheme 14).[147] Because in the enzymes the proximity of Cu to the heme is relatively fixed, the protein CO chemistry clearly will differ from what is found in the ^{5}L- and ^{6}L-containing systems.

4. Oxidized Heme–Copper Models

Prior to the information and insights obtained from X-ray crystallographic characterization of heme–copper oxidase enzyme derivatives (sections 2 and 4.1, vide infra), knowledge concerning the protein metal ion centers, and particularly the heme–copper binuclear center, came from more indirect spectroscopic data and reaction chemistry performed. This led to a "picture" of the heme–copper active-site structure, which in turn inspired (bio)inorganic chemists to try to generate synthetically derived model compounds for the purpose of more detailed structural and spectroscopic characterization.

4.1. Enzyme Structural, Spectroscopic, and Magnetization Studies

Oxidized mitochondrial cytochrome aa_3 can exist as a mixture of forms called *fast* and *slow*, defined as such according to the rate of reaction of the enzyme with exogenous anionic ligands such as fluoride (F^-), cyanide (CN^-), and formate ($HCOO^-$).[180,181] A *fast* form predominates when the enzyme is isolated under mildly alkaline conditions, whereas a *slow* form dominates in preparations exposed to low pH. The *fast* form of the enzyme has been proposed to consist of an EPR-silent $Fe^{III}-X-Cu^{II}$ moiety,[182,183] where X represents a bridging ligand that modulates antiferromagnetic coupling. Naturally occurring X groups, which have been proposed, include oxide (O^{2-}), hydroxide (OH^-), carboxylate ($RCOO^-$), chloride (Cl^-), sulfide (S^{2-}), cysteinato, or an imidazolate group. The magnetic state of heme a_3 within this coupled site has been deduced from Mössbauer spectroscopy (see parameters in Table 7, section 4.2.1) and concluded to be a high-spin iron(III) center.[184,185] However, the magnitude of the exchange coupling between the heme a_3 and the Cu_B remains unclear. Magnetic susceptibility studies of mammalian C*c*O indicated that the high-spin $S = {}^5/_2$ ferric heme a_3 has strong antiferromagnetic coupling to the spin $S = {}^1/_2$ Cu_B, yielding a net spin $S = 2$ ground state for the heme a_3-Cu_B center.[186] However, later saturation magnetization studies showed that a strong coupling model ($J > 100$ cm^{-1}) as well as a weak coupling model ($J < 4$ cm^{-1}) fit the magnetic data.[187]

In the *slow* preparation, the coupling between the heme a_3 and the Cu_B also leads to an $S = 2$ ground state.[188] However, the magnetic coupling and the zero-field-splitting parameters are quantitatively different from those of the *fast* enzyme and result in the observation of an active EPR spectrum.[183,186] A similar situation was found for the quinol oxidase cytochrome bo_3 from *E. coli*, in its oxidized state. Perpendicular mode X-band EPR spectra of oxidized quinol oxidases as well as the *slow* form of C*c*O show broad, fast relaxing features with a similar pattern of bands: a weak derivative signal below 100 mT ($g \sim 12$ region) and a broad band in the region 200–250 mT ($g \sim 3.2$).[189] In the parallel mode spectrum, only the low-field signal is present. Furthermore, studies simulating dual-mode EPR spectra of fluoride cytochrome bo_3 showed only a very weak exchange interaction ($J \sim 1$ cm^{-1}) between the two ions and also suggested that any intervening exogenous ligands (e.g., fluoride, formate, azide) play only a minor part in mediating the interaction.[190]

Prior to the post 1995 single-crystal X-ray structures, X-ray absorption spectroscopic (XAS) methods provided heme–copper oxidase active-site insights. Henkel et al. reported an $Fe_{a3}\cdots Cu_B$ separation of 3.96 Å for the native C*c*O from bovine heart mitochondria (by analysis of the K edge region of copper, iron, and zinc).[191] They suggested that the most probable bridge is a chlorine or sulfur atom, because an iron–sulfur or an iron–chloride contact could be identified on evaluating the fine structure of the iron edge. A slightly shorter $Fe_{a3}\cdots Cu_B$ distance (3.70 Å) was reported by Powers et al. for the resting state of cytochrome aa_3-600 from *Bacillus subtilis*; again a Cl or S scatterer was seen bridging Fe and Cu.[192] Furthermore, a similar $Fe_{a3}-Cl(S)-Cu_B$ core (Fe···Cu = 3.75 Å) was found for the fully oxidized "resting" form of bovine heart enzyme by EXAFS studies.[193] Between Cl and S, it is possible that the bridging ligand is Cl rather than S, because no conserved cysteines or methionines can conceivably provide a sulfur atom,[194–196] and of course in the light of the subsequent X-ray single-crystal studies. Thus, the possibility of Cl contamination during protein purification and manipulation cannot be ruled out.[196] A reinvestigation of the *B. subtilis* enzyme by both Cu EXAFS and ENDOR detected the presence of an

Table 5. X-ray Crystallographic Data Obtained for Mammalian and Bacterial Heme−Copper Oxidases in Different Situations: Fully Reduced, Carbon Monoxide Bound, Azide-Bound, and Fully Oxidized Forms of the Enzyme

	bovine heart				*P. dentrificans*	*R. sphaeroides*	*T. thermophilus*
	reduced	CO bound	N_3 bound	oxidized	oxidized	oxidized	oxidized
resolution, Å	2.35	2.8	2.9	2.30	2.7	2.3/2.8	2.4
Cu_B ligand	3 His	3 His, O	3 His, N	3 His, O	3 His, OH(?)	3 His, O	3 His, O
heme a_3 ligand	His	His, C	His, N	His, O	His, H_2O(?)	His, O(?)	His(?), O
Fe···Cu distance, Å	5.19	5.27	5.3	4.91	4.5	4.8	4.4
bridging ligand		CO	N_3	O_2^{2-}	H_2O··OH^-	OH^- or H_2O	O^{2-}, OH^-, or H_2O
Fe···X distance, Å		1.90	1.97	2.52	n.a.	3.6	2.3
Cu···Y distance, Å		2.47	1.90	2.16	n.a.	2.0	2.3
Fe···His distance, Å	1.9	2.0	1.9	1.9	2.1	2.2	3.3
His−Tyr cross-link	yes	yes	yes	yes	yes	not clear	yes
ref	18	18	18	18	19	31	30

O/N Cu(II) ligand with an exchangeable proton.[196] The authors thus suggested an Fe^{III}−(OH)−Cu^{II} group at the active site of the enzyme, but on the basis of some X-ray crystallography results[31] (see below) it is probable that the OH^- group is not a bridging ligand and is bound only to Cu_B.

In the past 10 years, the X-ray structures of cytochrome *c* oxidase from *P. denitrificans*,[15,19] bovine heart,[16,18] *T. thermophilus* (ba_3−C*c*O),[30] and *R. sphaeroides*[31] were determined for the fully oxidized form of the enzyme (see Table 5). Also, Yoshikawa et al. determined the structures of the bovine enzyme at the fully reduced and azide- and carbon monoxide-bound (section 3.3) states.[18] The heme a_3−Cu_B distances were found in the range of 4.4−4.91 Å for the fully oxidized form, but the identity of the electron density and, hence, the nature of ligands between the metal ions are still unclear. For the *P. denitrificans* enzyme, Michel and colleagues[19] favor the possibility of a water molecule as a heme a_3−iron ligand and a hydroxy ion as a Cu_B ligand. For the bovine fully oxidized form, Yoshikawa et al. tested the model proposed by Michel et al.[19] [heme a_3−(H_2O)···(OH^-)−Cu_B], but instead, they fit their data proposing this crystal derivative possesses a peroxide bridging ligand.[18] However, as discussed in section 3.2 (vide supra), we judge this is unlikely to be the case. The structure of the ba_3−C*c*O from *T. thermophilus* revealed the presence of one oxygen atom (μ-oxo species, μ-hydroxo species, or water molecule) bridging Fe_{a3} to Cu_B.[30] In this case, the metal−oxygen distance found in the active site (2.3 Å) is long to be considered as a real coordination bond in light of the known well-characterized μ-oxo and μ-hydroxo coordination compounds (see discussion in section 4.2.1). For the *R. sphaeroides* enzyme, an OH^- ligand (or water) was assumed to be coordinated to Cu_B, although it could not clearly be identified.[31] At the level of refinement available, this OH^- ligand is definitely not coordinated to heme a_3 but probably weakly interacting.

So, with all the biophysical studies, and now the X-ray crystal structures, the nature or identity of a bridging ligand that would mediate magnetic coupling (strong or weak) between heme a_3 and Cu_B is still unclear.

4.2. Heme–Copper Fe^{III}–X–Cu^{II} Complexes

As indicated by the above discussions on the enzyme spectroscopic and structural properties, the enigmatic nature of the heme−copper binuclear moiety has provoked considerable efforts by coordination chemists to generate synthetically derived models. The above-mentioned magnetic coupling is thought to be mediated by a bridging ligand, the nature of which is still under debate. Furthermore, the identification of the "correct ligation at the oxygen-binding site in the oxidized state" of the enzyme is critical for the ultimate elucidation of the details of the proton-pumping mechanism.[197]

While in the past 10 years many efforts have been directed toward O_2 reactivity with (P)Fe^{II} and Cu^I complexes (see section 3.2), the first biomimetic modeling studies have concentrated upon oxidized (porphyrinate)Fe^{III}−Cu^{II}L heterobinuclear compounds. Synthetic approaches include (i) the use of porphyrins modified with covalently linked chelates for copper (i.e., *a binucleating ligand*) and (ii) (porphyrinate)-Fe^{III}−X−Cu^{II}L complexes made through *self-assembly strategies*.

Although covalently linked systems frequently require lengthier synthetic procedures, they exhibit interesting features. They favor intramolecular heterobinuclear chemistry (rather than intermolecular Fe/Fe and/or Cu/Cu chemistry) and allow fine structural tuning in order to investigate relationships between structure and function. The majority of porphyrins used in the synthesis of binucleating ligands are based on TPP derivatives. The reasons are the advantages implicated in the synthesis and stability of *meso*-phenyl-substituted porphyrins, as well as the availability of *o*-phenyl substitution sites for adequate positioning of appended functional groups over the porphyrin ring.[2] Typical porphyrins used in self-assembled systems include octaethylporhyrin (H_2OEP), tetraphenylporphyrin (H_2TPP), and tetrakis(2,6-difluorophenyl)porphyrin (H_2F_8TPP), and a large number of copper complexes have been used.

Efforts in the synthesis of Fe^{III}−X−Cu^{II} model complexes include compounds with X = O^{2-},[87,88,92,96,112,198−200] OH^-,[112,201,202] CN^-,[203−207] RC(O)-O^-,[208,209] F^-,[210] Cl^-,[211] S^{2-},[212,213] and imidazolate groups.[214−216] Also, Boitrel and co-workers[217] have recently described a nonbridged Fe^{III}···Cu^{II} complex using a cyclam-strapped porphyrin binucleating ligand, where the Fe···Cu distance is 4.5 Å (as evaluated by EPR and NMR spesctroscopic methods), in the range of the known enzyme structures; this will not be further discussed. The model compounds

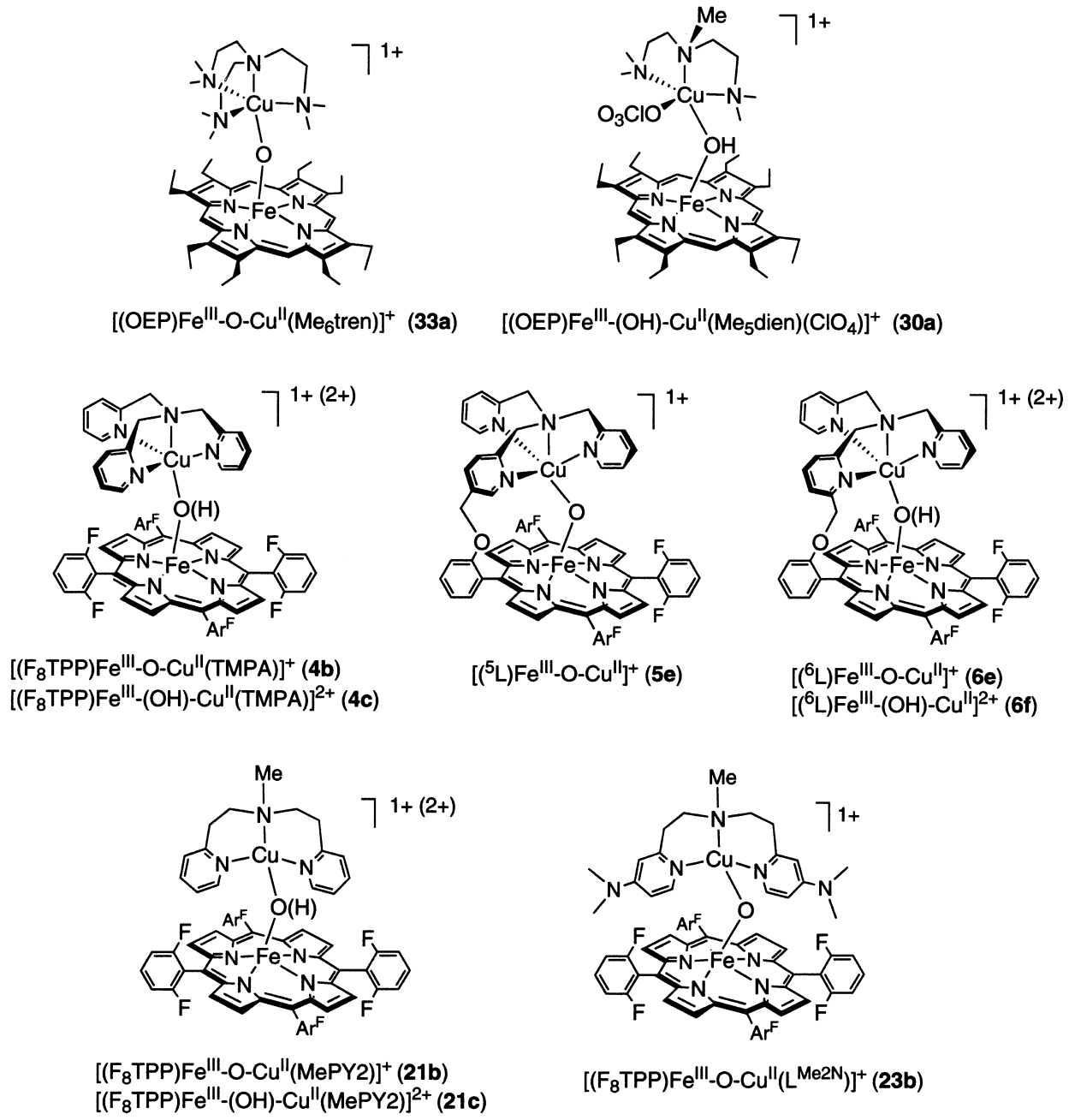

Figure 13. Oxo- and hydroxo-bridged heme–copper oxidase model complexes: **33a**,[199] **30a**,[201] **4b**,[92] **4c**,[202] **5e**,[97] **6e**,[96] **6f**,[97] **21b**,[112] **21c**,[112] **23b**.[87] X-ray structures of **33a**, **30a**, **4b**, **6e**, and **23b** are available. Also, see Table 6.

could represent different states and situations for the enzyme. For example, the Fe^{III}–X–Cu^{II} oxo- and hydroxo-bridged complexes could represent enzyme "resting-state" models or even turnover intermediates following O–O cleavage. Cyanide-bridged compounds may represent species responsible for cyanide poisoning.[204] Aside from the development of basic coordination chemistry of heme–copper complexes as possibly relevant to enzyme structure and spectroscopy, new types of compounds are the outcome of such studies. These may be of interest for their structures, spectroscopy, electronic coupling interactions, and acid–base behavior.

4.2.1. Oxo- and Hydroxo-Bridged Complexes

As discussed, in the past some authors have proposed an oxide ligand as possibly mediating the antiferromagnetic coupling in the heme/copper site for the fully oxidized enzyme.[92,218,219] This proposal was consistent with spectroscopic and magnetization studies on the enzyme and also supported by general knowledge concerning the coupling between metal ions known for μ-oxo dimetal complexes. Furthermore, the X-ray crystal structure of *T. thermophilus* ba_3–C*c*O shows an oxo or hydroxo species between the heme a_3 and Cu$_B$ sites (a water molecule is also possible).[30]

Just in the past decade, a number of oxo- and hydroxo-bridged heme–copper complexes have been synthesized and characterized. The molecular structures are shown in Figure 13; most of them are supported by X-ray diffraction on single crystals. All oxo- and hydroxo-bridged adducts exhibit strong antiferromagnetic coupling between the two metals.

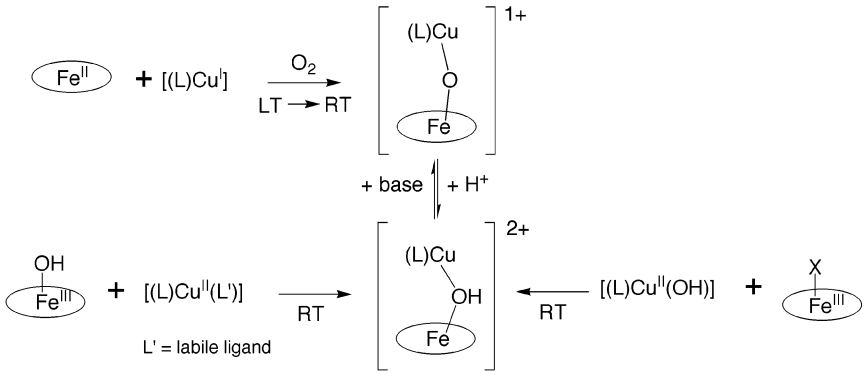

Figure 14. Different synthetic routes to generate μ-oxo and μ-hydroxo heme−copper oxidase models. The ellipse around the iron represents a porphyrin compound. See text for further discussion.

Synthesis. Syntheses of $Fe^{III}-O-Cu^{II}$ and $Fe^{III}-(OH)-Cu^{II}$ adducts following self-assembly strategies or using binucleating ligands have been carried employing four different routes.

(1) Equimolar quantities of Cu^{I} complex and (porphyrinate)Fe^{II} are combined in solution followed by oxygenation at low temperature and subsequent warming to room temperature (Figure 14). Addition of a coprecipitation solvent yields the complex as a solid sample.[92] $[(F_8TPP)Fe-O-Cu(TMPA)]^+$ (**4b**),[92] $[(F_8TPP)Fe-O-Cu(MePY2)]^+$ (**21b**),[112] $[(F_8TPP)Fe-O-Cu(L^{Me2N})]^+$ (**23b**),[87] $[(^6L)Fe-O-Cu]^+$ (**6e**),[96] and $[(^5L)Fe-O-Cu]^+$ (**5e**)[96] were successfully synthesized following this route. For the $(F_8TPP)Fe/Cu(TMPA)$ system, it was proven that a μ-peroxo complex is formed as an intermediate, and this decomposes by disproportionation to the corresponding μ-oxo complex and molecular oxygen.[80] In general, subsequent addition of 1 equiv of acid yields the μ-hydroxo product [i.e., $[(F_8TPP)Fe-(OH)-Cu(TMPA)]^{2+}$ (**4c**),[202] $[(F_8TPP)Fe-(OH)-Cu(MePY2)]^{2+}$ (**21c**),[112] $[(^6L)Fe-(OH)-Cu]^{2+}$ (**6f**)[97]].

(2) Acid−base reaction of a ligand−Cu^{II} complex and $[(P)Fe^{III}-OH]$ yields the μ-hydroxo adduct. In the presence of a base such as triethylamine, the μ-oxo compound is formed [i.e., $[(F_8TPP)Fe-(O/OH)-Cu(MePY2)]^+$ (**21b/21c**),[112] $[(^6L)Fe-O-Cu]^+$ (**6e**),[97] $[(^5L)Fe-O-Cu]^+$ (**5e**)[97]].

(3) Acid−base coupling of an axially labile $[(P)Fe^{III}-X]$ and copper−hydroxo $[LCu^{II}(OH)]$ species produces the μ-hydroxo complex. $[(OEP)Fe-(OH)-Cu(Me_5dien)(OClO_3)]^+$ (**30a**) was prepared by reaction of 2 equiv of $[(OEP)Fe-(OClO_3)]$ (**31a**) with 1 equiv of $[(Me_5dien)Cu(OH)]_2(ClO_4)_2$ (**32a**).[201] If this type of reaction is performed in the presence of a suitable base, the product is a μ-oxo complex; $[(OEP)Fe-O-Cu(Me_6tren)]^+$ (**33a**) was prepared following this route using $[(OEP)Fe-(OClO_3)]$ (**31a**), $[(Me_6tren)Cu(OH)]^+$ (**34a**), and lithium 2,6-di(*tert*butyl)-4-methylphenolate as a base.[199]

(4) There is one mention in the literature of a reaction between a Cu(I) complex and $[(TPP)Fe^{IV}(O^{2-})(py)]$ (**35**) reported to yield a μ-oxo complex (Scheme 15).[198] See discussion below in the present section.

Structural Studies. In general, oxo-bridged bimetallic cores of complexes exhibit near-linear Fe−O−Cu linkages with an Fe···Cu distance of 3.57−3.60 Å (see Table 6). The metal−oxygen distances are typically short for μ-oxo adducts; as one might expect, the $Fe^{III}-O$ distances are ∼0.1 Å less than the $Cu^{II}-O$ bond lengths (Table 6). Comparison of Fe−O−Cu X-ray data with those of the μ-oxo dimers $[(OEP)Fe]_2O$,[220] $[(TPP)Fe]_2O$, and $[(F_8TPP)Fe]_2O$[92] reveals small differences in Fe−O−M angles, Fe−O distances, average Fe−N distances, and $Fe-N_{plane}$ deviations (where $Fe-N_{plane}$ means the distance of the iron atom from the mean plane of the four pyrrole nitrogens). The structures are all consistent with the presence of high-spin Fe(III) porphyrinates.[221] With respect to Cu−O distances, even though there are no X-ray structural data on μ-oxo dimer $Cu^{II}-O-Cu^{II}$ complexes, the Cu−O bond distances are in the range of the values observed for now well-known higher valent bis-μ-oxodicopper(III) complexes [which originate from the reaction of {2(ligand−Cu^{I}) + O_2}, where Cu−O = 1.80−1.86 Å].[7]

Chart 2

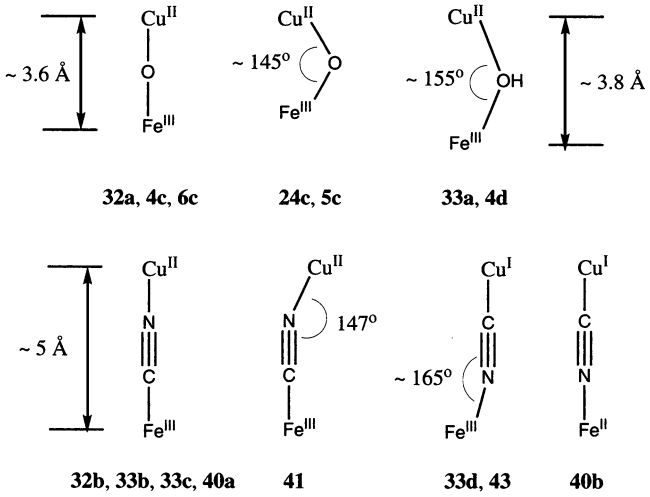

Two exceptions have been reported for the linearity of the Fe−O−Cu moiety (see Chart 2). One of these is a recently reported μ-oxo compound featuring a tridentate ligand for Cu, $[(F_8TPP)Fe-O-Cu(L^{Me2N})]^+$ (**23b**)[87] (see Figure 13). It exhibits an Fe−O−Cu core that is severely bent (143°) and a shorter Fe···Cu distance (3.42 Å) (Table 6). Whereas linear μ-oxo-bridged dimetal compounds in general feature strong magnetic coupling,[25,36] **23b** in any case also possesses this property.[87] The other exception to Fe−O−Cu linearity is exhibited by $[(^5L)Fe^{III}-O-Cu^{II}]^+$ (**5e**),[97] where ^5L is a binucleating ligand that possesses the

Table 6. Core Structural Parameters (Angstroms or Degrees) for Fe^{III}–X–Cu^{II} Complexes (All Are Binuclear Complexes, and Oxidation States Are Fe^{III} and Cu^{II} unless Otherwise Noted)

bridge (X)	compound	Fe···Cu	Fe–X	Cu–Y(X)	Fe–X–Cu	Fe–C–N	Cu–N–C	ref
oxo	[(OEP)Fe–O–Cu(Me_6tren)]$^+$.MeCN (**33a.MeCN**)	3.57	1.75	1.83	175			199
	[(OEP)Fe–O–Cu(Me_6tren)]$^+$.THF (**33a.THF**)	3.58	1.75	1.83	178			199
	[(OEP)Fe–O–Cu(Me_6tren)]$^+$ (**33a**)[a]	3.58	1.74	1.84	180			229
	[(F_8TPP)Fe–O–Cu(TMPA)]$^+$ (**4b**)	3.60	1.74	1.86	178			92
	[(F_8TPP)Fe–O–Cu(TMPA)]$^+$ (**4b**)[a]	3.55	1.72	1.83	176			202
	[(F_8TPP)Fe–O–Cu(L^{Me2N})]$^+$ (**23b**)	3.42	1.75	1.85	143			87
	[(^{6}L)Fe–O–Cu]$^+$ (**6e**)	3.59	1.75	1.85	171			96
	[(^{6}L)Fe–O–Cu]$^+$ (**6e**)[a]	3.58	1.75	1.84	177			97
	[(^{5}L)Fe–O–Cu]$^+$ (**5e**)[a]	3.40	1.77	1.84	141			97
hydroxo	[(OEP)Fe–(OH)–Cu(Me_5dien)(ClO_4)]$^{1+}$ (**30a**)	3.80	1.93	1.95	157			201
	[(OEP)Fe–(OH)–Cu(Me_5dien)(ClO_4)]$^{1+}$ (**30a**)[a]	3.80	1.93	1.99	153			229
	[(F_8TPP)Fe–(OH)–Cu(TMPA)]$^{2+}$ (**4c**)[a]	3.66	1.87	1.89	157			202
cyanide	[(py)(OEP)Fe–CN–Cu(Me_6tren)]$^{2+}$ (**33b**)	4.94	1.92	1.88		179	174	207
	[(py)(OEP)Fe–CN–Cu(Me_5dien)($OCMe_2$)]$^{2+}$(**30c**)	4.98	1.91	1.94		176	173	206
	[(py)(OEP)Fe–CN–Cu(Me_5dien)(OTf)]$^+$(**30b**)	4.98	1.90	1.95		177	170	207
	[(py)(OEP)Fe–CN–Cu(bnpy$_2$)(OTf)]$^+$ (**37a**)	4.94	1.86	2.02		176	163	206
	[(py)(OEP)Fe–CN–Cu(TMPA)]$^{2+}$ (**38a**)	4.96	1.91	1.91		174	175	204
	[(py)(F_8TPP)Fe–CN–Cu(TMPA)]$^{2+}$ (**4d**)		1.90	1.95		175	164	203
	[(py)(OEP)Fe–CN–Cu(TIM)]$^{2+}$ (**39**)	5.02	1.91	2.17		179	147	206
	[(py)(OEP)Fe–CN–Cu(cyclops)]$^+$ (**40**)	5.11	1.92	2.13		179	160	206
	(OEP)Fe–[CN–Cu(Me_6tren)]$_2$ (**33c**) trinuclear complex	4.99	1.94	1.94		173	172	207
	(F_8TPP)Fe–[CN–Cu(TMPA)]$_2$ (**4e**) trinuclear complex	5.03	1.98	1.92		177	175	203
		4.95	1.98	1.89		173	168	
	[{(py)(OEP)Fe–CN}$_2$–Cu(cyclam)]$^{2+}$ (**42**) trinuclear complex	5.15	1.91	2.45		177	140	206
	[(OEP)Fe–NC–Cu^I(Me_5dien)]$^+$ (**30d**)	4.90	2.00	1.86		165	169	206
	[(OEP)Fe–NC–Cu^I(MeNpy$_2$)]$^+$ (**41**)	4.95	2.00	1.87		162	177	204
	[(OEP–CH_2CN)Fe^{II}–NC–Cu^I(TMPA)]$^+$ (**38b**)	5.05	2.03	1.87		176	175	204
carboxylate	[(OEP)Fe–(O_2CH)–Cu(Me_5dien)(ClO_4)]$^+$ (**33e**)	5.86	1.97	1.98				208
	[(OEP)Fe–(OAc)–Cu(Me_5dien)]$^{2+}$ (**33f**)	4.43	1.96	1.94				208
	[(DPA-Por)Zn^{II}–(OAc)–Zn^{II}(Cl)] (**45**)[b]	4.6	2.14	1.99				230
	(OEP)Fe–[(O_2CH)–Cu(Me_6tren)]$_2$ (**33d**) trinuclear complex	5.42	2.10	1.92				208
fluoride	[(OEP)Fe–F–Cu(bnpy$_2$)($OClO_3$)]$^+$ (**39b**)	3.96	1.87	2.10	172			210
	[(OEP)Fe–F–Cu(bnpy$_2$)(MeCN)]$^+$ (**39c**)	4.05	1.86	2.22	166			210
chloride	[(H_2O)(P)Fe–Cl–Cu(N_4)]$^{2+}$ (**1e**)	4.9	2.55	2.41				211
sulfur	[(THF)(TPP)Fe–Cu(mnt)$_2$]– (**47**)	3.94	2.41	2.31	113			213
	[{(*p*-Cl_4TPP)Fe}$_2$–Cu(MNT)$_2$]– (**48**) trinuclear complex	3.83	2.48	2.25	108			231
imidazolate	(TPP)Fe–{Cu(Im)}$_2$ (**52**) trinuclear complex		1.98	1.98				232

[a] Parameters determined by XAS methods. [b] Dizinc(II) complex, (porphyrin)Zn–O, and (non-porphyrin)Zn–O distances are shown in Fe–X and Cu–Y(X) columns, respectively.

TMPA moiety covalently tethered to the periphery of the F_8TPP^{2-} porphyrinate (Figure 13). The Fe–O–Cu unit is severely contorted (141 ± 6°, from EXAFS studies), and the Fe···Cu separation is short (3.40 Å). It is noteworthy that the tethered close structural analogue [(^{6}L)Fe^{III}–O–Cu^{II}]$^+$ (**6e**), which differs only in the position of the porphyrin–TMPA linkage (6-pyridyl instead of 5-pyridyl) (see Figure 13), presents an almost linear Fe–O–Cu moiety.[96,97] This demonstrates that small variations in the ligand architecture can produce significant structural changes.

Comparison between the structural properties of the μ-oxo and μ-hydroxo compounds reveals distinctive trends (see Chart 2). On going from Fe^{III}–O–Cu^{II} to Fe^{III}–(OH)–Cu^{II}, the Fe–O bond distances lengthen considerably, from ∼1.74 to 1.90 Å (these distances are average values from all of the reported structures, see Table 6). The corresponding Cu–O distances also increase from 1.84 to 1.92 Å (average values), and they compare well to several X-ray crystal structures on Cu^{II}–(OH)–Cu^{II} complexes, in which Cu^{II}–OH distances are in the range of 1.85–1.96 Å.[222–227] Also, they compare closely to the value found in the mononuclear complex [Cu(Me_6tren)-(OH)]$^+$ (**34a**) (1.88 Å).[199] The M–O distance increments (comparing μ-oxo and μ-hydroxo adducts) are attributed to a diminution of oxygen atom anionic charge (from 2– to 1–). However, in the case of Fe–O distances, an added dominant contributing feature to bond lengthening is the implicit loss of some O-to-Fe π-bonding, according to the requirements of rehybridization about O [from the implicit "sp" of linear Fe–O–Cu, toward "sp^2" in bent Fe–(OH)–Cu].[202] The detailed nature of bonding and electronic structure in those complexes with highly bent Fe–O–Cu

Table 7. Mössbauer Data Obtained for Some Fe−O−Cu, Fe−(OH)−Cu, and Fe−(O_2CR)−Cu Heme−Copper Oxidase Model Complexes and for Some Enzymes

complex	ΔE_Q, mm/s	δ, mm/s	D_{Fe}, cm^{-1}	ref
$[(F_8TPP)Fe-O-Cu(TMPA)]^+$ (**4b**)	−1.26	0.46	4.5	92
$[(OEP)Fe-O-Cu(Me_6tren)]^+$ (**33a**)	−1.18	0.48	4.1	233
$[(F_8TPP)Fe-(OH)-Cu(TMPA)]^+$ (**4c**)	0.71	0.39		234
$[(OEP)Fe-(OH)-Cu(Me_5dien)(ClO_4)]^+$ (**30a**)	1.05	0.41	13.2	233
beef heart C*c*O	1.0	0.48		184
T. thermophilus C*c*O	1.3	0.41	∼3 (sc), 8 (wc)[a]	185
$[(py)(TPP)Fe-O-Cu(L)]^+$ (**36a**)	2.06	0.23		198
$[(OEP)Fe-(O_2CH)]$ (**31c**)	0.95	0.41	7.6	233
$[(OEP)Fe-(O_2CH)-Cu(Me_5dien)(ClO_4)]^+$ (**30e**)	1.56	0.41	17	233
$[(TPP)Fe-Cu(aib_3)]$ (**44**)	1.04	0.51		209

[a] sc = strong coupling; wc = weak coupling.

moiety, $[(F_8TPP)Fe-O-Cu(L^{Me2N})]^+$ (**23b**) and $[(^5L)-Fe-O-Cu]^+$ (**5e**), yet still possessing very short metal−O bonds, requires future elucidation.

The structural properties of μ-hydroxo compounds compare well with those observed for an enzyme preparation from the quinol oxidase aa_3-600 from *B. subtilis*.[228] A detailed EXAFS and ENDOR investigation of the Cu_B site of the isolated enzyme was carried out by preparing three different samples: (i) by standard procedures, (ii) with precautions to eliminate chloride (to avoid possible contamination), and (iii) at high pH (8.8) where the Fe−Cu magnetic coupling is broken and leads to observable EPR signals from Fe_{a3} and Cu_B. The results supported a Cu_B coordination of three histidines and one O-donor ligand carrying an exchangeable proton or protons such as water or hydroxide. The best fit for the three N(imidazole)/one O(hydroxyl) structure required a Cu−O(hydroxyl) bond distance of 1.90 ± 0.02 Å, closely resembling the Cu−O bond length found for μ-hydroxo model compounds discussed above (see Table 6). In addition, no intense outer-shell scattering is observed in the Fourier transform Cu_B EXAFS, in the same way that it was noted for μ-hydroxo heme−copper complexes.[202,229] However, Fe···Cu distances in these μ-hydroxo compounds (3.7−3.8 Å, Table 6) are short in comparison to the heme a_3···Cu_B distances found in the X-ray crystal structures of oxidized heme−copper oxidases (4.4−4.9 Å, see Table 5). Thus, an OH^- ligand only coordinated to Cu_B rather than bridging the Fe_{a3} and Cu_B is a more plausible formulation for an "as-isolated" structure of this quinol oxidase.

These heme$_{a3}$···Cu_B distances (4.4−4.9 Å) are also significantly longer than those found in the μ-oxo synthetic models (3.4−3.6 Å, Table 6). However, in the crystal structure report of the ba_3−C*c*O from *T. thermophilus*, the authors' proposal was that electron density ascribed to an oxygen atom located between the heme a_3 and Cu_B sites could be a μ-oxo or a μ-hydroxo species (or also a water molecule).[30] However, the oxygen atom is at a distance of 2.3 Å from each of the two metals, which is long to be considered a metal−oxygen coordination bond, certainly for an oxide or hydroxide molecule. Indeed, metal−oxo and metal−hydroxo distances are not longer than 2.0 Å in $Fe^{III}-O(H)-Cu^{II}$ compounds (Table 6). Of course, protein X-ray structure derived metal−ligand bond lengths may be somewhat in error, due to the resolution of the experiment (2.4 Å here). Nevertheless, with the metal−O distance reported, and the more accurate Fe···Cu distances observed (i.e., 4.4 Å, the shortest of any enzyme structure, Table 5), it is clearly not possible for an oxide or hydroxide ligand to bridge with true metal bonding, according to known inorganic (coordination) chemistry.

By EXAFS studies, linear Fe−O−Cu model complexes exhibit strong multiple scattering at both Fe and Cu K-edges, because of the near-linear three-atom arrangement.[202,229] This typical feature has not yet been observed in any EXAFS study made on heme−copper oxidases.

Mössbauer Spectroscopy and Magnetization Studies. Mössbauer spectroscopy has been used to characterize the ground-state electronic structure of Fe−O−Cu and Fe−(OH)−Cu complexes. The data unambiguously indicate that iron is high-spin ferric $S_{Fe} = {}^5/_2$ for all cases, except μ-oxo complex **36a** (see below). Isomer shifts (δ) are higher for μ-oxo than for μ-hydroxo complexes (Table 7), reflecting a more electron-rich bridging ligand for the μ-oxo compounds. The sign of quadrupole splitting (ΔE_Q) for oxo-bridged species is negative, opposite that observed for the hydroxo-bridged species, and the zero-field splitting (D_{Fe}) for $[(OEP)Fe-(OH)-Cu(Me_5dien)(ClO_4)]^+$ (**30a**) is significantly greater than those of μ-oxo compounds. Despite the fact these comparisons are made from only a few compounds (Table 7), it would appear that oxo- and hydroxo-bridged compounds are distinguishable by their Mössbauer data.[233]

As is noted above (section 4.1), Mössbauer spectroscopy has also been applied to the study of the coupled heme a_3−Cu_B site in cytochrome *c* oxidase, and spectral properties similar to that of the reported model complexes were observed. Mössbauer isomer shift (δ) and zero-field splitting (D_{Fe}) parameters for $[(F_8TPP)Fe-O-Cu(TMPA)]^+$ (**4b**), $[(OEP)Fe-O-Cu(Me_6tren)]^+$ (**33a**), and $[(OEP)Fe-(OH)-Cu(Me_5dien)(ClO_4)]^+$ (**30a**) compare well with those observed for the ferric heme a_3 of beef heart[3] and c_1aa_3 *T. thermophilus*[185] heme−copper oxidases (see Table 7). The quadrupole splitting (ΔE_Q) values also compare in an absolute sense, but only the μ-OH^- complexes compare in the positive sign for ΔE_Q (Table 7). For the case of *T. thermophilus*, the coupling between heme a_3 and the Cu_B was found to be antiferromagnetic, and the Mössbauer spectra were satisfactorily simulated using either a weak or a strong coupling

Table 8. Magnetic Moment (μ_{eff}, μ_B) and Coupling Constant (J, cm^{-1}) for μ-Oxo and μ-Hydroxo Model Complexes of Heme–Copper Oxidases

complex	μ_{eff}	$-J$	ref
$[(F_8TPP)Fe-O-Cu(TMPA)]^+$ (**4b**)	5.1	174	92
$[(OEP)Fe-O-Cu(Me_6tren)]^+$ (**33a**)	5.03	≥200	233
$[(F_8TPP)Fe-O-Cu(MePY2)]^+$ (**21b**)	5.15		112
$[(^6L)Fe-O-Cu]^+$ (**6e**)	5.0	>200	97, 234
$[(^5L)Fe-O-Cu]^+$ (**5e**)	4.9		97
$[(F_8TPP)Fe-(OH)-Cu(TMPA)]^{2+}$ (**4c**)	5.5	144	202, 234
$[(F_8TPP)Fe-(OH)-Cu(MePY2)]^{2+}$ (**21c**)	5.6		112
$[(OEP)Fe-(OH)-Cu(Me_5dien)(ClO_4)]^+$ (**30a**)		170	201
$[(py)(TPP)Fe-O-Cu(imidH_2\text{-}DAP)]^+$ (**36a**)	4.23		198

scheme. In the weak coupling scheme ($|J| \sim 1\ cm^{-1}$), the D_{Fe} was determined to be 8 cm^{-1}, whereas a value of ~3 cm^{-1} was found for the strong coupling scheme ($|J| > 10\ cm^{-1}$). Unfortunately, saturation magnetization measurements were not available to determine the strength of the exchange coupling. However, the observed D_{Fe} value for the μ-oxo synthetic model complexes is small and comparable to that determined for the strong coupling situation, indicating that it would be possible for a strongly coupled heme–Cu system to have a small value for D_{Fe}. However, all of these discussions and interpretations remain somewhat unclear, as we have noted above that structural considerations would suggest that μ-oxo bridging in heme–copper oxidase active sites is unlikely.

For most complexes, room temperature magnetic moments have been determined, whereas more detailed variable temperature magnetic studies have been carried out for $[(F_8TPP)Fe-O-Cu(TMPA)]^+$ (**4b**),[92] $[(OEP)Fe-O-Cu(Me_6tren)]^+$ (**33a**),[233] and the hydroxo-bridged $[(OEP)Fe-(OH)-Cu(Me_5dien)(ClO_4)]^+$ (**30a**)[233] (Table 8). The results indicate strong antiferromagnetic coupling between the ferric and cupric sites, yielding an $S = 2$ ground state for all complexes. The magnitude of the exchange coupling found for all solids occurs in the interval of 140 to ≥200 cm^{-1} [based on a Hamiltonian for antiferromagnetic coupling ($-JS_1 \cdot S_2$)] (see Table 8).

Although multifield saturation magnetization studies for the μ-hydroxo complexes $[(F_8TPP)Fe-(OH)-Cu(TMPA)]^{2+}$ (**4c**) and $[(F_8TPP)Fe-(OH)-Cu(MePY2)]^{2+}$ (**21c**) have not been reported, μ_{eff} could be determined by the Evans NMR method, giving values of 5.5 and 5.6 μ_B, respectively.[112,202] Thus, the implicit antiferromagnetic coupling in $[(F_8TPP)Fe-X-Cu(L)]^{+/(2+)}$ seems to be of lesser magnitude for $X = OH^-$ versus $X = O^{2-}$, although both bridging assemblies are considered to be of strong coupling. This conclusion is also supported by a recent variable temperature magnetic study on $[(F_8TPP)Fe-(OH)-Cu(TMPA)]^{2+}$ (**4c**) in which a J value of $-144\ cm^{-1}$ was found.[234]

A different ground-state electronic description has been described for the μ-oxo compound $[(py)(TPP)Fe-O-Cu(L)]^+$ (**36a**), which is synthesized according to the interesting method shown in Scheme 15. Variable temperature magnetic studies and Mössbauer measurements (Table 7) indicate strong antiferromagnetic coupling between Fe^{III} ($S = 3/2$) and

Scheme 15

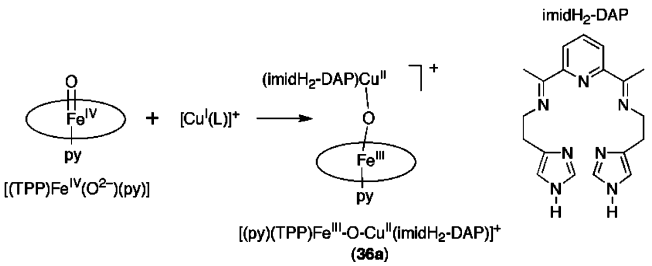

Cu^{II} ($S = 1/2$) to give an $S = 1$ ground state.[198] The complex formulation has not been confirmed by single-crystal X-ray diffraction, but by comparison to all of the other μ-oxo heme–Cu complexes now known, the presence of a pyridine (as axial ligand?) may be making the difference.

NMR Spectroscopy. This is a versatile technique to elucidate the spin and oxidation state of the metal in iron–porphyrinate complexes.[235–237] Pyrrole proton NMR signals are diagnostic in gauging the extent of magnetic interactions because a wide range of chemical shifts are exhibited in accordance with the iron ion's oxidation and spin state.

Low-spin Fe(III) porphyrins generally exhibit a pyrrole signal around −20 ppm [e.g., $[(py)(F_8TPP)Fe^{III}(CN)]$ (**3d**), −19.6 ppm],[203] whereas axially symmetric five-coordinate high-spin Fe(III) porphyrins [e.g., (TPP)Fe–Cl] show a pyrrole signal at ~80 ppm.[238] $[(F_8TPP)Fe-O-Cu(TMPA)]^+$ (**4b**) and $[(F_8TPP)Fe-O-Cu(MePY2)]^+$ (**21b**) exhibit pyrrole signals at 65 and 67.7 ppm, respectively.[236,239] The upfield-shifted signal observed for the μ-oxo compounds with respect to the high-spin Fe(III) porphyrins is consistent with reduction in the net paramagnetism, due to the antiferromagnetic coupling between the high-spin iron(III) ($S = 5/2$) and copper(II) ($S = 1/2$), which yields an $S = 2$ electronic ground state.[236] The possibility of intermediate spin ($S = 3/2$) mixing for Fe(III) (as has been found for $(TPP)Fe-ClO_4$, which has weak axial ligand) is ruled out on the basis of the above-discussed structural parameters, Mössbauer spectroscopy, and magnetization data. The downfield shifting to ~70 ppm observed in the μ-hydroxo complexes $[(F_8TPP)Fe-(OH)-Cu(TMPA)]^{2+}$ (**4c**) and $[(F_8TPP)Fe-(OH)-Cu(MePY2)]^{2+}$ (**21c**) suggests somewhat weaker coupling in these species, in agreement with the magnetic data (vide supra).[236,239]

Although ^1H NMR spectra of mononuclear Cu(II) complexes are typically precluded because of slow electronic relaxation ($\tau_S = 10^{-9}$ s) with consequent broad usually unobservable bands, antiferromagnetic coupling to Fe(III) promotes enhancement of the electron relaxation rate at the Cu(II) site.[236] This results in sharper bands such that the Cu(II) ligand protons become observable. Furthermore, these Cu(II)–ligand protons become upfield-shifted at lower temperatures, owing to the increased population of the $S = 1$ ground state. Thus, the above-mentioned μ-oxo and μ-hydroxo complexes offer excellent examples of heterobinuclear $S = 2$ copper-containing complexes that, due to their inherent strong coupling, illustrate the upfield- and downfield-shifted peak "signature"[240] over an unprecedently large chemical shift range.

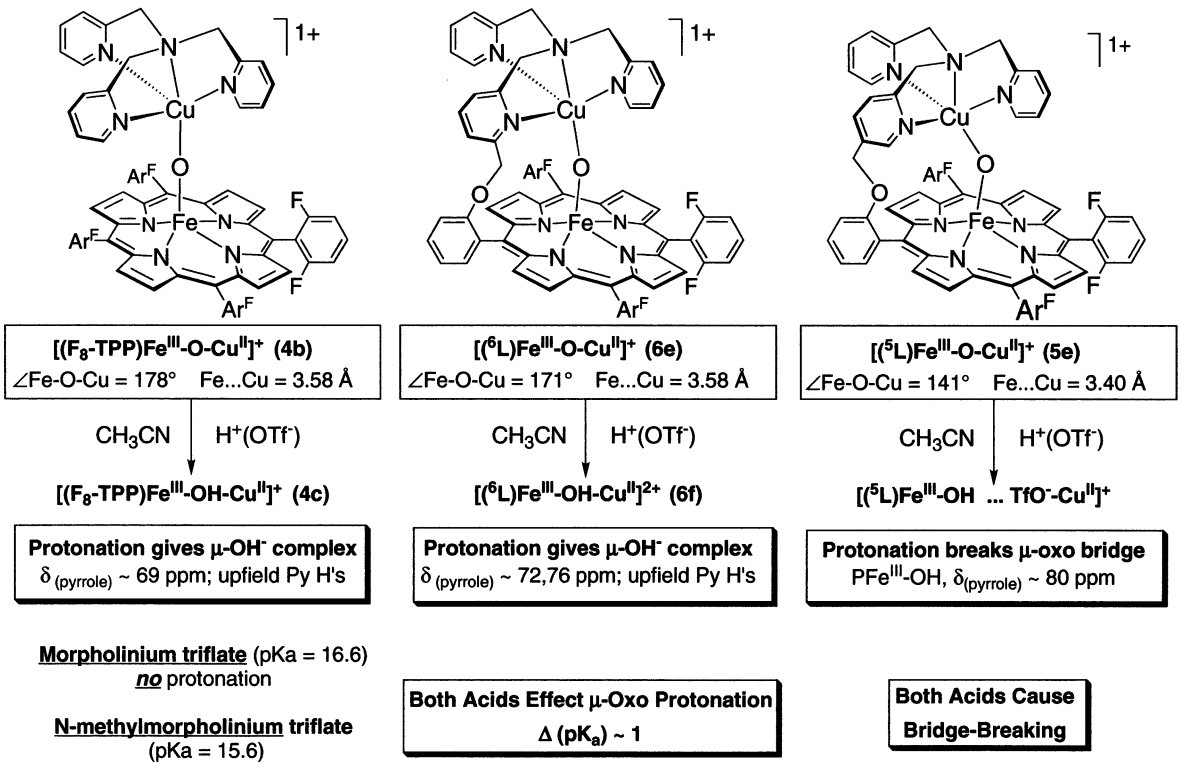

Figure 15. Binucleating ligands influence protonation of $[(L)Fe^{III}-O-Cu^{II}]^{+}$. Complexes $[(F_8TPP)Fe-O-Cu(TMPA)]^{+}$ (**4b**) can be protonated by *N*-methylmorpholinium triflate ($pK_a = 15.6$ in MeCN) but not by morpholinium triflate, giving a μ-hydroxo complex $[(F_8TPP)Fe-(OH)-Cu(TMPA)]^{2+}$ (**4c**).[202] However, both acids protonate $[(^6L)Fe^{III}-O-Cu^{II}]^{+}$ (**6e**) to give $[(^6L)Fe^{III}-(OH)-Cu^{II}]^{2+}$ (**6f**), indicating that **6e** is about 1 pK_a unit more basic than is **4b**. $[(^5L)Fe^{III}-O-Cu^{II}]^{2+}$ (**5e**), with a more bent Fe−O−Cu moiety, appears to be even easier to protonate, but a pK_a value could not be determined because the protonation is irreversible, leading to bridge breaking.[97]

Acid−Base Properties of $Fe^{III}-O(H)-Cu^{II}$ Heme−Copper Complexes. Protonation of μ-oxo iron−copper compounds is of possible importance in heme−copper oxidase function, because protons either are taken up to produce water from O_2 (scalar protons) or are translocated through cell membranes (vectorial protons).[197] Reversible acid−base equilibrium of μ-oxo and μ-hydroxo groups has been proven by ^{1}H NMR and UV−vis titration for the systems $[(F_8TPP)Fe-O(H)-Cu(TMPA)]^{+/(2+)}$ (**4b**/**4c**),[202] $[(^6L)-Fe-O(H)-Cu]^{+/(2+)}$ (**6e**/**6f**),[97] and $[(F_8TPP)Fe-O(H)-Cu(MePY2)]^{+/(2+)}$ (**21b**/**21c**).[112] Titrations with various acids having established acid/base properties in acetonitrile were carried out to determine pK_a values for these μ-hydroxo compounds (see Figure 15). The $Fe^{III}-(OH)-Cu^{II}$ complexes are unstable in water, as they hydrolyze and break, affording mononuclear products, including $(P)Fe^{III}-(OH)$ species. Literature citations[241] suggest that one can estimate an aqueous pK_a, being 7.5 ± 1 pK_a units lower than that in acetonitrile. From this approach, the aqueous $pK_a \sim 8 \pm 2.5$ for $[(F_8TPP)Fe-(OH)-Cu(TMPA)]^{2+}$ (**4c**),[202] $pK_a \sim 9$ for $[(^6L)Fe-(OH)-Cu]^{+}$ (**6f**),[97] and $pK_a \sim 9.6 \pm 2$ for $[(F_8TPP)Fe-(OH)-Cu(MePY2)]^{2+}$ (**21c**)[112] were determined. Thus, from the complementary perspective, the μ-oxo moiety in all of the $Fe^{III}-O-Cu^{II}$ adducts investigated is quite basic, and this finding contrasts with the lower basicity shown for other known μ-oxo Fe, Mn, and Ru complexes.[241−243] This relatively high basicity may be explained by the presence of the copper(II) ion, which is a metal with lower oxidation state and therefore decreased Lewis acidity (in comparison to Fe, Mn, and Ru in those complexes).

The protonation process has been monitored by ^{1}H NMR spectroscopy for $[(F_8TPP)Fe-O-Cu(TMPA)]^{1+}$ (**4b**) and $[(F_8TPP)Fe-O-Cu(MePY2)]^{1+}$ (**21b**), and an interesting phenomenon has been observed. When a μ-oxo adduct solution is titrated with small amounts of acid (<1 equiv), two distinctive sets of resonances (i.e., the pyrrole and/or the *m*- and *p*-phenyl hydrogens) are observed, one set from the μ-oxo compound and the other from its conjugate acid, rather than a single averaged peak.[202,239] This phenomenon is plausible because the exchange process is slow on the NMR scale. Such (relatively) slow protonation reactions, also confirmed in stopped-flow kinetic studies,[244] have also been observed in other oxo-bridged metal ion species, for example, bis(μ-oxo)−dimanganese(III)[245] and (μ-oxo)−diiron(III) complexes, including for $(OEP)Fe^{III}-O-Fe^{III}(OEP)$.[244] Protonation usually results in bending of the previously near-linear M−O−M′ core (see Chart 2). The required rehybridization around the μ-oxo atom to yield a μ-hydroxo product and concomitant structural rearrangement are generally seen to be the causes for the relatively slow proton-transfer reactions.[244]

The demonstration here of slow protonation of μ-oxo heme−O−Cu assemblies possibly could extend to putative protonation of heme−peroxo, heme−hydoperoxo, or heme−O_2(H)−Cu enzyme intermediates. This has been discussed[48,66] in the context of the enzymatic catalytic cycle; slow protonation may provide for the accumulation of certain intermediates

during turnover, allowing coupling of proton translocation chemistry.

4.2.2. Cyanide-Bridged Complexes

The lethal toxicity of cyanide has been traced to rapid and irreversible binding to C*c*O at the binuclear site, at which point it terminates the reduction of dioxygen to water catalyzed by this enzyme.[246] This has led to extensive thermodynamic and kinetic cyanide binding studies.[247−249] It is accepted that cyanide binds very slowly to the oxidized enzyme but rapidly and with high affinity to partially reduced forms. The number of electrons the enzyme must accept before cyanide may bind rapidly and the location of these within the set of redox sites available (Cu_A, cytochrome *a*, Cu_B, and cytochrome a_3) remains, however, under discussion.[250]

The mode of cyanide binding to the binuclear site heme a_3−Cu_B is also under debate.[251] The location of cyanide as a bridge connecting Cu_B and heme a_3 has become more acceptable, based in part on the observation that cyanide converts cytochrome a_3 from the high-spin to the low-spin state and substantially modifies the magnetic coupling to Cu_B.[251] However, proposals including terminal metal binding (heme or Cu_B) also exist.[252,253] Structural propositions have been based largely on the position and intensity of cyanide stretching frequencies ν_{CN} (see discussion below).

Efforts to provide a molecular basis for cyanide toxicity have also come from synthetic chemists devoted to modeling such enzyme−inhibitor complexes. These synthetic efforts and studies, largely due to Holm and co-workers, have afforded a database of bridged structures in which the structural parameters show correlation to the ν_{CN}.[204]

Synthesis. Synthetic model complexes for the heme−Cu cyanide adduct with fully oxidized bridged Fe^{III}−CN−Cu^{II} moiety and for the reduced forms, Fe^{III}−NC−Cu^{I} and Fe^{II}−NC−Cu^{I}, have been synthesized. Examples are shown in Figure 16. Most of these derive following *self-assembly strategies*, and they were derived starting from the iron−cyanide heme complex [(B)(P)Fe^{III}(CN)] (B = py or 1-MeIm) by reaction with the appropriate Cu(I,II) complex.[204,206,207] The iron−cyanide precursor was prepared in all cases from the corresponding μ-oxo dimer $[(P)Fe^{III}]_2O$ and trimethylsilyl cyanide in the presence of base.[254] The formation of the cyanide-bridged adducts proceeds by substitution of a labile ligand (water, acetonitrile, acetone, triflate) from the copper complex, by the free N terminus of the (P)Fe−CN precursor.

There is only one reported Fe^{III}−CN−Cu^{II} complex generated using a *binucleating ligand*, although the molecular structure could not be proven by X-ray crystallography.[205] It consists of a "picket-fence" heme with four nicotinamido groups positioned above the same face (**1d**, Figure 16). The synthesis for this μ-cyanide complex was carried out in the manner described above, with the Fe^{III}−CN moiety formed first, followed by addition of a copper(II) salt.

The use of a mononuclear cyanide−copper(II) complex instead of a cyanide−iron species as a precursor affords highly interesting but not biologically relevant trinuclear species Cu^{II}−NC−Fe^{III}−CN−Cu^{II} (Figure 17).[203,207]

Structural Studies. Largely due to the relatively recent work from the R. H. Holm laboratories, many Fe−(CN)−Cu complexes have been described and their X-ray crystal structures determined. Cyano (M−CN) versus isocyano (M−NC) bonding has been differentiated only by means of X-ray crystal structure refinement. Structural parameters for compounds are provided in Table 6.

In considering linkage isomerism and the metal center oxidation states, three different bridge assemblies are recognized in μ-cyanide heme−copper complexes:[204]

(i) [Fe^{III}−CN−Cu^{II}]. Most complexes belong to this category (Figure 16). In all binuclear complexes, structure refinement indicates that the carbon atom of the cyanide group is iron-bound. The bonding parameters of the heme fragment are consistent only with a low-spin iron(III) configuration.[221] Furthermore, they are essentially congruent with those of the heme fragment precursor [(py)(OEP)Fe^{III}(CN)] (**31b**)[255] (with the exception that in the heme−copper complex, the iron is just out of the porphyrinate plane toward the cyanide ligand, whereas the opposite is true for the iron-only complex).[206]

The cyanide-bridging ligand is bound to copper by the N atom with $Cu-N_{CN}$ distances ranging from 1.88 to 2.17 Å. The Fe−C−N angles are essentially linear throughout; however, Cu−N−C angles vary significantly (175−147°, Chart 2). Hodgson et al. demonstrated that it is possible to differentiate a linear and a bent four-body geometry (Fe−C−N−Cu) by XAS spectroscopy (using GNXAS analysis), due to different multiple-scattering effects.[256] Significantly, there is a trend of decreasing Cu−N−C angle with increasing Cu−NC bond length.[206] In general, there is no large structural change in the Cu^{II}−CN fragments when known mononuclear Cu−CN species are compared with the corresponding Fe^{III}−CN−Cu^{II} complex.[204] The reported cyanide-bridged complexes exhibit a varied stereochemistry on the Cu fragment, from trigonal bipyramidal [e.g., [(py)(OEP)Fe−CN−$Cu(Me_6tren)]^{2+}$ (**33b**)] to distorted square pyramidal [e.g., $[(py)(OEP)Fe-CN-Cu(Me_5dien)(OSO_2CF_3)]^{2+}$ (**30b**)].

(ii) [Fe^{III}−NC−Cu^{I}]. Two complexes featuring this moiety with reduced copper ion have been synthesized: $[(OEP)Fe^{III}-NC-Cu^{I}(Me_5dien)]^+$ (**30d**) and $[(OEP)Fe^{III}-NC-Cu^{I}(MeNpy_2)]^+$ (**41**) (Figure 16).[204] They are composed of a five-coordinate iron−porphyrinate, a nonlinear bridge (see Chart 2), and an irregular Cu(I) fragment. The mean $Fe-N_p$ bond lengths (2.04 and 2.05 Å, respectively) and displacement of the iron atom from the porphyrin mean plane (0.34 and 0.38 Å, respectively)[204,206] are consistent with high-spin iron(III) species.[221] This particular Fe−N−C−Cu linkage isomer is preferable from X-ray refinement;[204] remarkably, cyanide inverts its sequence with respect to the first configuration [i.e., in **(i)**] in which copper presents a 2+ oxidation state.

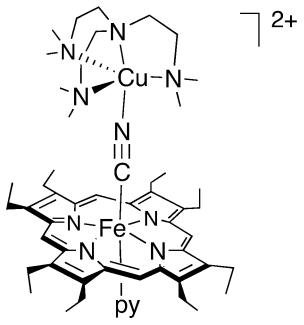

[(py)(OEP)Fe^{III}-CN-Cu^{II}(Me$_6$tren)]$^{2+}$ (**33b**)

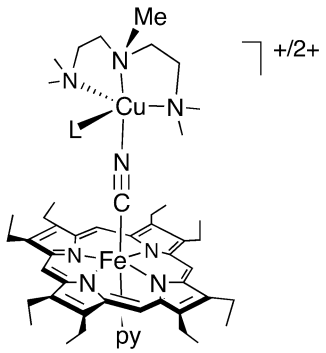

[(py)(OEP)Fe^{III}-CN-Cu^{II}(Me$_5$dien)(L)]$^{n+}$ L = (OSO$_2$CF$_3$)$^{1-}$ (**30b**) L = (Me$_2$CO) (**30c**)

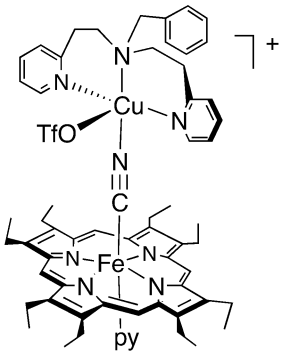

[(py)(OEP)Fe^{III}-CN-Cu^{II}(bnpy$_2$)(OTf)]$^{1+}$ (**37a**)

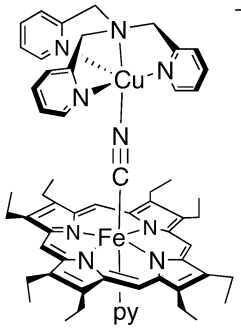

[(py)(OEP)Fe^{III}-CN-Cu^{II}(TMPA)]$^{2+}$ (**38a**)

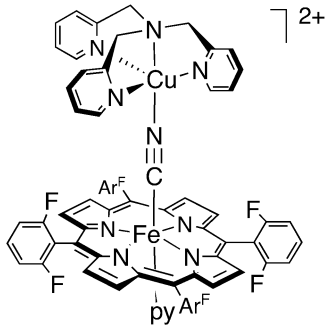

[(py)(F$_8$TPP)Fe^{III}-CN-Cu^{II}(TMPA)]$^{2+}$ (**4d**)

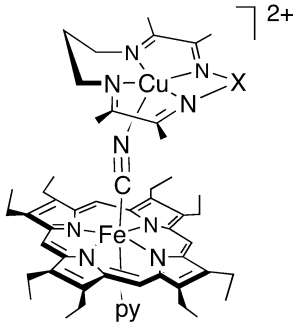

[(py)(OEP)Fe^{III}-CN-Cu^{II}(TIM)]$^{2+}$ X=(CH$_2$)$_3$ (**39**)

[(py)(OEP)Fe^{III}-CN-Cu^{II}(cyclops)]$^{2+}$ X=OBF$_2$O (**40**)

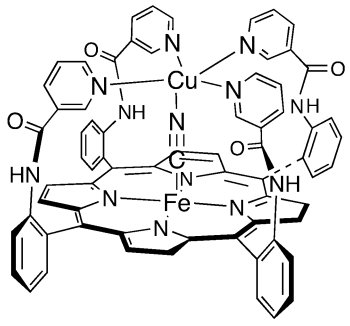

[(P)Fe^{III}-CN-Cu^{II}(N$_4$)]$^{2+}$ (**1d**)

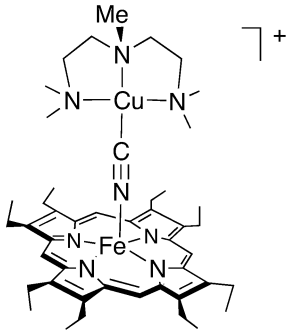

[(OEP)Fe^{III}-NC-Cu^{I}(Me$_5$dien)]$^{+}$ (**30d**)

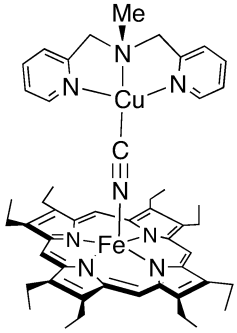

[(py)(OEP)Fe^{III}-NC-Cu^{I}(MeNpy$_2$)]$^{+}$ (**41**)

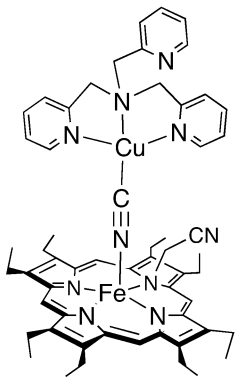

[(OEP-CH$_2$CN)Fe^{II}-NC-Cu^{I}(TMPA)]$^{+}$ (**38b**)

Figure 16. Binuclear cyanide-bridged heme−copper model complexes: **33b**,[207] **30b**,[207] **30c**,[206] **37a**,[206] **38a**,[204] **4d**,[203] **39**,[206] **40**,[206] **1d**,[205] **30d**,[206] **41**,[204] **38b**.[204] All structural formulas are supported by X-ray crystallography with the exception of **1d**.

It is notable that synthesis of these unique complexes starts with a carbon-bound Fe^{III}−CN moiety; thus, the synthesis involves a linkage isomer transformation.

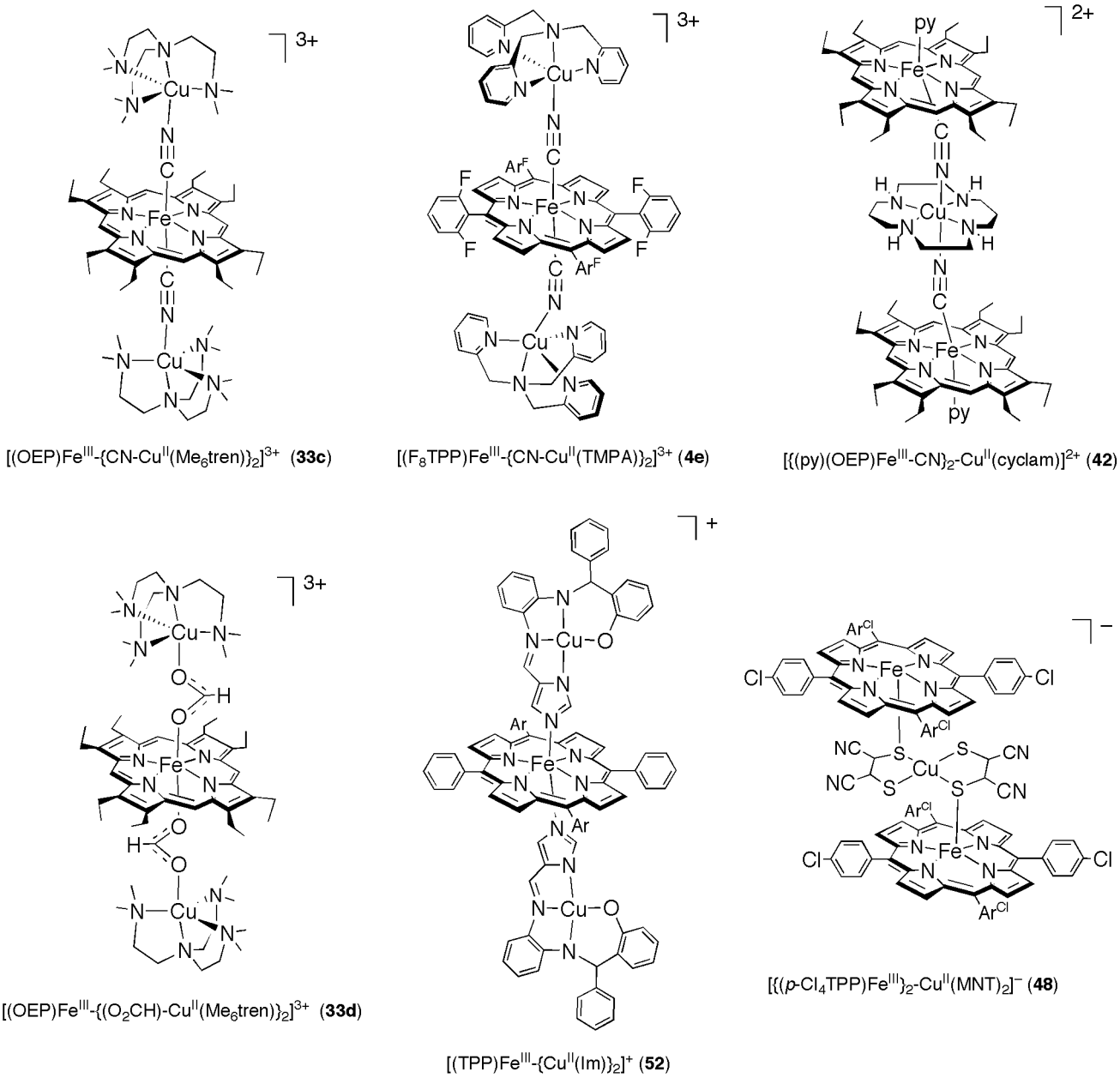

Figure 17. Trinuclear cyanide-, formate-, imidazolate-, and sulfur-bridged heme–copper model complexes: **33c**,[207] **4e**,[203] **42**,[206] **33d**,[208] **52**,[232] **48**.[231] All structural formulas are supported by X-ray crystallography.

(iii) [Fe^{II}–NC–Cu^{I}]. Only one compound has been reported featuring this bridge assembly, [(OEP–CH$_2$-CN)Fe^{II}–NC–Cu^{I}(TMPA)]$^+$ (**38b**) (Holm and co-workers employ the notation Npy$_3$ to refer to the TMPA ligand).[204] The complex contains a five-coordinate N-alkylated iron(II) porphyrinate and an irregular three-coordinate Cu^{I}(TMPA) fragment with one unbound pyridyl group (Figure 16). Here also, the Fe–N–C–Cu atom sequence is the preferred structural assignment, from X-ray refinement. On the basis of the well-known heme stereochemistry structural effects due to metal ion spin-state and radius, the complex is concluded to possess a high-spin porphyrinate–iron(II) fragment.[204]

From the data observed for the large series of model complexes, Holm and co-workers have been able to generalize structural/isomerism relationships. For Fe^{III}–X–Y–Cu, if the angle involving the iron atom is very close to or within the range of 175–180° and the angle involving the copper atom is not, then the bridge is most likely Fe–C–N–Cu. If the converse is true, the bridge is probably Fe–N–C–Cu, a situation that is common for copper(I)–cyanide complexes.[204]

Mössbauer Spectroscopy and Magnetization Studies. The μ-cyanide complex [(py)(OEP)Fe–CN–Cu(Me$_6$tren)]$^{2+}$ (**33b**) (Figure 16) was characterized by Mössbauer spectroscopy.[254] The zero-field spectrum at 4.2 K consists of a doublet with $\Delta E_Q = 1.23(2)$ mm/s (1.07 mm/s at 200 K) and $\delta_{Fe} = 0.22(2)$ mm/s. These data are similar to those of the heme precursor [(py)(OEP)Fe(CN)] (**31b**) (see Table 9). The complex is concluded to possess an *integer* spin, $S = 1$, with μ-cyanide-mediated ferromagnetic coupling between low-spin iron(III) and copper(II). Supporting evidence includes the observation of a quadrupole doublet in applied fields <0.1 T for frozen solutions

Table 9. Mössbauer Data Obtained for Some Fe−(CN)−Cu Complexes and Cyanide−Enzymes

complex	ΔE_Q, mm/s	δ, mm/s	ref
[(py)(OEP)Fe(CN)] (**31b**)	1.33	0.23	254
[(py)(OEP)Fe−CN−Cu(Me_6tren)]$^{2+}$ (**33b**)	1.23	0.22	254
[(P)Fe−CN−Cu(N_4)]$^{2+}$ (**1d**)	1.87	0.24	205
CN−C*c*O from beef heart	1.13	0.26	184
CN−C*c*O from *T. thermophilus*	1.25	0.28	185

as well as polycrystalline samples and compound EPR silence.[254]

The Mössbauer data found for the Gunter/Murray compound [(P)Fe−CN−Cu(N_4)]$^{2+}$ (**1d**), the very first well-characterized (but not by X-ray) heme−cyanide−copper enzyme model complex, are also typical for low-spin Fe^{III}−CN complexes (see Table 9).[205] The bulk magnetic susceptibility, EPR and Mössbauer data were interpreted in terms of a weak ferromagnetic coupling ($J = 0.25$ cm^{-1}).

A comparison of ΔE_Q and δ_{Fe} values for all of these model compounds and the cyanide-treated enzyme derivatives is given in Table 9. The data clearly reveal that these are excellent synthetic models, which very well mimic the cyanide-treated enzymes.

Infrared Spectroscopy. Infrared and Raman spectroscopies are powerful techniques useful in characterizing inorganic complexes, especially those possessing ligands with distinctive vibrational properties. Thus, structural propositions concerning cyanide derivatives of heme−copper oxidases have been based largely on the position and intensity of cyanide stretching (ν_{CN}) and metal−cyanide vibrations ($\nu_{M-(CN)}$ and $\delta_{M-(C-N)}$), in particular for bovine heart C*c*O[253,257−259] and several bacterial ubiquinol oxidases.[258,260,261]

Caughey and Yoshikawa concluded that in oxidized CN−C*c*O, cyanide is coordinated to copper(II) (ν_{CN} = 2151 cm^{-1}) but not as a bridging ligand.[253] The same authors reported that the IR band at 2058 cm^{-1} found for the fully reduced enzyme is due to an Fe_{a3}−CN moiety. In contrast, the feature at 2151 cm^{-1} for the fully oxidized form has been assigned to the Fe^{III}−CN unit whose nitrogen end is perturbed by hydrogen bonding.[259] Kitagawa and co-workers carried out a comparative study on the multiple CN-isotope-sensitive Raman spectra of CN^- adducts of hemoglobin (Hb), myoglobin (Mb), and C*c*O.[257] Thus, they assigned the ν_{Fe-CN} at 478 cm^{-1} (452 cm^{-1} for Hb and Mb) and the ν_{CN} at 2150 cm^{-1} (2122 and 2126 cm^{-1} for Hb and Mb, respectively) for C*c*O. The higher frequencies observed for the oxidase were attributed to the presence of a close-by copper, although they do not propose a cyanide-bridged situation.

The existence of structurally proven Fe−(CN), Cu−(CN), and Fe−(CN)−Cu entities in well-characterized coordination compounds represents important support in assessing the presence or absence of these molecular arrangements in the enzyme. Infrared data are also available for several linear and nonlinear cyanide-bridged model complexes containing the unit Fe^{III}−CN−Cu^{II}. Two examples have been reported for the reduced bridge Fe^{III}−NC−Cu^{I} and only one for a fully reduced Fe^{II}−NC−Cu^{I} species. Table 10 shows ν_{CN} data for free cyanide, copper−cyanide complexes, an iron−cyanide complex, bridged assemblies, and cyanide−oxidases in different oxidation states. These IR data were obtained in solution; small differences compared to solid sample data (not provided in Table 10) indicate that bridged structures of model complexes are maintained in solution.[204]

Oxidized Centers. [(py)(OEP)Fe(CN)] (**31b**) exhibits a ν_{CN} = 2121 cm^{-1}, where the cyanide group is bound to iron(III) through the carbon atom.[204] Ligation of copper(II) to the nitrogen end of cyanide in the linear bridged assemblies [(py)(OEP)Fe−CN−Cu(Me_6tren)]$^{2+}$ (**33b**) and [(py)(OEP)Fe−CN−Cu(TMPA)]$^{2+}$ (**38a**) raises ν_{CN} by ∼50−60 cm^{-1} (see Table 10). This increase is attributed to electron donation

Table 10. Cyanide Stretching Frequencies Found in Cyanide Oxidases and in Model Complexes (All IR Data Are in Solution unless Otherwise Noted)

group/bridge	compound/enzyme	ν_{CN}, cm^{-1}	ref
CN^-	NaCN	2080	263
Cu^{I}−CN	[Cu(HB(Me_2pz)$_3$(CN)] (**43**)	2077	204
Cu^{II}−CN	[Cu(TMPA)(CN)]$^+$ (**2c**)	2142	204
Fe^{III}−CN	[(py)(OEP)Fe(CN)] (**31b**)	2121	204
Fe^{III}−CN−Cu^{II}	[(py)(OEP)Fe−CN−Cu(Me_6tren)]$^{2+}$ (**33b**)	2179	204
	[(py)(OEP)Fe−CN−Cu(TMPA)]$^{2+}$(**38a**)	2172	204
	[(py)(OEP)Fe−CN−Cu(bnpy$_2$)(OTf)]$^+$(**37a**)	2164	206
	[(py)(OEP)Fe−CN−Cu(cyclops)]$^+$(**40**)	2153	206
	[(py)(OEP)Fe−CN−Cu(TIM)]$^{2+}$(**39**)	2143	206
	[(P)Fe−CN−Cu(N_4)]$^{2+}$(**1d**)	2143	205
Fe^{III}−NC−Cu^{I}	[(OEP)Fe−NC−Cu^{I}(Me_5dien)]$^+$ (**30d**)	2082	204
	[(OEP)Fe−NC−Cu^{I}(MeNpy$_2$)]$^+$(**41**)	2080	204
Fe^{II}−NC−Cu^{I}	[(OEP−CH_2CN)Fe^{II}−NC−Cu^{I}(TMPA)]$^+$(**38b**)	2107	204
fully oxidized	C*c*O (bovine heart)	2150−2152	252, 253, 257
	Cyt. *bo* (*E. coli*)	2146	260
	Cyt. a_1 (*A. aceti*)	2147, 2146	262
partially reduced	C*c*O (bovine heart)	2131, 2093	252, 253
fully reduced	C*c*O (bovine heart)	2058, 2045, 2037	252
	cyt. *bo* (*E. coli*)	2035	261
	cyt. a_1 (*A. aceti*)	2051	262

from the filled $5\sigma^*$ molecular orbital of cyanide to copper and kinematic coupling.[204] These elevated ν_{CN} model compound values are rather different from those reported for the fully oxidized enzymes, 2146–2152 cm^{-1} (see Table 10).[252,253,257,260,262] However, when the Cu–N–C angle decreases to near 150° for certain copper–ligand situations, the Cu–N bond length increases and ν_{CN} decreases (Tables 6 and 10). This situation can be explained in terms of the electronic structures **A** and **B**, shown below. As the

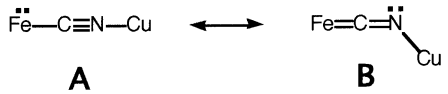

Cu–N–C angle decreases and the bridge deviates from linearity in **A**, the cyanide triple bonding diminishes as the contribution from **B** increases in the presence of a π-donor atom such as low-spin iron(III). Consequently, the ν_{CN} values are lower for the nonlinear assemblies [e.g. [(py)(OEP)Fe–CN–Cu(cyclops)]$^+$ (**40**) and [(py)(OEP)Fe–CN–Cu(TIM)]$^{2+}$ (**39**)], closely approaching the values found for the fully oxidized enzymes (see Table 10).[204]

The low-spin ferriheme–(CN)–Cu complex reported by Murray and co-workers, [(P)Fe–CN–Cu(N_4)]$^{2+}$(**1d**), has ν_{CN} = 2143 cm^{-1} (in MeOH–$CHCl_3$ solution),[205] also in close agreement with the fully oxidized enzyme results (Table 10). Without an X-ray structure, it is hard to conclude whether this complex has a linear or bent [at the copper(II)] Fe–C–N–Cu unit. The "picket-fence" ligand architecture might suggest a linear arrangement is likely, but perhaps one of the pyridine donors (Figure 16) does not ligate and allows a bent μ-cyanide configuration. The more compelling data would seem to come from the data discussed for [(py)(OEP)Fe–CN–Cu(cyclops)]$^+$ (**40**) and [(py)(OEP)Fe–CN–Cu(TIM)]$^{2+}$ (**39**) (vide infra), and because all three complexes (**1d**, **39**, and **40**) closely match the enzyme data in ν_{CN} values (Table 10), a bent μ-cyanide heme–Cu moiety seems to be quite plausible for the enzyme.

Reduced Centers. In Fe^{III}–NC–Cu^I assemblies in model compounds (**30d** and **41**, Figure 16), the bridge has isomerized upon coordination to copper(I) resulting in Cu–C rather than Fe–C binding and ν_{CN} frequencies ~40 cm^{-1} lower than that of [(py)(OEP)Fe(CN)] (**31b**) and ~90 cm^{-1} below those of fully oxidized Fe^{III}–CN–Cu^{II} (see Table 10). Also, the observed values are very close to that of the Cu^I–CN complex [Cu(HB(Me_2pz)$_3$(CN)]$^-$ (**43**). These facts strongly suggest that electron donation from copper(I) to the vacant $2\pi^*$ molecular orbital of cyanide dominates in this type of assembly and that kinematic coupling and the presence of iron(III) at the nitrogen end are minor factors in determining C–N stretching frequencies.[204]

Fully Reduced Complex. With the assistance of only one compound (**38b**), it is difficult to determine the effect of the oxidation state of iron (III vs II) on ν_{CN} in Cu(I) bridged, in comparison to model complexes containing an Fe^{III}–NC–Cu^I versus an Fe^{II}–NC–Cu^I moiety. Nevertheless, the higher stretching frequency observed for [(OEP–CH_2CN)Fe^{II}–NC–Cu^I(TMPA)]$^+$ (**38b**) is consistent with more linear arrangement (175–176°) (see structures **A** and **B** above).[204]

Thus, bridges containing the Cu^I–CN fragment are clearly distinguishable from those with Cu^{II}–NC. However, the two types of bridges [i.e., iron(III) vs iron(II)] containing copper(I) are not necessarily distinguishable by IR spectroscopy.

NMR Spectroscopy. NMR spectroscopy is also (see section 4.2.1) useful in the characterization of cyanide-containing heme or heme–copper complexes. A precursor in the synthesis of copper–(μ-CN)–iron complexes, [(py)(F_8TPP)Fe^{III}(CN)] (**3d**), exhibits a pyrrole resonance at −19.6 ppm,[203] which is typical for a low-spin iron(III) situation.[238] After reaction with [Cu^{II}(TMPA)(CH_3CN)]$^{2+}$ (**2b**) and formation of [(py)(F_8TPP)Fe–CN–Cu(TMPA)]$^{2+}$ (**4d**), the pyrrole resonance moves downfield to −11.1 ppm. This shift is consistent with a low-spin Fe^{III} ($S = {}^1/_2$) ferromagnetically coupled to a Cu^{II} ($S = {}^1/_2$), giving rise to an $S = 1$ ground-state spin system. This characterization is also supported by the room temperature magnetic moment, $\mu_{eff} = 2.7\ \mu_B$.[203]

In a phenomenon similar to that observed for antiferromagnetically coupled copper(II)–iron(III) systems (see section 4.2.1), ferromagnetic coupling in copper(II)–(μ-CN)–iron(III) complexes enhances the electronic relaxation time of copper(II). Thus, it becomes possible to see sharper protons signals in [(py)(F_8TPP)Fe–CN–Cu(TMPA)]$^{2+}$ (**4d**), for copper(II) ligand hydrogens, relative to the mononuclear complex [Cu^{II}(TMPA)(CN)]$^+$ (**2c**).[203]

4.2.3. Carboxylate-Bridged Complexes

Exogenous ligands such as formate [HC(O)O^-], cyanide, carbon monoxide, nitrogen monoxide (NO), and azide have been used as probes of the binuclear site of the heme–copper oxidases. Among those, formate binding has been extensively studied and shows a distinctive property.[181,189,264,265] Incubation of the *fast* preparation of the enzyme (see discussion about *fast* and *slow* forms in section 4.1) with formate in alkaline medium produces a form of the enzyme virtually indistinguishable in kinetics and spectroscopic properties from the *slow* preparation.[51,266] The behavior has not been fully explained but has provoked important discussions. Explanations from perturbations in protein tertiary structure to specific binding of formate at the binuclear site have been put forward.[208] Furthermore, it has been suggested that endogenous carboxylate (i.e., amino acid residue derived) might bridge heme a_3 and Cu_B, as the enzyme formate derivative possesses physical properties similar to those of the *slow* form.[265,267,268] Thus, the structural and spectroscopic characterization of formate or carboxylate adducts of oxidized heme–Cu coordination complexes is of interest.

Synthesis. As in the synthesis of Fe^{III}–O(H)–Cu^{II} (see section 4.2.1) and Fe^{III}–(CN)–Cu^{II} (see section 4.2.2) compounds, condensation of an iron(III) porphyrin and a copper(II) complex, one carrying the bridging species and the other a labile ligand, proved to be successful. For instance, [Fe^{III}(OEP)($OClO_3$)] (**31a**) was used as a heme precursor and copper(II)

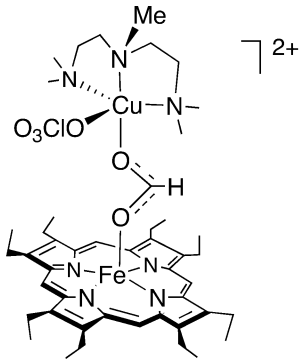

$[(OEP)Fe^{III}\text{-}(O_2CH)\text{-}Cu^{II}(Me_5dien)(OClO_3)]^{2+}$

(**33e**) (*anti–anti*)

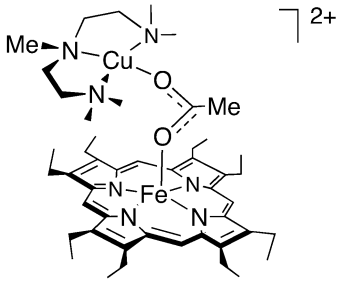

$[(OEP)Fe^{III}\text{-}(OAc)\text{-}Cu^{II}(Me_5dien)]^{2+}$

(**33f**) (*syn–anti*)

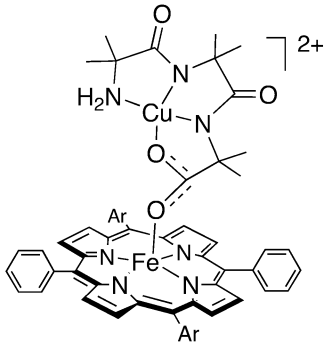

$[(TPP)Fe^{III}/Cu^{II}(aib_3)]$ (**44**)

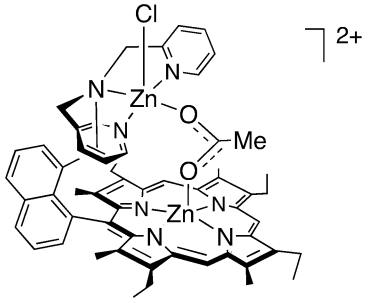

$[(DPA\text{-}Por)Zn^{II}\text{-}(OAc)\text{-}Zn^{II}(Cl)]$

(**45**) (*syn–anti*)

Figure 18. Carboxylate-bridged heme−copper model complexes: **33e**,[208] **33f**,[208] **44**,[209] **45**.[230] Under the formulas are indicated the bridge modalities. See below for further explanation.

complexes [i.e., $[(Me_5dien)Cu^{II}(carboxylate)](ClO_4)$] carried the eventual bridging carboxylate ligands (formate and acetate). Complexes $[(OEP)Fe^{III}-(O_2CH)-Cu^{II}(Me_5dien)(OClO_3)]^+$ (**33e**) and $[(OEP)Fe^{III}-(OAc)-Cu^{II}(Me_5dien)]^{2+}$ (**33f**) (Figure 18) were successfully prepared in this manner. Such syntheses of μ-carboxylate adducts proceeds only in low yields, as different subproducts are generally formed, for example $[Fe^{III}(OEP)(O_2C-R)]$ ($R = -H, -CH_3$) and $Fe^{III}-(OH)-Cu^{II}$ species. However, the desired μ-carboxylate compounds could be isolated as pure samples by multiple recrystallization.[208]

Another binuclear compound that appears to contain a μ-carboxylate bridge between a heme and a copper(II) complex is $[(TPP)Fe^{III}-Cu^{II}(aib_3)]$ (**44**) (Figure 18).[209] It was prepared by addition of 1 equiv of $Cu^{III}(aib_3)$ (aib_3 = tripeptide of α-aminoisobutyric acid) to a THF solution of $Fe^{II}(TPP)$. However, it could not be isolated as a solid because of the thermal, photochemical, and oxygen instability.[209] Following a *binucleating* ligand strategy, a μ-acetate complex bridging two zinc(II) ions was synthesized to structurally model the C*c*O active site.[230] The complex, $[(DPA\text{-}Por)Zn^{II}-(OAc)-Zn^{II}(Cl)]$ (**45**) (Figure 18) was characterized by ^1H NMR and single-crystal X-ray diffraction.[230]

An interesting trinuclear assembly, $Cu^{II}-(O_2CH)-Fe^{III}-(O_2CH)-Cu^{II}$, was generated by equimolar (or 1:2 molar ratio) reaction of $[(OEP)Fe^{III}(O_2CH)]$ (**31c**) and $[Cu^{II}(Me_6tren)(O_2CH)]^+$ (**34b**)[208] and closely resembles the trinuclear cyanide-bridged analogues reviewed in section 4.2.2 (Figure 17).

Structural Studies. Carboxylates act as mono- and bidentate terminal ligands and can assume the four bridging modes depicted below.[208,269] Struc-

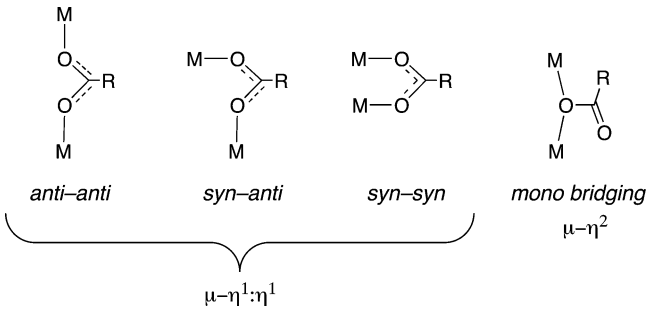

tural features of the copper and iron fragments in $[(OEP)Fe^{III}-(O_2CH)-Cu^{II}(Me_5dien)(OClO_3)]^+$ (**33e**) and $[(OEP)Fe^{III}-(OAc)-Cu^{II}(Me_5dien)]^{2+}$ (**33f**) do not significantly vary in comparison to the relevant mononuclear precursor or analogue. In both cases, iron(III) exhibits high-spin configuration.[208]

$[(OEP)Fe^{III}-(O_2CH)-Cu^{II}(Me_5dien)(OClO_3)]^+$ (**33e**) exhibits an *anti-anti* bridge configuration, which explains the long Fe···Cu distance of 5.86 Å (see Table 6). The same structure is observed in the formate-bridged polymeric species $[Mn(TPP)(O_2-$

CH)]$_n$.[270] In contrast, the related heme−copper binuclear μ-carboxylate complex [(OEP)Fe^{III}−(OAc)−Cu^{II}(Me$_5$dien)]$^{2+}$ (**33f**) and the dizinc(II) complex **45** exhibit a *syn-anti* acetate-bridging coordination. Thus, the M···M separation is considerably reduced (4.43 Å for **33f** and ∼4.6 Å for **45**) compared to that in **33e**.

A number of researchers have suggested that a formate (or endogenous carboxylate) can or does bridge the heme a_3 and Cu$_B$ enzyme binuclear center.[265,267,268] In light of data on the relevant coordination complexes (vide supra), it might be reasonable to expect that formate could be positioned in an enzyme *syn-anti* configuration. This affirmation is based on the Fe···Cu distance found in **33f** and **45**, which compares well with the distances found in the oxidized forms of the oxidase for bovine heart and for bacterial derivatives (Fe···Cu = 4.4−4.9 Å, see section 4.1). The *anti-anti*-configured complex [(OEP)-Fe^{III}−(O$_2$CH)−Cu^{II}(Me$_5$dien)(OClO$_3$)]$^+$ (**33e**) places the two metal centers ∼1 Å farther apart than the separation found for the oxidized mammalian enzyme (4.9 Å), the longest metal−metal separation yet observed (see Table 5). In conclusion, if formate or an endogenous carboxylate bridges the heme−copper oxidase binuclear center metal ions, model compound studies suggest it would do so in the *syn-anti* configuration. In light of the now known X-ray structures and knowledge of the identity of amino acid residues near the heme−Cu active site, a protein-derived carboxylate is an unlikely possibility. Also see the discussion on Mössbauer spectroscopy and magnetization studies below.

Mössbauer Spectroscopy and Magnetization Studies. Mössbauer spectroscopy and magnetization measurements were performed to elucidate the ground-state electronic structure of the carboxylate-bridged assemblies [(OEP)Fe^{III}−(O$_2$CH)−Cu^{II}(Me$_5$-dien)(OClO$_3$)]$^+$ (**33e**)[233] and [(TPP)Fe^{III}−Cu^{II}(aib$_3$)] (**44**).[209] Unfortunately, [(OEP)Fe^{III}−(OAc)−Cu^{II}(Me$_5$-dien)]$^{2+}$ (**33f**), which better represents a hypothetical carboxylate-bridged situation in C*c*O due to its *syn-anti* bridge mode, was not studied by these techniques. Data obtained for the carboxylate-bridged complexes together with those of the mononuclear species [(OEP)Fe^{III}−(O$_2$CH)] (**31c**) are provided in Table 7. Isomer shift and quadrupole splitting values of all three complexes are in the range observed for five-coordinate high-spin porphyrinate−iron(III) compounds.[271]

The large difference in magnitude for the antiferromagnetic exchange coupling observed for [(OEP)-Fe^{III}−(O$_2$CH)−Cu^{II}(Me$_5$dien)(OClO$_3$)]$^+$ (**33e**) (*anti-anti* conformation, $J = 18$ cm^{-1})[233] and μ-oxo(hydroxo) compounds ($J \geq 140$ cm^{-1}, see section 4.2.1) is noteworthy. Furthermore, it was concluded from the solution magnetic moment (5.5 ± 0.2 μ_B, Evans method) and EPR and Mössbauer spectroscopic data that [(TPP)Fe^{III}−Cu^{II}(aib$_3$)] (**44**) also exhibits a weak heme−copper antiferromagnetic coupling.[209] However, the magnetic moment seems to be too low to be considered as weak coupling. Nevertheless, the μ-carboxylate group appears to be a less effective propagator of exchange coupling than μ-oxo or μ-hydroxo groups in heme−Cu assemblies; this would be expected given the increased number of atoms bridging the paramagnetic metal ion centers. One would expect that the exchange interaction depends to some extent on the bridge conformation (*syn-syn*, *syn-anti*, *anti-anti*). However, the observed J value for [(OEP)-Fe^{III}−(O$_2$CH)−Cu^{II}(Me$_5$dien)(OClO$_3$)]$^+$ (**33e**) is ∼1 order of magnitude smaller in comparison with μ-oxo and μ-hydroxo complexes. Thus, one can make the general conclusion that heme−copper μ-carboxylate electronic interactions are weak.

Interesting observations are made when the physical properties of oxidized formate-bound and *slow* forms of the enzyme are compared with those of [(OEP)Fe^{III}−(O$_2$CH)−Cu^{II}(Me$_5$dien)(OClO$_3$)]$^+$ (**33e**). First, Day et al.[187] have reported a negative zero-field splitting ($D_{Fe} = -7$ cm^{-1}) for the *slow* form of bovine heart C*c*O. In contrast, the Mössbauer studies on **33e** show an unusually large value for the zero-field splitting ($D_{Fe} = 17$ cm^{-1}).[233] Second, oxidized formate-bound bovine heart C*c*O and *E. coli* cytochrome *bo*$_3$ yield EPR signals,[189,272] whereas Münck and co-workers have reported failing to observe any EPR signal at X-band frequencies in either the parallel or perpendicular mode for the μ-carboxylate model compound **33e**.[233] Third, Dye and co-workers[183] reported a J value >200 cm^{-1} for the formate-bound bovine heart C*c*O, which contrasts with the small value found in the model complex (*anti-anti* conformation, $J = 18$ cm^{-1}). With these data, it is most unlikely that the formate-bound enzyme as well as the *slow* form of the enzyme contains a carboxylate group (endogenous carboxylate for the *slow* form) bridging the heme a_3 and Cu$_B$ sites through a μ-η^1:η^1 conformation (see diagram above). However, the possibility of a formate or endogenous carboxylate bridging the metal centers by μ-η^2 mode (utilizing a single oxygen atom, diagram) could be considered. Perhaps such a moiety would exhibit strong coupling between heme and copper metal centers, because it has only one atom between metal ions, but there are no models (i.e., well-characterized coordination complexes) to corroborate such a conclusion.

4.2.4. Other X-Bridged Complexes

In sections 4.2.1−4.2.3 we examined μ-oxo and μ-hydroxo complexes as possible candidates of the oxidized form of the enzyme, μ-cyanide complexes as mimetic compounds of the cyanide-inhibited form of the enzyme, and μ-carboxylate as a possible representative of the slow form. Other ions such as Cl$^-$, F$^-$, S^{2-}, and N^{3-} may bridge the heme a_3 and Cu$_B$ site in determined situations such as after certain isolation procedures[196] or after the addition of exogenous ligands to the enzymatic preparation. On the other hand, histidine imidazolate and cysteine thiolate had emerged as a heme/Cu$_B$ bridge candidate in the 1970s and 1980s,[273] stimulating the bioinorganic community on the preparation of such model compounds. However, this hypothesis lost consensus in the past decade, in light of the X-ray structures determined for the fully oxidized enzyme. Here we review reported model complexes that exhibit these other bridge entities, as they often reflect intense synthetic efforts and the molecules obtained and

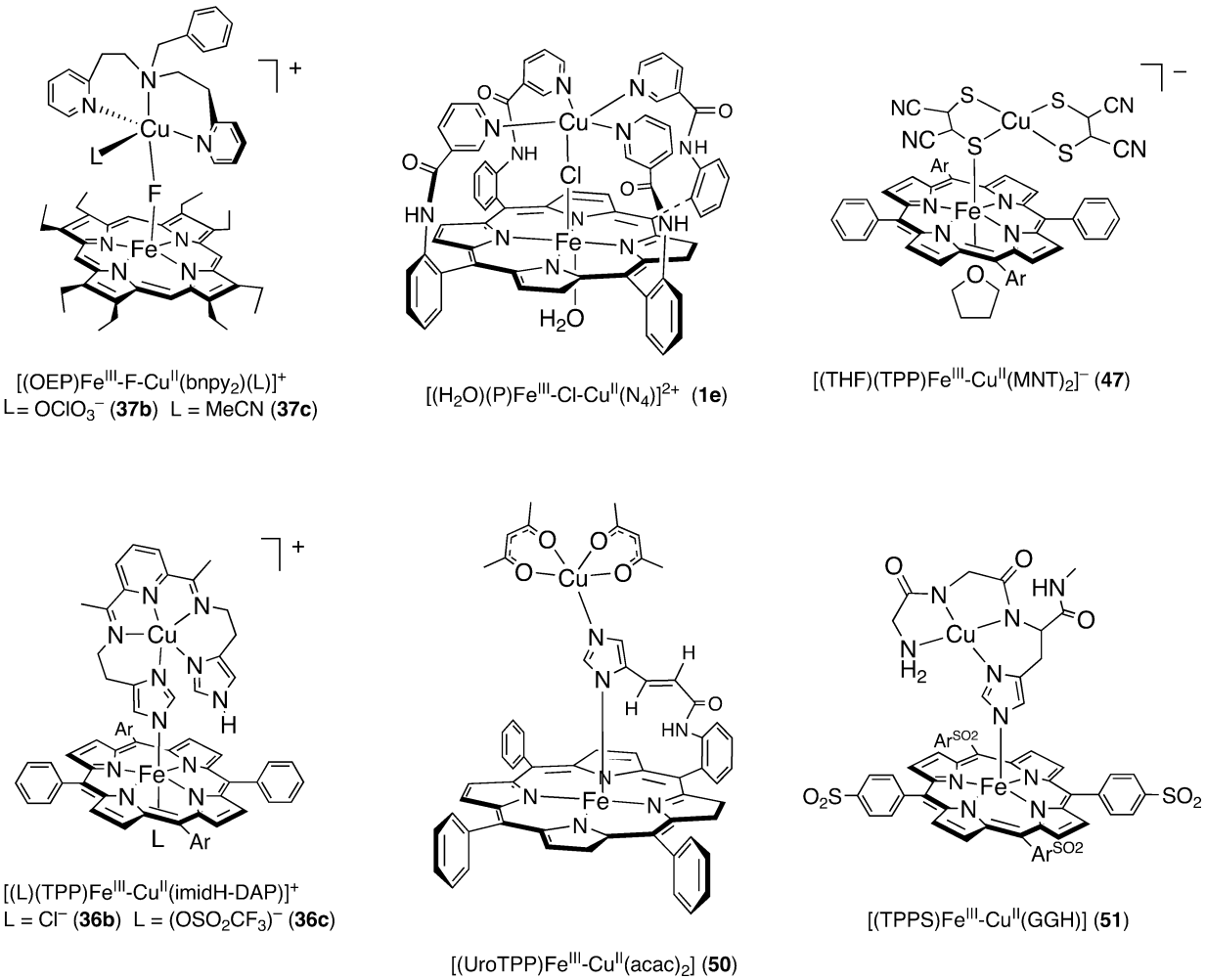

Figure 19. Binuclear fluoride-, chloride-, sulfur-, and imidazolate-bridged heme−copper model complexes: **37b**,[210] **37c**,[210] **1e**,[211] **47**,[213] **36b**,[214] **36c**,[214] **50**,[215] **51**.[216] Structural formulations for **37b**, **37c**, **1e**, and **47** are supported by X-ray diffraction.

characterized are novel heterobinuclear species with interesting electronic or structural features.

Fluoride-Bridged Complexes. There are two μ-fluoride heme−copper compounds reported in the literature, from Holm and co-workers. These are [(OEP)Fe^{III}−F−Cu^{II}($bnpy_2$)($OClO_3$)]$^+$ (**37b**) and [(OEP)-Fe^{III}−F−Cu^{II}($bnpy_2$)(MeCN)]$^+$ (**37c**) (Figure 19).[210] Both complexes were synthesized by reaction of (OEP)Fe^{III}($OClO_3$) (**31a**) and the fluoride-bridged complex [$Cu^{II}_2F_2(bnpy_2)_2$]$^{2+}$ (**46**), with the only difference of the solvent used for the synthesis; the first was prepared in acetone, whereas the second one was prepared in acetonitrile. X-ray structures were determined for both complexes. The two are similar and contain high-spin five-coordinate iron(III) porphyrinate moieties. The Fe^{III}−F−Cu^{II} bridges are slightly bent, 172° for **37b** and 166° for **37c**, and the Fe···Cu distances are 3.96 and 4.05 Å, respectively (see Table 6). These structural parameters resemble those observed for the μ-hydroxo compound [(OEP)Fe^{III}−(OH)−Cu^{II}(Me_5dien)($OClO_3$)]$^+$ (**30a**) [X-ray: Fe^{III}−(OH)−Cu^{II}, 157°, Fe···Cu, 3.80 Å].[201] However, the authors ruled out the possibility of a misidentification, that is, having a hydroxo ion as the bridge ligand (instead of fluoride), following in-depth testing of the oxygen atom in X-ray refinement procedures.

Compounds **37b** and **37c** exhibit a weak magnetic coupling through the fluoride bridge,[210] in contrast with the strong antiferromagnetic interaction observed for μ-oxo and μ-hydroxo heme−copper compounds (see section 4.2.1).

Chloride-Bridged Complexes. Reaction of (P)-Fe^{III}−Cl [P = *meso*-αααα-tetra(*o*-nicotinamidophenyl)porphyrinate] with 1 equiv of copper(II) perchlorate yields the μ-chloride compound [(H_2O)(P)Fe^{III}−Cl−Cu^{II}(N_4)]$^{2+}$ (**1e**) (Note: P and N_4 represent the coordinate sites of a *binucleating* ligand).[211] The X-ray structure was determined, although crystal quality prevented a high-resolution structure. The iron atom is octahedrally coordinated, with a water molecule in the sixth coordination site [Fe−O = 2.081(13) Å]. Considering the Fe−N_p distances [2.01 (7) Å] and magnetic studies, the electronic situation for the iron(III) seems to be that for a high-spin state. However, the possibility of an admixed ($S = {}^3/_2, {}^5/_2$) spin state is not ruled out. Note that in the pre-X-ray structure protein EXAFS studies, where a chloride was proposed as a bridging ligand, the data were interpreted to give an iron···copper distance of 3.7−4.0 Å,[191−193] much shorter than the ∼4.9 Å observed here for **1e** (see Table 6).

As it is observed for fluoride (vide supra), chloride ion produces a weak exchange coupling between an iron(III)−porphyrinate and a copper(II) complex. This fact is supported by the active EPR spectrum observed for **1e**, which exhibits typical signals for high-

spin iron(III)−porphyrinate ($g \sim 6$) and for copper(II) ($g \sim 2$). However, the magnetic behavior was unusual and could not be interpreted in terms of the usual $-2JS_1 \cdot S_2$ exchange-coupled Hamiltonian. Mössbauer and variable temperature magnetic studies indicated an iron(III) in some form of $S = {}^5/_2$ and $S = {}^3/_2$ spin equilibrium (or admixed spin state $S = {}^3/_2, {}^5/_2$), where spin contributions vary with temperature.[211]

Sulfur-Bridged Complexes. There are three very similar binuclear sulfur-bridged heme−copper compounds, each of which contains the same μ-sulfur anion [(THF)(TPP)Fe^{III}−$Cu^{II}(MNT)_2]^-$ (**47**, Figure 19) and a different porphyrin cation $[(TPP)M^{III}(THF)(L)]^+$ (M = Fe, Ga, Al).[213] Their preparation was inspired by enzyme EXAFS studies that suggested a thiolate sulfur atom as a heme a_3−Cu_B bridging ligand.[193] Reaction of (TPP)Fe^{II} and $[Cu^{III}(MNT)_2]^-$ was reported to yield the anionic μ-sulfur complex **47**.[212] All three compounds were characterized by single-crystal X-ray diffraction; structural data for one of them are shown in Table 6. The assignment of the iron spin state based on the metrical parameters was quite difficult; however, Mössbauer data indicated an intermediate spin state for the iron(III) of all sulfur-bridged anions. After careful analysis, the authors concluded that the μ-sulfur heme−copper complex **47** is EPR silent. As the exchange coupling between the metal ions was found to be weak, they proposed a "relaxation broadening mediated by a small degree of exchange coupling through the bridging sulfur atom" to explain the silent EPR spectra. Furthermore, inspired by the unusual behavior of this and other trinuclear μ-sulfur complexes,[231,274] Elliott and Akabori[275] proposed an alternative mechanism to explain heme a_3−Cu_B oxidase enzyme EPR silence. They suggested that a combination of dipolar coupling and a small exchange coupling between the copper(II) and the rapidly relaxing $S = {}^3/_2$ iron(III) would cause sufficient EPR broadening so as to make any signal nonobservable. However, there has not since been any consensus concerning such a proposal.

Three μ-sulfide trinuclear complexes having an Fe^{III}−S−Cu^{II}−S−Fe^{III} connectivity are structurally similar to the μ-cyanide complex **42** (see compound **48**, as an example, in Figure 17), in the sense that two iron(III)−porphyrinate units sandwich a copper(II) moiety. Variable temperature magnetic studies showed a weak antiferromagnetic coupling for all three complexes ($J \sim -2$ cm^{-1}). "Weak" EPR signals observed were interpreted as being due to the above-mentioned relaxation broadening mechanism.[231]

Imidazolate-Bridged Complexes. A couple of μ-imidazolate heme−copper complexes with the formula $[(L)(TPP)Fe^{III}$−$Cu^{II}(imidH\text{-}DAP)]^+$ (**36b**, L = chloride, **36c**, L = triflate) (Figure 19) were prepared by equimolar reaction of the corresponding iron(III)−porphyrinate [(TPP)Fe^{III}−(L)] complexes and $[Cu^{II}(imidH_2DAP)]^{2+}$, in the presence of 1 equiv of base.[214] The compounds were isolated as solid samples and characterized by elemental analysis, EPR, Mössbauer spectroscopy, and magnetization techniques. The latter carried out on $[(Cl)(TPP)Fe^{III}$−$Cu^{II}(imidH_2\text{-}DAP)]^+$ (**36b**) show $\mu_{eff} = 2.0$ μ_B, consistent with a weak antiferromagnetic coupling between low-spin iron(III) (spin state determined by EPR and Mössbauer spectroscopies) and copper(II) mediated by the imidazolate bridge. In contrast, the magnitude of the exchange for the analogue $[(OSO_2CF_3)(TPP)Fe^{III}$−$Cu^{II}(imidH_2DAP)]^+$ (**36c**) was interpreted as being a significantly large, strong coupling based on EPR silence and the observed magnetic behavior. However, the reasons for the different behaviors in the two compounds are not clear.

For a related μ-imidazolate complex $[(TPP)Mn^{II}$−$Cu^{II}(imidH\text{-}DAP)]^+$ (**36d**), strong antiferromagnetic coupling between $S = {}^5/_2$ manganese(II)−porphyrinate (a spin mimic of heme a_3) and $S = {}^1/_2$ copper(II) was claimed.[276] This interpretation is supported by the compound EPR silence and observation of a depressed magnetic moment (5.11 μ_B at room temperature, decreasing to 4.17 μ_B at 20 K). However, a similar imidazolate-bridged compound $[(TPP)Mn^{III}$−$Cu^{II}(imid)]^+$ (**49**) exhibits weak exchange coupling ($J = -6.0$ cm^{-1}, where $H = -2JS_{5/2} \cdot S_{1/2}$), suggesting that probably Mn^{III} rather than Mn^{II} is present in complex **36d** and that the magnetic data should be re-evaluated.[277] Furthermore, Reed and co-workers[277] raised the question of whether different iron(III)−imidazolate−copper(II) complexes could exhibit extremely different magnetic behaviors, judging that this situation is unlikely.

Using an appended-tail porphyrin possessing a terminal imidazole group, an imidazolate-bridged complex can be prepared by reaction of the iron(III)−porphyrinate and a copper(II) complex, in the presence of 1 equiv of base. The magnetic and EPR characterization carried out on the isolated solid (compound **50**, Figure 19) indicates that there is essentially no exchange coupling between the high-spin iron(III) and the copper(II) ions.[215] Another heme−copper complex prepared in aqueous solution that appears to contain an imidazolate group as a bridging ligand was synthesized by the addition of 1 equiv of copper(II) complex $[Cu^{II}(GCH)]$ (GCH = glycyl-glycyl-L-histidine-*N*-methylamine) to a (TPPS)Fe^{III} (TPPS = tetra(*p*-sulfophenylporphyrinate)] solution at pH 4.8. The formation of the complex (**51**, Figure 19) was monitored by electrochemical methods and visible and EPR spectroscopies. The authors' interpretations included the suggestion of coupling between a low-spin iron(III) and copper(II), although magnetic studies to confirm this hypothesis were not reported.[216]

Beyond the fact that it is not clear whether imidazolate is a weak or a strong propagator of exchange coupling between heme and copper(II) complexes, the nature of the exchange for most of the imidazolate-bridged complexes described is *antiferromagnetic*. Surprisingly, a trinuclear Cu^{II}−Im−Fe^{III}−Im−Cu^{II} species (compound **52**, see Figure 17) whose structure resembles those found for trinuclear cyanide- and formate-bridged heme−copper(II) complexes (also Figure 17), exhibits a *ferromagnetic* interaction between metal centers.[232] The complex was prepared by reaction of $[(TPP)Fe^{III}](B_{11}CH_2)$ and Cu(Im), where Im represents a Schiff base generated by sequential condensation of 5-chloro-2-hydroxobenzophenone, 1,2-diaminobenzene, and imidazole-4-carboxaldehyde.

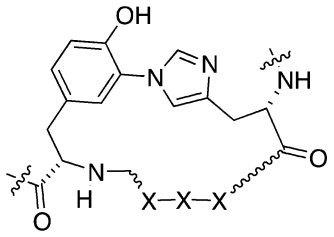

Figure 20. Cyclic pentapeptide-containing histidine–tyrosine cross-link. X is an amino acid residue.

EPR spectroscopic and magnetic studies on **52** and a nickel(II)-containing analogue lead to the conclusion about this unusual *ferromagnetic* behavior, which was interpreted in terms of the symmetries of the magnetic orbitals. The unpaired electron of iron(III) located in the d_{xz} (or d_{yz}) orbital, which exhibits π symmetry with respect to the iron–imidazolate bond, would be orthogonally interacting with the $d_{x^2-y^2}$ unpaired electron of copper(II), which has σ symmetry with respect to the copper imidazolate bond.[232]

5. Histidine–Tyrosine Cross-Link at the Heme–Copper Center

In recent years, copper and heme/copper-containing enzymes have been shown to possess post-translationally modified redox active amino acid cofactors at or near their active sites.[278–282] These pairwise cross-linked structural motifs, for example, histidine–tyrosine (for heme–copper oxidases, discussed here),[15–19,30,283] histidine–cysteine (in binuclear copper active sites in tyrosinase,[284] hemocyanins,[285] and catechol oxidase[286]), and tyrosine–cysteine (in the copper enzyme galactose oxidase[287]), are integral parts of the ligand architecture of the metal center, where the crucial redox-induced chemical reactions take place. These cross-linked amino acids have been identified to possess significantly altered physical properties (i.e., pK_a, redox properties) from their individual amino acid constituents.[288–291] The modifications have typically involved an unusual or interesting organic transformation of the amino acid, which remained unanticipated prior to high-resolution X-ray crystallographic structural characterization of the enzyme active site. After these findings, efforts have focused on the mechanism of formation of the cofactor, that is, the biosynthesis of the novel cross-link,[292] and of course an understanding of the contribution or role of the cross-link in enzyme mechanism.[19,23,56,293–295]

At the site for heme a_3/Cu_B binuclear center where O_2-binding, O–O cleavage, and coupling to membrane proton translocation occurs is found the unique post-translationally modified covalent cross-link between C_6 of tyrosine-244 (in bovine heart enzyme nomenclature) and $N_{\epsilon 2}$ of the histidine-240 imidazole group;[18] the latter is one of the endogenous ligands of Cu_B. [Note: Tyr-280 is cross-linked to His-276 in *P. denitrificans*,[19] whereas it is Tyr-237 and His-233 in *T. thermophilus*.][30] Thus, the His–Tyr cross-link is a cyclic pentapeptide (Figure 20), originating from a protein α-helix in enzyme subunit I, and is located at the end of the so-called K-channel for proton translocation.[296,297] Since its discovery and due to the proximity to the binuclear active center, a number of functional as well as structural roles have been proposed.[18,56,137,295] Investigations on biomimetic systems have just begun in very recent years, aimed at gaining insight into the exact beneficiary role(s) of the novel histidine–tyrosine cross-link.[288–291,298] In this section, we focus on the histidine–tyrosine cross-link that has been characterized by crystallographic and biochemical studies, their proposed roles in the O_2 reduction at the active site, and the recent advancements in histidine–tyrosine model chemistry.

5.1. Characterization and Roles of the Histidine–Tyrosine Cross-Link

5.1.1. Structural Characterization of the Cross-Linked Histidine–Tyrosine at the Active Site

The crystal structures of cytochrome *c* oxidase from *P. denitrificans* was initially reported in 1995 to a resolution of 2.8 Å and was later improved to 2.7 Å for the four- and two-subunit enzymes, respectively.[15,19] Initially, the His–Tyr cross-link was not identified. Iwata and co-workers[15] found that the His-276 Cu_B ligand was in van der Waals contact with Tyr-280 and suggested that these two residues may be hydrogen bonded, possibly stabilizing the Cu_B site. In the later structure (2.7 Å resolution) containing only the subunits I and II, it was concluded that a covalent cross-link between these two residues exists.[19] Yoshikawa's bovine cytochrome *c* oxidase structure was also solved initially at a 2.8 Å resolution[16,17] and later refined to 2.3 Å,[18] whereupon it was also concluded that there was a covalent bond between $N_{\epsilon 2}$ of the His-240 imidazole group and $C_{\epsilon 2}$ of Tyr-244. Confirmation for this linkage came from the solved X-ray structures of the fully reduced, fully reduced CO-bound, and fully oxidized azide-bound form.[18] More recently, the cross-link has been also verified from X-ray structures on cytochrome *c* oxidase from *T. thermophilus*.[30] The crystal structure of the C*c*O from *R. sphaeroides* is not clear on this point, as the distance between $C_{\epsilon 2}$ of Tyr-288 and the $N_{\epsilon 2}$ of His-284 was refined to 2.5 Å, too long for a covalent bond, yet too close to assume a nonbonding distance; it was suggested to possibly represent a mixture of enzyme populations with and without the His–Tyr N–C bond linkage.[31]

5.1.2. Biochemical Evidence for the Histidine–Tyrosine Cross-Link

Although the published crystal structures have presented the supporting evidence for the presence of the covalent cross-link between histidine and tyrosine, protein chemical analysis is required to firmly confirm and establish the covalent cross-link formation was not from the treatment of high energy X-ray treatment of the crystals in the presence of O_2, copper, iron, and the susceptible histidine and tyrosine amino acid side chains.

Buse and co-workers[292] have used the 13-subunit bovine and the 2-subunit *P. denitrificans* aa_3 cytochrome *c* oxidases and the caa_3- and ba_3 cytochrome *c* oxidases from *T. thermophilus* to carry out protein

chemical analysis. C-terminal half-fragments of the polypeptides obtained by the acid hydrolysis method were subjected to biochemical analysis, leading to the finding that the His and Tyr residues were unavailable for phenylthiohydantoin derivatization. This is explained by the presence of the covalent cross-link through the C−N bond, thus establishing it as a functional natural unit.

The mass of the purified 42-mer, that peptide fragment used for the derivatization analysis mentioned above, has been determined by electrospray ionization mass spectrometry (ESI-MS) with a resolution of ±2 mass units. The average mass calculated is 4816.76 Da, and the determined molecular weight is 4814.8 ± 0.4 Da. The decrease of 2 mass units from the theoretical value (assuming a linear normal peptide) is then explained by the His−Tyr N−C covalent bond, as two hydrogen atoms are removed (one from histidine NH and one from tyrosine CH) as a result of the oxidative coupling (formally) that has occurred.

In all, these studies biochemically confirm the presence of the His−Tyr cross-link at the binuclear active site, thus suggesting it has a natural role in enzyme function and that it most likely results from a post-translational modification process.

5.1.3. Spectroscopic Studies

Recent multifaceted spectroscopic investigations on heme−copper oxidases have been focused on the identification of the spectral features identified with the cross-linked histidine−tyrosine group and their changes associated with active-site dynamic conformational changes, protonation/deprotonation as well as redox or chemical events occurring at the binuclear center.[129,137,154,166,299,300]

In one effort, Hellwig and co-workers[154] have applied a combined electrochemical and FTIR spectroscopic technique to identify the vibrational modes of tyrosine in cytochrome *c* oxidase from *P. denitrificans* through Tyr isotopic labeling and study of a mutant in which Tyr-280 is replaced by a histidine. The variations of a band observed at 1270/1268 cm^{-1} at different pH values have been attributed to Tyr-280, and it has been suggested that these reflect a pH-dependent change in extinction coefficient upon variation in the direct environment close to the Tyr residue; alternatively, it might reflect a change of the protonation state of Tyr-280. A downshift of ∼95mV in the heme a_3 redox potential has been estimated for the Tyr-280 mutant of the enzyme as compared to that of the wild-type enzyme from the observed triphasic redox titration curve. The shift in the redox potential has been interpreted to arise from the substantial structural changes in the environment of heme a_3 accompanying the Tyr-280/His mutation. In addition, loss of Cu_B (∼50%) from the active site is also reported. Thus, the histidine−tyrosine cofactors at the Cu_B site of bovine heart C*c*O and also bacterial homologues have been suggested to be "electrostatically coupled to the binuclear active site".[301]

In a closely related low-temperature CO photolysis FTIR study, spectroscopic signatures of the covalently cross-linked histidine−tyrosine of the cytochrome bo_3 quinol oxidase from *E. coli* have been identified.[299] Among the several infrared features identified in the region of the imidazole and phenol stretching modes (1350−1650 cm^{-1}), two of these at ca. 1480 and 1550 cm^{-1} have been definitively assigned to arise from the His-284/Tyr-288 bi-ring structure. The vibration at 1549 cm^{-1} has been seen in both a histidine−tyrosine model compound (vide infra) and cytochrome bo_3 and cytochrome aa_3 from *P. denitrificans*; thus, all are assigned as being unique to the His−Tyr cross-link, with a substantial contribution from the inter-ring covalent C−N bond.[154,299] Despite the lack of conclusive evidence for the covalent cross-link between His-284 and Tyr-288 from the crystal structure of cytochrome *c* oxidase from *R. sphaeroides*, IR spectral features (for example, 1479, 1528, 1517, and 1587 cm^{-1}) similar to that observed for the cross-linked His−Tyr in cytochrome bo_3 and cytochrome aa_3 confirm the presence of a His−Tyr moiety in this oxidase.[302]

5.1.4. Proposed Role of the Cross-Linked Histidine–Tyrosine Active Site Cofactor

Since its discovery, there have been several suggestions for the role of the His−Tyr cross-link in heme−copper oxidases.[19,21,137,293−295] Initially, the generation of the cross-link has been proposed to modulate one or more of the properties of either residue.[18]

Full reduction of dioxygen requires four electrons and four protons. We now discuss a O_2 reduction mechanism that includes consideration of the His−Tyr cofactor (Figure 21), taken from various recent discussions.[18,23,56,77,278,282,303] As before, the essential elements are that dioxygen binds to the heme a_3−Cu_B binuclear center, leading to a spectroscopically detectable Fe−O_2 intermediate (**A**), which subsequently converts to **P** and **F** intermediates, before the oxidized form of the enzyme is regenerated. Reduction of **P** and **F** intermediates is limited by proton transfer. The **P** state has been conclusively identified as an oxoferryl species [Fe(IV)═O]; thus, the formation of **P** requires four electrons.

Three of the electrons are clearly provided by heme a_3−Cu_B [where iron(II) converts to iron(IV) and Cu_B goes from copper(I) to copper(II)], where the remaining one electron must be provided from other enzyme groups. The source of this final electron required for O−O cleavage is less certain. There are a number of possibilities that could be considered, in light of precedent from other heme enzymes or considerations: (a) In peroxidases[304] and catalases[305,306] the source of this electron is often the heme macrocycle resulting in the formation of porphyrin π-cation radical. Neither optical[307−309] nor resonance Raman spectroscopic evidence[310] at this time provides any support for the occurrence of this process in heme−copper oxidases. (b) Oxidation of heme iron from iron(IV) to iron(V) has been recently proposed,[73,294] but this possibility is unprecedented among other heme enzymes and supporting evidence has not yet emerged. (c) Another potential source of the additional reducing equivalent is Cu_B, which conceivably may be oxidizable to the 3+ valence state, and there have

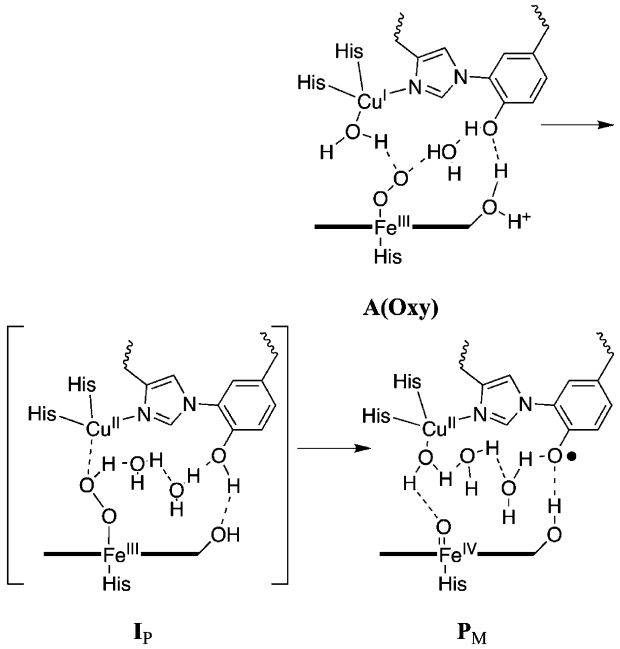

Figure 21. That part of the heme−copper enzyme O_2 reduction mechanism indicating the possible important role of the tyrosine of the His−Tyr cross-link cofactor, adapted from recent discussions (see text for references). **A**, oxy species; $\mathbf{I_P}$, an as yet undetected transient ferric hydroperoxide or μ-peroxo $Fe^{III}-(O_2^{2-})-Cu^{II}$ species; $\mathbf{P_M}$, the O−O cleavage an oxy−ferryl spectroscopically observed intermediate, with electron provided from the Tyr of the His−Tyr cofactor, where a key active site water molecules facilitates proton transfer and stabilization. See text for further discussion.

been suggestions[23,309] that trivalent copper might be stabilized by the His−Tyr cross-link. However, the occurrence of copper(III) has never been demonstrated in copper enzymes. It is known in inorganic chemistry, but only with deprotonated amide or oxide ligands present,[6,7,311−313] not anything like the His_3 ligand environment in heme−copper oxidases. (d) Another possible source of the additional electron may be an amino acid residue, such as is established for the heme proteins cytochrome *c* peroxidase[304] (a tryptophan) and prostaglandin H synthase[314] (a tyrosine).

It is of course most compelling to think the electron can or does derive from the tyrosine of the His−Tyr cross-link, as mentioned in section 3.1 and depicted here in Figure 21. We start with intermediate **A**, the O_2 adduct of the reduced enzyme, an oxymyoglobin analogue. Although never having been detected, a further one-electron-reduced peroxo species derived from oxidation of copper(I) to copper(II) could lead either to a ferric hydroperoxo intermediate or to a bridged Fe^{III}−peroxo−Cu^{II} $\mathbf{I_P}$. The key O−O cleavage then occurs through net hydrogen-atom transfer (but with the electron from tyrosine and proton from a water), leading to $\mathbf{P_M}$. [Note: The protons necessary in this process may be derived from the shortest pathway (K-channel) proposed among other pathways, which includes a hydrogen-bonding network with the farnesyl side chain of the heme a_3, His-276−Tyr-280 (the cross-linked His−Tyr), Ser-291, Lys-354("K"), and Thr-351 (*P. denitrificans* numbering).][296,297]

Evidence for the His−Tyr• Radical. Thus, a His−Tyr radical is proposed to form in dioxygen reduction from the mixed-valent (MV) enzyme, accompanied by formation of $\mathbf{P_M}$.[21−23] However, the EPR signals expected have not been observed. If it were present, its absence could be attributed to spin coupling between the $S = {}^1/_2$ Cu_B^{2+} and the $S = {}^1/_2$ tyrosyl radical. A suggestion[21] made is that spin coupling might serve to delocalize the oxidizing equivalent so that Cu_B assumes a partial 3+ character, leaving a tyrosinate anion. A recent report indicates a radical EPR signal can be detected (at 80 K, $g_{iso} \sim 2.0055$) from a H_2O_2-treated (pH 6.0) fully oxidized cytochrome *c* oxidase. Although the yield of radical is low (20%), it was assigned as a His−Tyr radical, following perturbation of the EPR signal resulting from selective deuteration of the tyrosine.[76] The researchers suggest that the lower yield of radical may represent a partial uncoupling of the Cu_B/His−Tyr moiety.[21,76]

Through infrared spectroscopic studies on the *R. sphaeroides* C*c*O O_2 reaction, spectral features characteristic of a neutral tyrosyl radical (1479 cm^{-1}) and tyrosinate (1455 and 1515 cm^{-1}) at the $\mathbf{P_M}$ and $\mathbf{P_R}$ level intermediates were identified.[302] Optical spectroscopic (UV−vis and IR) differences for intermediates have been recently elucidated and were determined to arise from a different number of redox states of the binuclear center, proposed as [Fe_{a3}-(IV)═O Cu_B(II)−OH− (TyrO•)] for $\mathbf{P_M}$ and [Fe_{a3}-(IV)═O Cu_B(II)−OH− (TyrO$^-$)] for $\mathbf{P_R}$, with heme *a* being in the oxidized ferric state in both forms.[55,315] In addition, through a perfusion-induced attenuated total reflection FTIR spectroscopic investigation on the intermediates ($\mathbf{P_M}$, **F**, **O**) generated from bovine and *P. denitrificans* C*c*O, spectral features characteristic of tyrosyl radical have also been identified.[316] In particular, the 1542/1547 and 1313/1314 cm^{-1} troughs were observed in the $\mathbf{P_M}$ spectra but were absent in the **F** state, suggesting that the tyrosyl radical is most likely formed in the $\mathbf{P_M}$ state.[316] The vibrations can be associated with the tyrosine, on the basis of model studies (vide infra). Evidence has also been presented for the presence of His−Tyr radical at the Cu_B site in the $\mathbf{P_M}$ state in an experiment where a Tyr• radical (which is generated as part of the His−Tyr cofactor) could be specifically labeled with radioactive $^{125}I^-$ and then identified by peptide mapping procedures.[23]

Studies on simple organic cofactor histidine−tyrosine models (vide infra) also suggest that the covalent modification could facilitate hydrogen atom donation to heme-bound dioxygen by modulating the phenolic pK_a.[288−291] Theoretical studies[56,78] suggest that O−O cleavage and tyrosyl radical formation cannot occur unless a base (suggested to be the farnesyl hydroxyl) assists the phenol proton removal (Figure 21). It is also interesting to note that mutants which lack the His−Tyr group (including, for example, a Tyr-280/Phe mutant) have been shown to lose a heme a_3 farnesyl H-bonding interaction, and there is loss of copper and alteration of the heme a_3 redox potential;[156] many of the mutants are catalytically inactive. A contrasting report indicates that a *P. denitrificans*

Y280H mutant which lacks the His−Tyr cross-link at the Cu_B site in fact does lead to the generation of the oxygenated intermediates (oxoferryl species) with spectroscopic features similar to those observed for the wild-type enzyme.[137] These studies suggest our lack of a complete understanding of the mechanistic role of the His−Tyr unit in O_2 reduction.

Other Possible Roles. Other roles, besides in the O−O cleavage process, have been suggested for the active site His−Tyr moiety.[137,295] It has been shown that approximately half of the charge is translocated in each of the phases of the heme−copper oxidase enzyme mechanism, the oxidative phase O_2 is reduced and cleaved where the metal centers are left in their oxidized state, and the reductive phase four-electron reduction occurs, giving back fully reduced enzyme.[317] The redox energy must be stored in the protein after O_2 reduction is completed, requiring the existence of metastable conformations.[317,318] There are suggestions that there are protein sites such as the His−Tyr moiety, which must be redox sensitive and undergo protonation/deprotonation events (i.e., at the His N−H or Tyr O−H) associated with the catalytic activity, playing essential roles in functionally important conformational changes and redox-linked proton pumping.[129]

These suggestions come in part from XAS studies revealing that there is a Cu_B His ligand which is labile, dissociating from the metal ion in its reduced state.[319,320] (Note, however, that protein X-ray structures do not "see" such differences around Cu_B in oxidized vs reduced enzyme forms.) From a recent copper model compound study (described further below), it has been suggested that His−Tyr oxidation to a Tyr• radical should make the imidazole a weaker ligand for copper ion (see diagram below); thus,

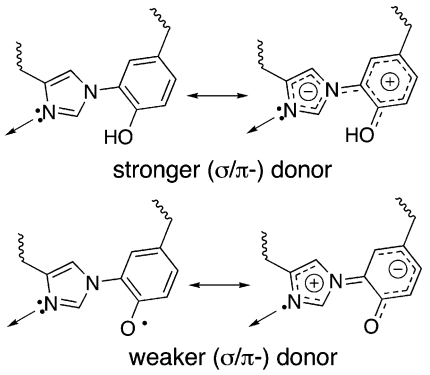

imidazole dissociation from Cu_B (cupric?) would facilitate binding of other ligands such as hydroxide (or water), the latter produced via the O−O cleavage process (Figure 21).[295]

Thus, ligand lability in either or both the reduced and oxidized states of Cu_B, including possibly the Cu_B deligation of the His−Tyr moiety, may greatly contribute to redox-driven and proton-linked conformational (or ligation) changes, contributing importantly to enzyme function. A dissociated His−Tyr moiety may drive helix distortion, providing a means for energy storage (to be used in the later reductive phase) and/or facilitation of protonation−deprotonation steps important in translocation chemistry.[295]

Scheme 16

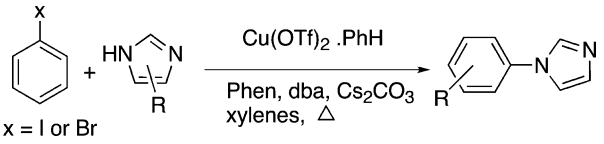

5.2. Histidine–Tyrosine Model Compound Chemistry

Since the discovery of the histidine−tyrosine covalent cross-link, there have been a number of reports of simple organic cofactor mimics as well as copper-containing chelate models that bear covalently linked imidazole−phenol structures.[154,288−291,298,299] The major goal in all cases is to produce synthetic mimics of the cross-linked His−Tyr structure and to elucidate their physiochemical properties. It is hoped that such investigations would pave the way for an in-depth understanding of the function and benefit of this novel cofactor in the dioxygen reduction event and perhaps its coupling to proton translocation.

5.2.1. Synthetic Methodology

Synthesis of N-substituted *o*-hydroxyphenyl-imidazole as a model for the cross-linked histidine−tyrosine requires N-arylation of imidazoles. *N*-Arylimidazoles have usually been constructed by two types of direct coupling, that is, nucleophilic aromatic substitution[321−324] or Ullmann-type coupling.[325,326] Construction of covalently linked imidazole−phenols through an aromatic substitution method would require the use of substrates with an electron-withdrawing substituent in both the imidazole and phenol moieties; this method might not be widely applicable when the synthesis of a suitable mimic with an appropriate biomimetic substituent (i.e., 4-alkylimidazole or 4-alkylphenol) is considered. Ullmann-type couplings are usually carried out at high temperatures, which also limits its application to only thermally insensitive compounds.

Buchwald[327] has demonstrated condensation between aryl halides and imidazoles with catalytic amounts of $(CuOTf)_2$·benzene/1,10-phenanthroline-(phen)/*trans*,*trans*-dibenzylidene acetone (dba)/Cs_2CO_3 at temperatures in the range of 110−125 °C (Scheme 16). The necessity for base and the elevated temperatures are expected to limit this approach.[328] Other efficient methods have been established for generating *N*-arylimidazoles, via coupling of arylboronic acid and aryllead reagents (instead of aryl halides) with imidazoles; these reactions occur under relatively mild reaction conditions.[329,330] Chan and coworkers[331] have described a $Cu(OAc)_2$-promoted N-arylation of commercially available arylboronic acids with imidazoles at room temperature. Collman et al.[329,332] extended this method and have demonstrated that same N-arylation can be accomplished in the presence of a catalytic amount of $[Cu(OH)\cdot TMEDA]_2Cl_2$ (TMEDA = *N*,*N*,*N*′,*N*′-tetramethylethylenediamine) without the addition of any base at room temperature (Scheme 17). However, both the Collman and Buchwald procedures have been reported to afford mixtures of regioisomers when the coupling is performed on 4-substituted imidazoles.[327,329]

Scheme 17

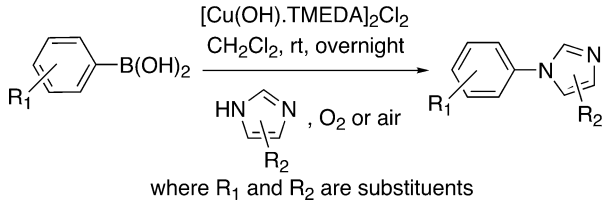

Scheme 18

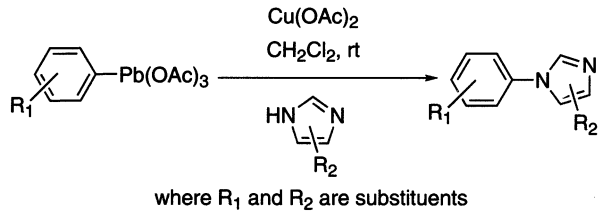

Table 11. Reported Simple Organic Cofactor Models for the Histidine−Tyrosine Cross-Link in Heme−Copper Oxidases

Covalently cross-linked Imidazole-phenol model compounds	Numbering of the models and its substituents
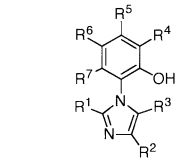 Models **53-62**	**53** ($R^1 = CO_2Me$, $R^2 - R^7 = H$) **54** ($R^2 = CO_2Me$, R^1, $R^3 - R^7 = H$) **55** ($R^3 = CO_2Me$, R^1, R^2, $R^4 - R^7 = H$) **56** ($R^1 - R^7 = H$) **57** ($R^6 = Me$, R^1-R^5, $R^7 = H$) **58** ($R^2 = R^6 = Me$, R^1, R^3-R^5, $R^7 = H$) **59** ($R^2 = CH_2$-C(NHAc)(COOMe), R^1, R^3-$R^7 = H$)
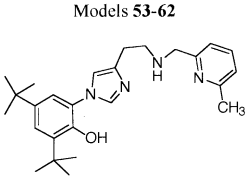 Copper chelating model-**63**	**60** ($R^1 = R^6 = Me$, R^2-R^5, $R^7 = H$) **61** (R^1-$R^3 = D$, $R^6 = CD_3$, R^4-R^5, $R^7 = H$) **62** (R^1-$R^3 = H$, $R^6 = CD_3$, R^4, R^5, $R^7 = D$) **63** = $L^{N3}OH$
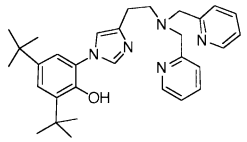 Copper chelating model-**64**	**64** = $L^{N4}OH$

Elliot et al.[330] have reported the coupling of imidazoles with arylleadtriacetate (Scheme 18) in the presence of catalytic $Cu(OAc)_2$, resulting in exclusive formation of 1,4-disubstituted imidazoles. Arylleadtriacetate is usually prepared either by direct plumbation of aryl halides or through the intermediacy of aryltin compounds.[333,334] They have extended this method to obtain a suitably protected version of the histidine−tyrosine dipeptide found in the active site of the enzyme.[289] Kamaraj et al.[298] have recently accomplished the construction of tridentate and tetradentate chelate ligands (Table 11, compounds **63** and **64**) for copper including an imidazole−phenol donor, and the preliminary results on the dioxygen reactivity of the Cu(I) complexes have been reported (discussed further below).

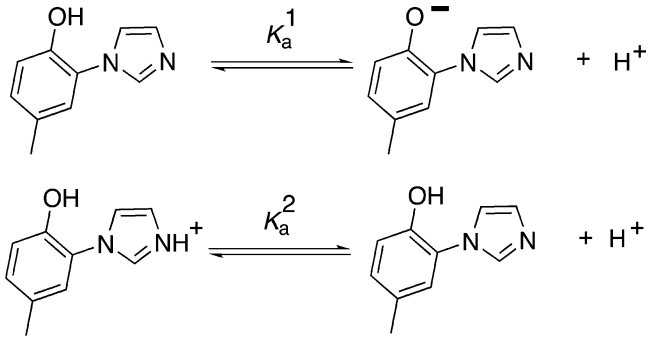

Figure 22. Dissociation equilibria for histidine−tyrosine models. See Table 12.

Table 12. pK_a Values of Histidine−Tyrosine Models

compound	pK_a (imidazole)	pK_a (phenol)	ref
53	4.05	6.58	291
54	4.25	6.80	291
55	4.30	6.89	291
56	6.12	7.86	291
57	5.54	8.60	288
59	5.54	8.34	289
imidazole	7.10		290
histidine	6.00		335
p-cresol		10.3	290
tyrosine		9.21	336

5.2.2. Physicochemical Studies

One major aspect of interest is to establish the properties of the models of the cross-linked histidine−tyrosine unit and closely compare those with corresponding properties of the individual imidazole and phenol components. A number of physical methods have been employed, including electrochemical and FT-IR, UV-resonance Raman (UVRR), and EPR spectroscopies, etc., to probe the effect of cross-link on the property of the imidazole−phenol models (**53**−**62**, Table 11) with an objective to extend the information obtained to understand the mechanistic role of the cross-linked histidine−tyrosine cofactor in enzyme catalysis. For the organic His−Tyr models, that is, in the absence of copper ion, measurement of imidazole and phenol pK_a values and identification of spectroscopic features for the histidine−tyrosyl radical are of interest.[154,288−291,299]

Spectrophotometric and titrimetric studies on imidazole−phenols **53**−**57** and **59** (Table 11) have revealed two pK_a values (Table 12), which were assigned to protons on the ϵ-nitrogen of the imidazole and phenolic hydroxide (Figure 22).[288−291] Significantly reduced values for the pK_a of the phenol and imidazole are observed as common characteristics of the cross-link models. The modulation of the phenol pK_a varies over a significant range (6.6−8.6, Table 12), which may be due to the effect of substituents. The increased acidity apparently due to the cross-link, both at the imidazole and phenol (Table 12), suggests an increased π-delocalization, which would depend on the coplanarity of the phenol and imidazole rings.[288−290] The pK_a of the substituted phenolate may be lowered via resonance stabilization of the conjugate anion by the N-linked imidazole or by stabilization of the phenolate through an inductive electron withdrawing effect.[288] An additional reduc-

tion of pK_a could be expected when the imidazole was coordinated to a copper ion (as in the enzymes) and should depend also on the oxidation state and coordination geometry.[290] However, no such experimental data are yet available. The cross-link of the imidazole−phenol model compounds also lowers the imidazole pK_a, which might significantly weaken its copper-coordinating ability. Again, no investigations yet bear on this point.

UVRR studies on the cross-linked imidazole−phenol models **56**, **57**, and **60**−**62** and their isotopically substituted (^{18}O) analogues have demonstrated that some imidazole vibrations are resonance enhanced upon excitation of phenol $\pi-\pi^*$ transitions, whereas they are absent for corresponding equimolar mixtures of imidazole and *p*-cresol.[290] This indicates delocalization of π-electrons between the imidazole and phenol. A significant intensity change occurs when neutral and anionic phenolic forms are compared [note, for example, that the Y8a band of the anionic form is much stronger (∼4 times) than that of the neutral form upon excitation, and its frequency is lower in the anionic form], and there is a resulting closer approach to data obtained for an enzyme pH difference spectrum. The authors suggest that imidazole Cu_B ligation may serve to stabilize a closer to coplanar His−Tyr situation.[290]

Although imidazole/neutral-phenol ring dihedral angles are known in heme−copper oxidases (44°, 66°, 57°; all presumed to be neutral phenol form),[18,19,30] organic cofactor models (36.3°, 42.2°),[289,337] and copper-containing complexes (83.1°, 73.0°; see below),[298] corresponding values for deprotonated forms are not available. Dihedral angles may be different in crystal forms versus solutions and may vary with redox state. Theoretical studies suggested that the effect of imidazole substitution on phenol acidity for an imidazole−phenol moiety can vary significantly.[338,339] The pK_a difference relative to unsubstituted phenol decreases from −9.4 to −4.9 to −3.5 units for gas phase, protein, and water solution, respectively. This calculated dielectric dependency has been rationalized to arise from the changes in dihedral angle. In the calculations the neutral species has an angle of ∼59°, whereas the anionic form corresponding value is ∼27°. This study also suggests that the pK_a value of the cross-linked phenol can be further lowered by a low dielectric protein environment and would be affected by the nature of the specific surrounding residues. A small decrease of ArO−H bond dissociation energy of ∼1 kcal/mol in a cross-linked phenol has been estimated by comparison to an unmodified phenol.[339] A similar magnitude of decrease in the oxygen−hydrogen bond strength (0.7 kcal/mol) has been directly measured (electrochemically) in the imidazole−phenol model compound **57** (Table 11).[288]

Cyclic voltammetric studies on **57** and *p*-cresol displayed irreversible behavior. The observed anodic peak was 66 ± 3 mV greater than that measured for *p*-cresol, which has been attributed to the electron-withdrawing effect of the imidazole substituent.[288] Differential pulse voltammetry studies revealed three dissociation constants for the pH dependence of the midpoint potential for a one-electron oxidation of the model compound **57**. Among the three pK_a values, the former two have been assigned to protonation of imidazole and phenol, respectively (Table 12). On the basis of the direction of the change in slope at the third pK_a at ∼4.80, it has been suggested to be associated with the protonation of the imidazole of the cross-linked phenol oxidized radical species (see diagram below).[288]

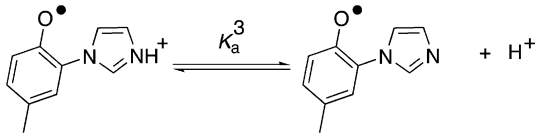

Phenoxyl Radicals. Radical species generated by UV photolysis within several cross-link models (**57**−**59**)[288−290] and tyrosine-containing dipeptides[340] have been identified as phenoxyl ring radicals by EPR and UV−vis spectroscopy. Significant mixing of the imidazole and phenoxyl electronic states occurs, and a small delocalization of spin density onto the imidazole ring has been suggested, on the basis of the observation of a significant shift (∼100 nm) in the radical UV−visible spectrum, compared with an unmodified tyrosyl radical.[289] With simple tyrosine-containing dipeptides (Tyr−His, Tyr−Pro, and Pro−Tyr) lacking the covalent cross-link, phenoxyl radicals produced by UV photolysis indicate conformationally sensitive delocalization of spin density onto the dipeptide amino and carboxylate groups occurs. The authors suggest that this property, which may also occur with other functional groups, may have important implications for electron-transfer pathways in proteins.[340] As it may pertain to heme−copper oxidases, other researchers[288−290] suggest that the His−Tyr covalent bond may enable enhanced migration of an electron between the two rings.

UVRR studies on imidazole−phenol models **56**, **57**, and **60**−**62** show that the presence of an imidazole C_2 substituent appreciably increases the C−O double-bond character in the phenoxyl radical state. It was suggested that in the absence of a C_2 bulky group, the cross-linked structure may better approach coplanarity.[290] A C−O stretching RR band was observed at 1530 cm^{-1} for the radical state of **56**, **57**, and **60**−**62**. The *g* values of the radical-generated **56**−**59** vary over the range 2.0045−2.0058. The authors suggest that a tyrosyl radical generated during heme−copper oxidase turnover would need only to have a transient existence and stability so that the subsequent one-electron reduction is highly favorable.[278,288]

Copper-Containing Model Complexes. In an attempt to model and understand the redox-linked conformational gate to proton translocation, Colbran and co-workers[295] have investigated the copper coordination chemistry of tris(pyridylmethyl)amine ligands with one of the pyridine arms having a hydroquinone (H_2L^2) or a quinone substituent (L^3) at the sixth position (Figure 23). They demonstrated that two-electron oxidation of a square planar complex [Cu(k^3N−H_2L^2)Cl_2] is linked to the loss of two protons accompanied by a conformational change (i.e., binding of the previously "dangling" hydroquinone-containing pyridine arm to the copper and simulta-

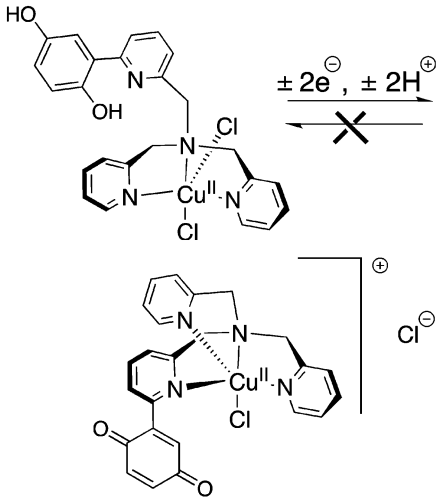

Figure 23. Oxidation of [Cu(k^3N−H_2L^2)Cl_2] (top) to [Cu(k^4N−L^3)Cl]$^+$ (bottom), a model for a copper−ligand complex redox-linked conformational transformation (i.e., ligation and geometric changes), also accompanied by proton movement (i.e., loss).

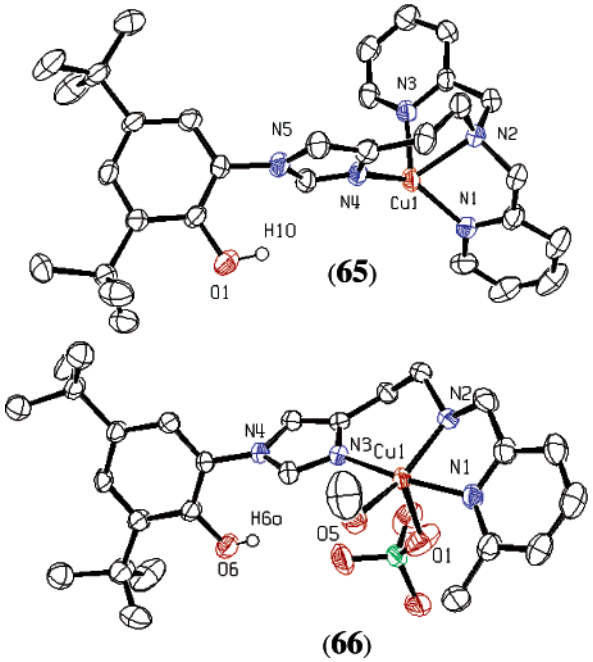

Figure 24. ORTEP diagrams showing the cationic portions of [Cu^I(L^{N4}OH)](B(C_6F_5)$_4$) (**65**) (top) and [Cu^{II}(L^{N3}-OH)(MeOH)($OClO_3^-$)]($OClO_3^-$) (**66**) (bottom).

neous loss of 2H$^+$ to form a quinone), affording a trigonal bipyramidal product [Cu(k^4N−L^3)Cl]$^+$ (Figure 23). Thus, this system provides a crude but quite interesting example for a critically important step in a proton-pumping cycle.

Kamaraj et al.[298] prepared first-generation models of the Cu_B−His−Tyr moiety, employing ligands **63** and **64** (Table 11), synthesizing copper (I/II) complexes. The X-ray structures of copper(I) complex [Cu^I(L^{N4}OH)]$^+$ (**65**) and the cupric compound [Cu^{II}-(L^{N3}OH)(MeOH)($OClO_3^-$)]$^+$ (**66**) are shown in Figure 24. For mononuclear complex **65**, the copper(I) geometry is distorted trigonal pyramidal with three aromatic nitrogens (pyridine and imidazole) in the basal plane, whereas the copper(II) ion in **66** is pentacoordinate, possessing ligation from the three nitrogen donors of the tridentate chelate plus methanol and perchlorate ligands. The imidazole−phenol moiety in both complexes enjoys nitrogen−copper ligation, also yielding a phenol proximate to the copper ion, similar to that seen in the natural enzyme active sites. The resulting Cu···(O) distances are in the range of 5−6 Å, analogous to those in the protein crystal structures.[18,19,30] The observed phenol/imidazole dihedral angles in these model compound (**65** and **66**) structures are larger than observed for the proteins (vide supra), suggesting only a minimal electronic interaction exists between the copper ion and the phenol through the C−N covalent cross-link, at least in the solid state. The measured Cu(II)/Cu(I) redox potentials for [Cu^I(L^{N4}OH)](B(C_6F_5)$_4$) (**65**), its anisole analogue, and [Cu^I(TMPA)(MeCN)]ClO_4 (**2a**, Figure 6) are nearly identical ($E_{1/2} \cong -0.42$ V vs $FeCp_2/FeCp_2^+$ in acetonitrile), indicating that the imidazole−phenol cross-link does not directly influence the redox properties. This is of course consistent with the large imidazole−phenol dihedral angles (vide supra) resulting in an apparent minimal electronic communication of the copper ion and the phenol part of the ligand.

Initial dioxygen reactivity studies of the copper(I) forms of the ligand−Cu complexes were carried out to see if phenoxyl radical species might form. No such chemistry was observed. Both the tridentate and tetradentate chelate copper(I) complexes react with dioxygen at low temperatures to give spectroscopically (UV−vis) peroxo−dicopper(II) Cu−O_2−Cu intermediates, apparently preorganized for subsequent deprotonation of the cross-linked imidazole−phenol moiety and subsequent phenolate dimer product formation. It was suggested that the phenol moiety acted as a proton donor toward the basic peroxide intermediate species formed.[298]

Summary. Models for the histidine−tyrosine cross-link have led to new or newly applied synthetic organic chemistry development and the determination of how the cross-link effects modify pK_a values, phenol-bond dissociation energies, properties of the phenoxyl radicals, and other physical properties. Only a few examples of copper complexes with an imidazole−phenol moiety exist and, as of this writing, none with a heme−copper complex with the cross-link of interest (but see ***9. Note Added in Proof***).

6. Models for the Dicopper Cu_A Electron-Transfer Site

Most cytochrome *c* oxidases have the primary electron acceptor Cu_A site in subunit II (Figure 3 in section 2), mediating one-electron-transfer (ET) processes from cytochrome *c* to the low-spin heme *a* site.[10] Cu_A was once thought to be a mononuclear redox center, analogous to the type 1 centers in blue copper proteins, but is now known to consist of a thiolate-bridged binuclear site, as illustrated in Figure 25. The electron transfer facilitated by Cu_A is remarkably fast, both for the intramolecular ET ($k = 1 \times 10^4$ s^{-1}, $Cu_A \rightarrow$ heme *a*)[29,341] and for the intermolecular ET ($k = 6 \times 10^4$ s^{-1}, cytochrome *c* → Cu_A),[342] considering the fact that the metal centers are separated by ~20 Å[18] (Figure 3) and ~18 Å (as

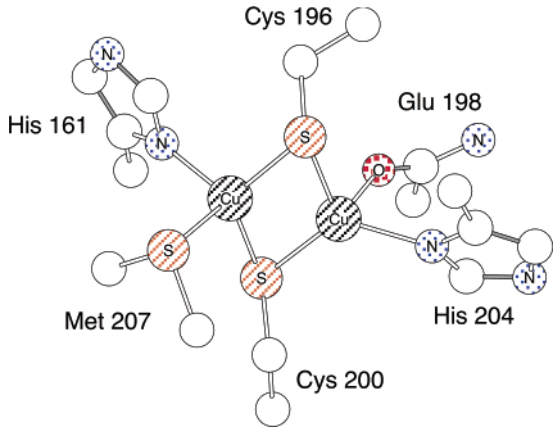

Figure 25. Chem 3D representation of the Cu_A site in bovine cytochrome *c* oxidase, as taken from the X-ray coordinates (PDB 10CR).

predicted by modeling studies),[27] respectively. Understanding the unique structure of Cu_A with respect to its ET functionality has been a focus of intense research, and synthetic modeling chemistry, in particular, has made considerable contributions in elucidating the geometric and electronic structures of Cu_A.

6.1. Cu_A Site in Cytochrome *c* Oxidase

Physical studies of the Cu_A site in C*c*O were previously hampered by the presence of the heme groups, whose dominant spectroscopic features often interfered with those from the copper centers. Such difficulties have been overcome relatively recently through a genetic-engineering approach, in which the water-soluble Cu_A C*c*O domains from *B. subtilis*,[343] *P. denitrificans*,[344] and *T. thermophilus*[345] can be separately expressed. In addition, protein engineering has led to the reconstitution of the Cu_A site into the CyoA subunit of quinol oxidase from *E. coli*,[346,347] and into a copper-binding site of *Pseudomonas aeruginosa* azurin[348] and *Thiobacillus versutus* amicyanin.[349] A great deal of insight has been obtained from studies using these constructs; these are relevant or related to the very similar electron-transfer copper A site of nitrous oxide reductase (N_2OR), the terminal denitrification enzyme that catalyzes the reduction of N_2O ($N_2O + 2H^+ + 2e^- \rightarrow N_2 + H_2O$).[350]

Cu_A exists in two redox states. The reduced form has two cuprous ions ($Cu^I \cdots Cu^I$), whereas the oxidized form has a fully delocalized mixed-valence core ($Cu^{II}Cu^I \leftrightarrow Cu^ICu^{II} \equiv Cu^{1.5} \cdots Cu^{1.5}$) in which the unpaired electron gives rise to an EPR spectroscopic seven-line hyperfine pattern, expected for delocalization over two copper ions, each possessing a nuclear spin $I = {}^3/_2$. Although controversial at the time, a binuclear structure was in fact first (correctly) proposed by Antholine and Kroneck, following their multifrequency EPR observations and analyses.[350,351]

Several C*c*O[15−19,30,31] and N_2OR[352,353] crystal structures and that for the engineered Cu_A-containing proteins[354−356] are now available, confirming the Cu_A binuclear structure suggested by the spectroscopic methods. The geometry of the Cu_A site from reduced bovine cytochrome *c* oxidase[18] is shown in Figure 25. The two copper ions are bridged by the sulfur atoms of Cys-196 and Cys-200, forming a planar diamond core with a short metal-to-metal distance of 2.58 Å. Each copper ion is terminally coordinated by histidine ligands that are trans to each other. One copper atom is also weakly coordinated by a methionine sulfur ligand, whereas the second copper ion is also weakly bound to a backbone carbonyl oxygen of a glutamic acid residue. These structural features are generally conserved in the natural and the engineered Cu_A sites (Table 13). The short distance between the two copper centers is in good agreement with that observed from XAS and EXAFS studies,[357,358] in which a direct Cu−Cu bond has been proposed, whereas the presence of the weak ligands (Met and Glu) could not be detected by EXAFS analyses. Only minor changes in the core Cu_2S_2 structures are observed between the oxidized and the reduced forms, where the reduced form has slightly longer Cu−Cu and C−S bond lengths (Table 13). The robust Cu_A cluster, which is essentially unchanged upon one-electron redox change, has been suggested to provide a structural framework for the low reorganization energy of Cu_A, λ, which can be directly related to its fast ET rate.[358]

The MV "oxidized" form of the Cu_A center has a number of distinctive spectral features (Table 14). In addition to its characteristic EPR spectroscopic properties (see above), MV−Cu_A exhibits an intense purple color with strong absorption bands around 480 and 530 nm, originating from the S(Cys) → Cu charge-transfer transitions.[359−361] Resonance Raman spectroscopy also reveals a large number of vibra-

Table 13. Comparisons of the Bond Distances (Angstroms) for the Different Forms of Cu_A

	bovine heart		*T. thermophilus*			Cu_A azurin
	reduced	oxidized	reduced	oxidized	oxidized	oxidized
method	X-ray	X-ray	EXAFS	EXAFS	X-ray	X-ray
resolution (Å)	2.35	2.30	*a*	*a*	1.6	1.65[b]
Cu···Cu	2.58	2.45	2.51	2.43	2.51	2.39
Cu−S(Cys)	2.21−2.34	2.17−2.27	2.33	2.29	2.2−2.42	2.16−2.43
Cu−N(His161)	1.96	1.93	1.96	1.97	2.11	2.05
Cu−N(His204)	1.97	1.93			1.88	2.16
Cu−S(Met)	2.67	2.66	NA[c]	NA	2.46	3.07
Cu−O(Glu)	2.41	2.39	NA	NA	2.62	2.16
ref	18	18	357	357	354	355

[a] Distances are accurate to ±0.02 Å; coordination numbers are accurate to ±25%; the coordination numbers in the simulations were fixed at 1 N, 2 S, and 1 Cu scatter per Cu_A absorber (ref 357). [b] Two independent Cu_A azurin molecules are in the asymmetric unit with root-mean-square deviation of 0.27 Å between them (ref 355). [c] Not observed.

Table 14. Physical Properties of the Mixed-Valence Cu_A Site

spectroscopic method		data	ref
EPR[a]	hyperfine pattern	7 lines	350
	g_x	2.00	
	g_y	2.03	
	g_z	2.18	
	A^{Cu}, Guass A_x	22.70	
	A_y	24.50	
	A_z	38.00	
ENDOR[a]	A^N, MHz	7−11	362
		15.6−20.3	
UV−vis, MCD,[b] nm (ϵ, M^{-1} cm^{-1})	S → Cu CT	480 (3000)	359−361
	S → Cu CT	530 (2600)	363
	$\psi \rightarrow \psi^*$	~800 (1600)	
Raman,[b] cm^{-1} ($\Delta^{34}S$)	Cu_2S_2 breathing	339 (−5.1)	359−361
	Cu−S/Cu−N stretching	260 (−4.1)	
	Cu−S twisting	270	
	Cu_2S_2 accordian bending	~130	
reduction potential		250 mV[d]	364

[a] From bovine C*c*O. [b] From *P. denitrificans* Cu_A domian C*c*O. [c] From *B. subtilis* Cu_A domain C*c*O. [d] Potential vs NHE.

tional modes from the $Cu_2S_2(Im)_2$ core, providing further information and insights concerning the coordination and bonding in Cu_A.[359−361]

The electronic structure of Cu_A has also been studied using both experimental and theoretical approaches. Solomon,[361,365,366] Thomson,[367] Kroneck,[368] and their co-workers carried out detailed spectroscopic and molecular orbital calculations on both Cu_A-containing enzymes and a MV model compound (discussed below). The research group of Solomon suggests that the elongated axial ligands (Met sulfur and oxygen donor from Gln or Glu) leads to Cu−Cu compression, which then produces strong orbital overlap and valence delocalization, a lower reorganization energy, and thus efficient ET. In addition, the importance of the short and highly covalent Cu_A Cys−Cu bonds was highlighted, as contributing to efficient long-range ET, allowing multiple ET pathways, as a S(Cys) path is competitive with a shorter N(His) pathway. However, in a separate study using DFT calculations [on the molecule $(Im)(S(CH_3)_2)Cu(SCH_3)_2Cu(Im)(CH_3CONHCH_3)$, representing the Cu_A center], Ryde and co-workers[369] conclude that variation in the axial ligand does not likely change the structure or reduction potential of Cu_A significantly. The authors rather suggest a small change in stiff bonds (of the core structure) in Cu_A as a more important factor.

6.2. Cu_A Site Synthetic Models

The characteristic features of the binuclear Cu_A electron-transfer center are its fully delocalized MV ($Cu^{II}Cu^I \leftrightarrow Cu^ICu^{II} \equiv Cu^{1.5}\cdots Cu^{1.5}$) nature, a so-called class III nature,[370] meaning from the inorganic chemistry literature that it is delocalized even at low temperatures. Further, the extremely short Cu···Cu distance and apparent metal−metal bonding, with thiolate bridging, makes the heme−copper oxidase and nitrous oxide reductase Cu_A electron-transfer center unique. In the past 10 years, there have been considerable inorganic chemistry advances, especially in the generation of class III dicopper complexes, also possessing very short Cu···Cu separations. Included in these are systems that employ macrobicylic polyaza,[371−375] μ-1,3-carboxylate,[376−380] and deprotonated urea[381] ligands.

Nelson,[371] Barr,[374] Thomson and McGarvey,[382] and their co-workers have synthesized MV dicopper complexes with the formula $[Cu_2L]^{3+}$ (**67a**, **68**, **69a**) (Figure 26), each using very similar macrobicyclic octaaza ligands. Compound **67a** contains an unsaturated Schiff base ligand, whereas the ligand in **68** is the saturated reduced form. Complex **69a** is a variation of **67a** with a longer alkyl chain between nitrogen atom donors. These appear to be the first examples of complexes with short Cu−Cu distances as in Cu_A.

The structures of **67a**, **68**, and **69a** have been determined by X-ray crystallography, revealing that each copper ion has almost identical trigonal bipyramidal geometry, with Cu−Cu distances of 2.380(5), 2.364(1), and 2.419(1), respectively. EPR[383] and electronic absorption[382] spectroscopies have revealed the presence of a Cu−Cu bond between the two metal ions through direct orbital (d_{z^2}) overlap (Table 15). EPR spectra obtained for these complexes display the characteristic seven-line pattern arising from spin delocalization over the two copper ($I = {}^3/_2$) ions. The hyperfine couplings $A_\perp$ in **67a**, **68**, and **69a** are relatively large compared to that found for the Cu_A site of C*c*O (Table 14), indicating that these model complexes do not have the extensive delocalization of spin density onto the ligands found in Cu_A.[383] Despite the differences in unsaturation of the ligand skeleton, **67a**, **68**, and **69a** have similar electronic absorption spectra, with quite intense ($\epsilon > 1000$ M^{-1} cm^{-1}) features in the near-IR region (Table 15). MCD, resonance Raman, and theoretical studies confirm that the visible and near-IR absorption bands originate from d−d transitions of coupled metal centers, and the most intense feature of the near-IR absorption corresponds to a $\sigma \rightarrow \sigma^*$ transition.[384] Resonance Raman studies[373] also show that the Cu−Cu bonds in **67a**, **68**, and **69a** are much stronger than that in the natural Cu_A site, suggesting that the weaker Cu−Cu interaction in the enzyme reflects the bonding interaction between copper and the thiolate bridging,

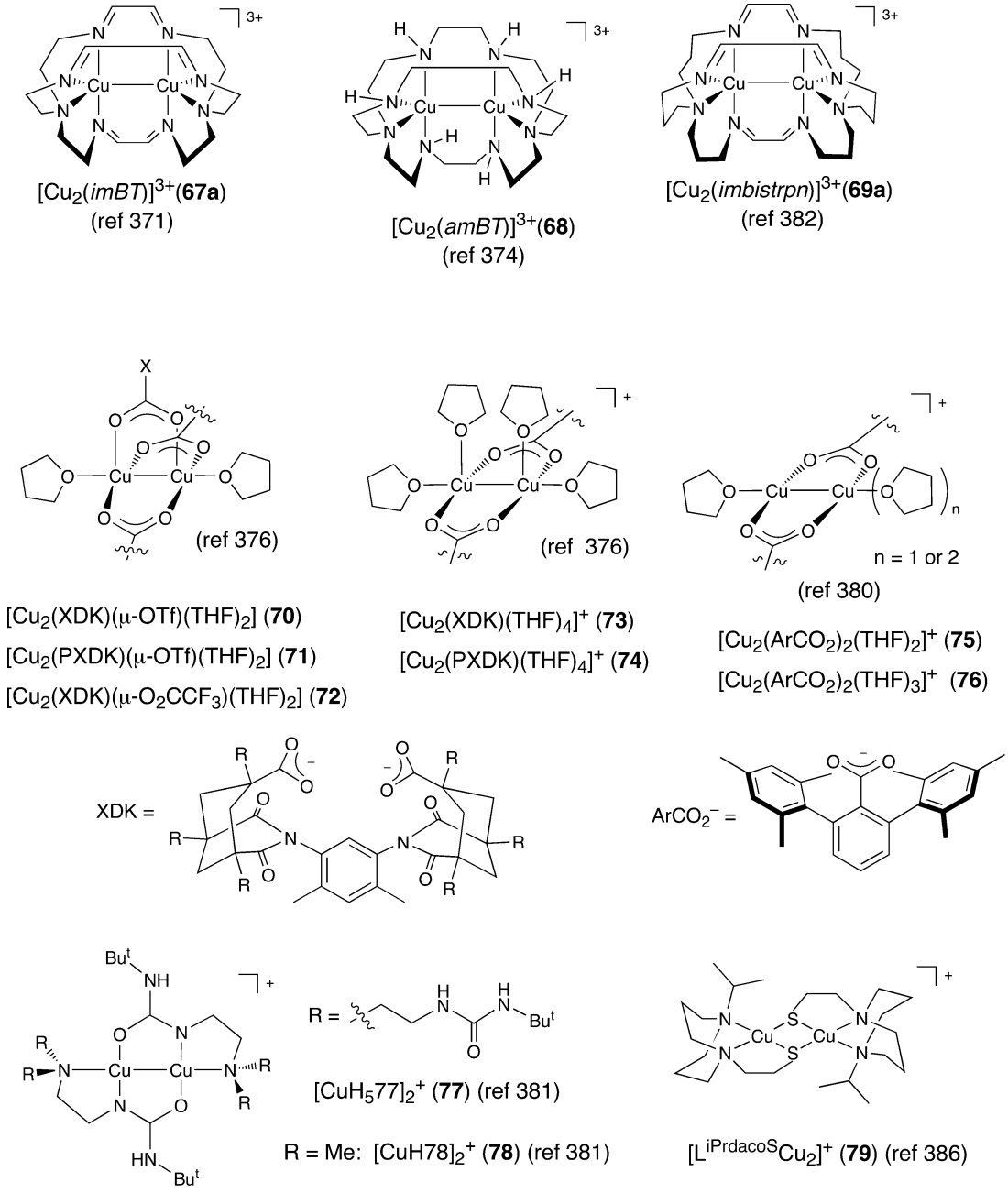

Figure 26. Mixed-valence dicopper(I,II) complexes.

Table 15. Spectroscopic Features of the Selected Mixed-Valence Cu_A Model Complexes

	67a	68	73	77	79
Cu−Cu distance, Å	2.385(5)	2.364	2.4246(12)	2.39	2.9306(9)
EPR	7 lines	7 lines	7 lines	7 lines	7 lines
	$g_{\|\|} = 2.004$	$g_{\|\|} = 2.02$	$g_1 = 2.030$	$g = 2.023$	$g_1 = 2.010$
	$g_\perp = 2.148$	$g_\perp = 2.15$	$g_2 = 2.158$	$g = 2070$	$g_2 = 2.046$
			$g_3 = 2.312$	$g = 2.197$	$g_3 = 2.204$
	$A_{\|\|} = 11$ G	$A_{\|\|} = 22$ G	$A_1 = 20.0$ G	$A = 14$ G	$A_2 = 36.3$ G
	$A_\perp = 111$ G	$A_\perp = 115$ G	$A_2 = 55.0$ G	$A = 38$ G	$A_3 = 49.9$ G
			$A_3 = 122.5$ G	$A = 147$ G	
UV−vis, nm (ϵ, M^{-1} cm^{-1})	600−650 (1500−3500)	662 (2900)	536 (1600)	466 (1600)	358 (2700)
	750−780 (5000)	736 (4500)	923 (1200)	568 (1400)	602 (800), 786 (sh)
				707 (4000)	1466 (1200)
ref	371, 372	374	376	381	386

which may play an important role in its ET functionality. In a separate Raman excitation profile and calculation study,[375] the existence of the isomeric forms of **68** is revealed, in which the torsional coordinate $N_{eq}-Cu-Cu-N_{eq}$ is strongly coupled to the Cu−Cu bond stretch, influencing electronic structure and the potential energy surface of the complex. Although such behavior is not yet apparent in the C*c*O Cu_A site, the authors[375] suggest that the possibility of such control by a subtle change in the

ligand environment could be important in the enzyme function.

The one-electron-reduced form of the MV complexes **67a** and **69a**, dicopper(I) compounds $[Cu^{I}_2(im\text{BT})]^{2+}$ (**67b**), and $[Cu^{I}_2(imbistrpn)]^{2+}$ (**69b**) have also been synthesized.[373] The X-ray crystal structures of **67b** and **69b** reveal considerable elongation in the Cu−Cu bond distances: 2.380(5) → 2.448(1) Å for **67a** → **67b**; 2.491(1) → 2.928(4) Å for **69a** → **69b**. A similar trend in the Cu−Cu distance change is also observed in the enzyme Cu_A site (see Table 13).

Another group of class III MV dicopper complexes contain carboxylate-bridging ligands (compounds **70**−**76**, Figure 26). Lippard and co-workers[376] have utilized the *m*-xylenediamine bis(Kemp's triacid imide) (H_2XDK) or the propyl derivative of H_2XDK (H_2PXDK) as bridging ligands, in which the effects of steric hindrance and preorganization of the ligating carboxylate groups stabilize the mixed-valence core. In this system, the copper ions are coordinated by oxygen atom ligands, including negatively charged carboxylate and neutral oxygen atom from THF, in contrast to the octaazacryptand chelates, which provide only neutral nitrogen donor atoms for copper (vide supra). Despite the quite different ligand environment, the MV complexes **70**−**74** reveal physical properties very similar to those in **67a**, **68**, and **69a**. X-ray crystal structures of $[Cu_2(XDK)(\mu\text{-OTf})(THF)_2]$ (**70**), $[Cu_2(XDK)(\mu\text{-}O_2CCF_3)(THF)_2]$ (**72**), and $[Cu_2(PXDK)(THF)_4]$ (**74**) reveal that each copper ion has a square pyramidal geometry with short Cu···Cu distances of 2.4093(8), 2.3988(8), and 2.4246(12) Å, respectively. EPR studies demonstrate that the complexes **70**−**74** have fully delocalized electronic structures, again exhibiting seven-line signals (Table 15). Molecular orbital calculations on simplified models of **70**−**74** have also been carried out, revealing a Cu−Cu-bonding interaction in SHOMO and SOMO, which comprise σ-type overlap between the two $d_{x^2-y^2}$ orbitals. In a complementary approach, Tolman, Que, and co-workers have prepared similar class III MV dicopper compounds $[Cu_2(ArCO_2)_2(THF)_n]^+$ (**75** and **76**), employing a self-assembly strategy with sterically hindered benzoate ligands (Figure 26).[380] Both **75** and **76** have characteristic spectroscopic features for the fully delocalized $Cu^{1.5}Cu^{1.5}$ cores, including a short Cu···Cu distance [e.g., 2.3876(12) Å for **76**] and the seven-line EPR spectral pattern. An unusually large solvent dependence of UV−vis maxima in the low-energy regions is observed (e.g., for **75**, 736 to 788 to 941 nm for CH_2Cl_2, toluene, and THF, respectively). The researchers explain this behavior by a perturbation of the metal−metal interactions caused by the solvent or counterion binding. Using the concept of "μ-carboxylate bridging" in synthesizing fully delocalized MV dicopper complexes, several other examples have also been reported.[377−379,385]

Borovik and co-workers[381] have prepared their MV dicopper complexes, utilizing the tripodal ligand tris-[(*N′-tert*-butylureayl)-*N*-ethyl)]amine (H_6**77**), which has three *N*-ethylene-*N′-tert*-butyl urea arms attached to an apical nitrogen atom (Figure 26). The fully delocalized MV complex **77** has been characterized by X-ray crystallography, revealing that the two copper ions are linked through two mono-deprotonated urea ligands, which coordinate as a μ-1,3-(κN:κO) ureate bridge to produce a Cu···Cu distance of 2.39 Å (Table 15). A similar type III copper complex, **78**, has been also prepared with the analogous bidentate ligand (Figure 26). The structural properties of the $Cu^{1.5}Cu^{1.5}$ core in **78** are nearly identical to those in **77**. Both complexes also have a fully delocalized electronic structure, as judged by EPR spectroscopy.

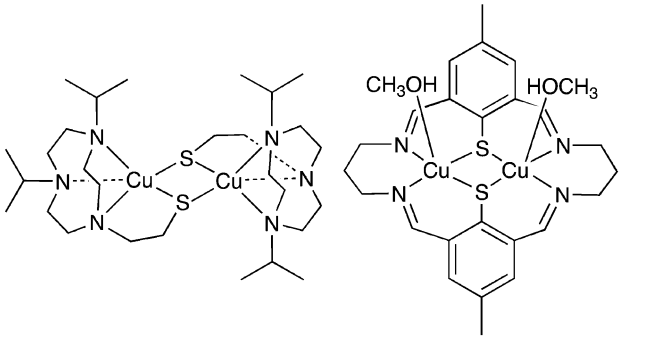

$[L^{N3S}Cu_2]^+$ (**80**) (ref 387) $[Cu_2(L)(HOMe)_2(NO_3^-)]^+$ (**81**) (ref 388)

Figure 27. Thiolate-bridged dicopper(II) complexes.

Tolman and co-workers[386] have reported the first example of dithiolate-bridged MV complex $[(L^{i\text{Prdaco}S}\text{-}Cu)_2](O_3SCF_3)$ (**79**) (Figure 26) that closely mimics the MV-Cu_A geometry and other spectroscopic features. Complex **79** is synthesized from a reaction mixture with a 3:2 ratio of $NaL^{i\text{Prdaco}S}$ and $Cu(O_3SCF_3)_2$, where the extra half-equivalent of $NaL^{i\text{Prdaco}S}$ provides a reducing equivalent for copper(II), affording the MV complex. The X-ray crystal determination of **79** reveals a planar MV Cu_2S_2 core with a Cu···Cu distance of 2.92 Å, which is considerably longer than that found in protein Cu_A structures (Table 15). The MV description of **79** is further supported by X-band EPR spectroscopy, exhibiting the seven-line hyperfine pattern (Table 15). Complex **79** has less intense and red-shifted visible bands compared to Cu_A, seen by UV−vis spectroscopy. The class III (fully delocalized) MV $\psi \rightarrow \psi^*$ transition of **79** is also observed at 5600 cm^{-1} by near-IR resonance Raman spectroscopy, at a much lower energy than that observed for Cu_A ($\sim$13000 cm^{-1}).[361,365,366] The electronic structure of **79**, in comparison with that of Cu_A, has been further studied through absorption, MCD, and X-ray absorption spectroscopies, and an MO-splitting description has been provided.[361,365,366] The conclusion is that valence delocalization in **79** is mediated by the bridging thiolate ligands rather than by direct Cu−Cu overlap; in Cu_A (with direct short Cu−Cu bond), electron delocalization is provided by both Cu−Cu and Cu−S interactions.

Although homovalent dicopper(II) species are not observed in enzyme Cu_A sites, studies of such complexes can increase the understanding of the geometric and electronic structures of related MV Cu_2S_2 cores. As an analogue of $[(L^{i\text{Prdaco}S}Cu)_2](O_3SCF_3)$ (**79**), Tolman and co-workers[387] have also synthesized a thiolate-bridged dicopper(II) complex $[\{(L^{N3S})Cu\}_2]^{2+}$ (**80**) (Figure 27), utilizing a 1,4-diisopropyl-1,4,7-

triazacyclononane (L^{N3S}) ligand. The X-ray crystal structure of **80** reveals a distinct "butterfly" distortion of the $Cu_2(\mu\text{-}SR)_2$ core with a Cu···Cu distance of 3.34 Å, which is significantly longer than the core structure of the MV analogue **79**. Complex **80** is EPR silent, suggesting magnetic coupling between the two Cu(II) ions, and further variable temperature variable field (VTVH) magnetic circular dichroism (MCD) intensity measurements reveal that **80** has an $S = 1$ ferromagnetic ground state.[361] Low-temperature solid-state absorption and MCD spectra of **80** have been also obtained, exhibiting spectral features similar to those from MV analogue **79**, with the dramatic exception of the latter possessing the intense near-IR feature typical of MV systems (vide supra).

Schröder and co-workers[388] have synthesized a dicopper(II) complex $[Cu_2L(HOMe)_2(NO_3^-)]^+$ (**81**) (Figure 27), utilizing a binucleating ligand that contains two thiolate-bridging groups for copper. Complex **81** is prepared from a metal displacement process involving $Cu(NO_3)_2$ reaction with a ligand–dizinc(II) complex $[Zn_2L(O_2CMe)]^+$. The structure of **81** has been determined by X-ray crystallography, revealing the Cu···Cu distance of 3.26 Å with a Cu_2S_2 core that is distorted in a manner similar to that found in **80**. Complex **81** shows two reversible one-electron reductions by coulometry, at −0.605 and −0.805 V (vs Fc/Fc^+), assigned to the formation of corresponding $[Cu^{II}Cu^{I}]$ and $[Cu^{I}Cu^{I}]$ complexes. No interactions between the two copper ions in **81** are observed from magnetochemical measurements ($\mu_{eff} = 1.8\ \mu_B$) and EPR spectroscopy.

7. Concluding Remarks

Great strides have been made in the synthetic modeling of heme–copper oxidases. The overall purpose of such studies is to elucidate fundamental aspects of the relevant coordination chemistry, metal ion ligation, coordination structures, spectroscopy and spectroscopic structural correlation, and reactivity. Interests and approaches have changed somewhat since the 1995 and subsequently reported enzyme X-ray structures, which of course have given a much stronger basis for any conclusions about spectroscopy, reactivity, and function. Nonetheless, there are many unresolved issues and new questions and directions to consider.

As mentioned, many modeling investigations have focused on synthetic approaches for generating bridged and oxidized form $Fe^{III}–X–Cu^{II}$ assemblies, trying to get at a possible identity for X, and to resolve issues about magnetic coupling between the heme and copper(II) centers. In fact, we conclude that these issues are not yet resolved. In resting state oxidized enzyme, water, and/or hydroxide would appear to be bound both to iron and to copper ions, and with >4.3 Å (minimally) heme a_3 Fe and Cu_B distances observed thus far, it seems most likely that there is at best weak magnetic coupling between the metal centers, as has been suggested from a few of the magnetic or spectroscopic studies (see section 4.1). Other questions are, what are the "fast" and "slow" forms of the enzyme (see section 4.1) in terms of metal ion ligation, coordination geometries, or other factors? It does not appear either model studies or the enzyme X-ray structural have yet revealed relevant insights.

Perhaps one of the most successful model investigations comes from Holm and co-workers, with a series of cyanide-bridged heme–copper assemblies (section 4.2.2). The systematic approach and thorough structural and physical characterization lead to the strong conclusion that cyanide binding and cyanide toxicity can or do involve a cyanide bridging between heme a_3 iron and Cu_B. Although the biological relevance is clear, additional benefits come by way of the new contributions to basic inorganic chemistry.

Recent significant advances also have come in the discovery and characterization by the groups of Holm and Karlin of μ-oxo and μ-hydroxo heme–Cu assemblies, derived either from acid–base chemistry or from the dioxygen reactivity of reduced species [reactions of iron(II) and copper(I) complexes and subsequent O–O cleavage via disproportionation]. The relevance to actual enzyme chemistry is unclear, but these heterobinuclear heme–Cu compounds are remarkable in their kinetic stability, as (porphyrinate)Fe^{III}–OH and especially μ-oxo [(porphyrinate)-$Fe^{III}]_2$–O complexes are thermodynamic sinks. Again, new coordination chemistry advances, synthetic, structural, and spectroscopic, have come about from these studies intended to shed light on heme–copper oxidase chemistry. The chemistry of the μ-oxo heme–copper assemblies will have continuing interest with respect to enzyme modeling. We suggest that, for example, these compounds may be excellent precursors for reactions with hydrogen peroxide, potentially leading to species of interest (i.e., compound **P** or **F** or other relevant transients) and relevance to the enzyme O_2 reduction pathway.

The newest directions in heme–copper oxidase modeling have come from examination of compounds with reduced heme and copper ion complex 1:1 mixtures or heterobinuclear constructs. Thus, generation and characterization of carbon monoxide adducts of heme and/or copper provide preliminary insights into the binding of this O_2 surrogate and allow probing of the heme–copper environment. However, it is dioxygen reactivity that has really led to exciting developments, including biomimetic functional modeling studies using electrochemical approaches (see paper by Collman et al.),[90] and O_2 reactivity studies leading to discrete superoxo–heme (with copper present) and heme–peroxo–copper assemblies. The latter may be directly relevant to an enzyme transient intermediate or may be a precursor to such (i.e., by protonation giving a heme hydroperoxo Fe^{III}–OOH···Cu^{II} moiety). Collman reported the first example of a heme–peroxo–copper complex in 1994, and Karlin's group has greatly developed this area, reporting a variety of examples also demonstrating that peroxo spectroscopic signatures (and perhaps structures) can be influenced by binucleating ligand superstructure and copper-ligand denticity. Naruta recently reported the first X-ray structure, confirming the nature of such species, with an example of an unsymmetrically bridged peroxo moiety bound to the heme in a side-on η^2 fashion, whereas it is η^1 to copper (section 3.2.1). Thus, there

are very promising future prospects for successful model compound study of dioxygen reactivity in a heme−copper environment. Much still needs to be done in characterizing these O_2-derived complex structures, including electronic/spectroscopic studies. Does side-on and end-on peroxo ligation exist, and what are the structural−spectroscopic implications and consequences for reactivity? Most of the complexes studied by Karlin and Naruta are high-spin; what will happen in the presence of a strong axial base ligand (as is present as the His proximal group at heme a_3) in terms of spin-state of the heme model? Will this alter peroxo structure and subsequent reactivity? Very importantly, reactivity studies of these heme−peroxo complexes with electrons/protons will need to be carried out, attempting to mimic the enzyme O_2 reduction pathway(s) and the O−O-bond cleavage process.

Another exciting new direction for modeling comes from the relatively recent revelation concerning the heme−copper oxidase Cu−ligand covalent histidine−tyrosine cross-link. Model studies have begun, but much remains for the future in order to understand how this alters Cu_B or Tyr redox potential or the acid−base (p*K*) behavior of the His or Tyr or Cu_B ligand(s) present. And what is the connection to the O−O bond cleavage? Is the His−Tyr group an electron and/or proton source, or other? We should shortly see model compounds that incorporate a heme and copper in a binucleating ligand assembly, along with a model for the His−Tyr cross-link. A very interesting question that should be addressed is how in fact does the His−Tyr cross-link form in the first place? Does the oxidative coupling (formally) of a His and Tyr residue require O_2 or hydrogen peroxide? Does it require only Cu_B or both heme and Cu metal centers? Is the proenzyme first reaction turnover (i.e., the post-translational modification step) evolved to form the His−Tyr link and can models be designed to help elucidate the mechanism of this process?

The Cu_A dicopper center is a relatively exciting new species or prosthetic group in bioinorganic chemistry, as a one-electron transfer conduit for many heme−copper oxidases and nitrous oxide reductase. It has novel features, probably the first with a copper−copper bond, a stable mixed-valent delocalized (formally) $Cu^{1.5}$−$Cu^{1.5}$ redox state, and cysteine-bridging ligands. Some beautiful molecules have been described in the past 10 years, possessing very short Cu···Cu distances and quite probably metal−metal bonds. With its sulfur thiolate bridges and its stabilized mixed-valent delocalized state, the Tolman and co-worker model compound (section 6.2) is very elegant and an achievement in bioinorganic synthetic modeling. Yet, it is imperfect as it does not shuttle (electrochemically) between the mixed-valent and fully reduced dicopper(I) state, nor does it possess a short Cu···Cu distance. Thus, to fully elucidate its chemical nature, still better Cu_A models are needed, and the considerable challenge will be to find a way to synthesize this dicopper entity, which is surely kinetically stabilized by its biological environment. Researchers must find a synthetic kinetic pathway to generate a model with thiolate bridges, accessible fully reduced and mixed-valent states, and a copper−copper bond.

Although synthetic modeling of the redox-active heme−copper oxidase metal centers and His−Tyr cross-link has considerably advanced, significant and exciting future challenges remain.

8. Abbreviations

HCO	heme−copper oxidase
C*c*O	cytochrome *c* oxidase
MV	mixed valence
FR	fully reduced
TMPA	tris(2-pyridylmethyl)amine
TPP	tetraphenylporphyrinate
F_8TPP	tetrakis(2,6-difluorophenyl)porphyrinate
OEP	octaethylporphyrinate
TMP	tetramesitylporphyrinate
$CoCp_2$	cobaltocene
THF	tetrahydrofuran
ESI-MS	electron spray ionization mass spectrometry
EXAFS	extended X-ray absorption fine structure
EPR	electron paramagnetic resonance
XAS	X-ray absorption spectroscopy
MCD	magnetic circular dichroism
TACN	triazacyclononane
DHIm	1,5-dicyclohexylimidazole
PY2	bis(pyridylethyl)amine
MePY2	*N*,*N*-bis[2-(2-pyridylethyl]methylamine
HO	heme oxygenase
1,2-Me_2IM	1,2-dimethylimidazole
aib_3	tripeptide of α-aminoisobutyric acid
OTf	triflate
GcH	glycyl-glycyl-L-His-methylamine
TMEDA	*N*,*N*,*N*′,*N*′-tetramethylethylenediamine
phen	1,10-phenanthroline
dba	*trans*,*trans*-dibenzylideneacetone
ET	electron transfer
N_2OR	nitrous oxide reductase

9. Note Added in Proof

After submission of this paper, Naruta and co-workers (Liu et al. *Chem. Commun.* **2004**, 120) reported a new porphyrin with a covalently appended copper chelate possessing a cross-linked imidazole−phenol group; the iron(II)−copper(I) complex with this ligand reacts with dioxygen to form a low-temperature stable peroxo species.

10. Acknowledgment

We thank the National Institutes of Health (K.D.K., GM60353) and CONICET-Argentina and Universidad Nacional de San Luis-Argentina (E.E.C.) for financial support in the preparation of this paper.

11. References

(1) Kitajima, N. *Adv. Inorg. Chem.* **1992**, *39*, 1.
(2) Collman, J. P.; Boulatov, R.; Sunderland, C. J. *Porphyrin Handb.* **2003**, *11*, 1.
(3) Karlin, K. D. *Science* **1993**, *261*, 701.
(4) Momenteau, M.; Reed, C. A. *Chem. Rev.* **1994**, *94*, 659.
(5) Traylor, T. G.; Traylor, P. S. In *Active Oxygen: Active Oxygen in Biochemistry*; Valentine, J. S., Foote, C. S., Greenberg, A., Liebman, J. F., Eds.; Chapman and Hall: New York, 1995.
(6) (a) Mirica, L. M.; Ottenwaelder, X.; Stack, T. D. P. *Chem. Rev.* **2004**, *104*, 1013. (b) Lewis, E. A.; Tolman, W. B. *Chem. Rev.* **2004**, *104*, 1047.
(7) Que, L., Jr.; Tolman, W. B. *Angew. Chem., Int. Ed.* **2002**, *41*, 1114.

(8) Zhang, C. X.; Liang, H.-C.; Humphreys, K. J.; Karlin, K. D. In *Catalytic Activation of Dioxygen by Metal Complexes*; Simandi, L., Ed.; Kluwer: Dordrecht, The Netherlands, 2003; Vol. 26, Catalysis by Metal Complexes; James, Brian R., van Leewen, Piet W. N. M., Eds.
(9) Karlin, K. D.; Zuberbühler, A. D. In *Bioinorganic Catalysis*, 2nd ed., revised and expanded; Reedijk, J., Bouwman, E., Eds.; Dekker: New York, 1999.
(10) Ferguson-Miller, S.; Babcock, G. T. *Chem. Rev.* **1996**, *96*, 2889.
(11) Michel, H.; Behr, J.; Harrenga, A.; Kannt, A. *Annu. Rev. Biophys. Biomol. Struct.* **1998**, *27*, 329.
(12) García-Horsman, J. A.; Barquera, B.; Rumbley, J.; Ma, J.; Gennis, R. B. *J. Bacteriol.* **1994**, *176*, 5587.
(13) Calhoun, M. W.; Thomas, J. W.; Gennis, R. B. *Trends Biochem. Sci.* **1994**, *19*, 325−330.
(14) Babcock, G. T.; Wikström, M. *Nature* **1992**, *356*, 301.
(15) Iwata, S.; Ostermeier, C.; Ludwig, B.; Michel, H. *Nature* **1995**, *376*, 660.
(16) Tsukihara, T.; Aoyama, H.; Yamashita, E.; Tomizaki, T.; Yamaguchi, H.; Shinzawa-Itoh, K.; Nakashima, R.; Yaono, R.; Yoshikawa, S. *Science* **1995**, *269*, 1069.
(17) Tsukihara, T.; Aoyama, H.; Yamashita, E.; Tomizaki, T.; Yamaguchi, H.; Shinzawa-Itoh, K.; Nakashima, R.; Yaono, R.; Yoshikawa, S. *Science* **1996**, *272*, 1136.
(18) Yoshikawa, S.; Shinzawa-Itoh, K.; Nakashima, R.; Yaono, R.; Yamashita, E.; Inoue, N.; Yao, M.; Jei-Fei, M.; Libeu, C. P.; Mizushima, T.; Yamaguchi, H.; Tomizaki, T.; Tsukihara, T. *Science* **1998**, *280*, 1723.
(19) Ostermeier, C.; Harrenga, A.; Ermler, U.; Michel, H. *Proc. Natl. Acad. Sci. U.S.A.* **1997**, *94*, 10547.
(20) Harrenga, A.; Michel, H. *J. Biol. Chem.* **1999**, *274*, 33296.
(21) Proshlyakov, D. A.; Pressler, M. A.; Babcock, G. T. *Proc. Natl. Acad. Sci. U.S.A.* **1998**, *95*, 8020.
(22) Babcock, G. T. *Proc. Natl. Acad. Sci. U.S.A.* **1999**, *96*, 12971.
(23) Proshlyakov, D. A.; Pressler, M. A.; DeMaso, C.; Leykam, J. F.; DeWitt, D. L.; Babcock, G. T. *Science* **2000**, *290*, 1588.
(24) Hill, B. C. *J. Biol. Chem.* **1991**, *266*, 2219.
(25) Pan, L. P.; Hibdon, S.; Liu, R. Q.; Durham, B.; Millett, F. *Biochemistry* **1993**, *32*, 8492.
(26) Malatesta, F.; Nicoletti, F.; Zickermann, V.; Ludwig, B.; Brunori, M. *FEBS Lett.* **1998**, *434*, 322.
(27) Roberts, V. A.; Pique, M. E. *J. Biol. Chem.* **1999**, *274*, 38051.
(28) Zhen, Y.; Hoganson, C. W.; Babcock, G. T.; Ferguson-Miller, S. *J. Biol. Chem.* **1999**, *274*, 38032.
(29) Winkler, J. R.; Malmstroem, B. G.; Gray, H. B. *Biophys. Chem.* **1995**, *54*, 199.
(30) Soulimane, T.; Buse, G.; Bourenkov, G. P.; Bartunik, H. D.; Huber, R.; Than, M. E. *EMBO J.* **2000**, *19*, 1766.
(31) Svensson-Ek, M.; Abramson, J.; Larsson, G.; Tornroth, S.; Brzezinski, P.; Iwata, S. *J. Mol. Biol.* **2002**, *321*, 329.
(32) Abramson, J.; Riistama, S.; Larsson, G.; Jasaitis, A.; Svensson-Ek, M.; Laakkonen, L.; Puustinen, A.; Iwata, S.; Wikstrom, M. *Nat. Struct. Biol.* **2000**, *7*, 910.
(33) Kitagawa, T.; Ogura, T. *Prog. Inorg. Chem.* **1997**, *45*, 431.
(34) Adelroth, P.; Ek, M.; Brzezinski, P. *Biochim. Biophys. Acta* **1998**, *1367*, 107.
(35) Einarsdottir, O. *Biochim. Biophys. Acta* **1995**, *1229*, 129.
(36) Gibson, Q. H.; Greenwood, C. *Biochem. J.* **1963**, *86*, 541.
(37) Greenwood, C.; Gibson, Q. H. *J. Biol. Chem.* **1967**, *242*, 1782.
(38) MacArthur, R.; Sucheta, A.; Chong, F. F. S.; Einarsdóttir, O. *Proc. Natl. Acad. Sci. U.S.A.* **1995**, *92*, 8105.
(39) Hill, B. C.; Greenwood, C. *Biochem. J.* **1983**, *215*, 659.
(40) Verkhovsky, M. I.; Morgan, J. E.; Puustinen, A.; Wikstrom, M. *Biochemistry* **1996**, *35*, 16241.
(41) Varotsis, C.; Woodruff, W. H.; Babcock, G. T. *J. Am. Chem. Soc.* **1989**, *111*, 6439.
(42) Ogura, T.; Takahashi, S.; Shinzawa-Itoh, K.; Yoshikawa, S.; Kitagawa, T. *J. Am. Chem. Soc.* **1990**, *112*, 5630.
(43) Han, S.; Ching, Y. C.; Rousseau, D. L. *Proc. Natl. Adac. Sci. U.S.A.* **1990**, *87*, 2491.
(44) Han, S.; Ching, Y. C.; Rousseau, D. L. *Biochemistry* **1990**, *29*, 1380.
(45) Ogura, T.; Takahashi, S.; Hirota, S.; Shinzawa-Itoh, K.; Yoshikawa, S.; Appelman, E. H.; Kitagawa, T. *J. Am. Chem. Soc.* **1993**, *115*, 8527.
(46) Oliveberg, M.; Malmström, B. G. *Biochemistry* **1992**, *31*, 3560.
(47) Blackmore, R. S.; Greenwood, C.; Gibson, Q. H. *J. Biol. Chem.* **1991**, *266*, 19245.
(48) Varotsis, C.; Zhang, Y.; Appelman, E. H.; Babcock, G. T. *Proc. Natl. Acad. Sci. U.S.A.* **1993**, *90*, 237.
(49) Chance, B.; Saronio, C.; Leigh, J. S., Jr. *J. Biol. Chem.* **1975**, *250*, 9226.
(50) Morgan, J. E.; Verkhovsky, M. I.; Wikstrom, M. *Biochemistry* **1996**, *35*, 12235.
(51) Weng, L. C.; Baker, G. M. *Biochemistry* **1991**, *30*, 5727.
(52) Proshlyakov, D. A.; Ogura, T.; Shinzawa-Itoh, K.; Yoshikawa, S.; Appelman, E. H.; Kitagawa, T. *J. Biol. Chem.* **1994**, *269*, 29385.
(53) Proshlyakov, D. A.; Ogura, T.; Shinzawa-Itoh, K.; Yoshikawa, S.; Kitagawa, T. *Biochemistry* **1996**, *35*, 8580.
(54) Fabian, M.; Wong, W. W.; Gennis, R. B.; Palmer, G. *Proc. Natl. Acad. Sci. U.S.A.* **1999**, *96*, 13114.
(55) Einarsdottir, O.; Szundi, I.; Van Eps, N.; Sucheta, A. *J. Inorg. Biochem.* **2002**, *91*, 87.
(56) Blomberg, M. R. A.; Siegbahn, P. E. M.; Wikstroem, M. *Inorg. Chem.* **2003**, *42*, 5231.
(57) Hill, B. C.; Greenwood, C. *Biochem. J.* **1984**, *218*, 913.
(58) Han, S.; Ching, Y. C.; Rousseau, D. L. *Proc. Natl. Acad. Sci. U.S.A.* **1990**, *87*, 8408.
(59) Verkhovsky, M. I.; Morgan, J. E.; Wikstrom, M. *Biochemistry* **1994**, *33*, 3079.
(60) Sucheta, A.; Istvan Szundi, I.; Einarsdóttir, O. *Biochemistry* **1998**, *37*, 17905.
(61) Karpefors, M.; Aedelroth, P.; Namslauer, A.; Zhen, Y.; Brzezinski, P. *Biochemistry* **2000**, *39*, 14664.
(62) Morgan, J. E.; Verkhovsky, M. I.; Palmer, G.; Wikstroem, M. *Biochemistry* **2001**, *40*, 6882.
(63) Szundi, I.; Liao, G.-L.; Einarsdottir, O. *Biochemistry* **2001**, *40*, 2332.
(64) Paula, S.; Sucheta, A.; Szundi, I.; Einarsdottir, O. *Biochemistry* **1999**, *38*, 3025.
(65) Varotsis, C.; Babcock, G. T. *Biochemistry* **1990**, *29*, 7357.
(66) Hallén, S.; Nilsson, T. *Biochemistry* **1992**, *31*, 11853.
(67) Szundi, I.; Van Eps, N.; Einarsdöttir, O. *Biochemistry* **2003**, *42*, 5074.
(68) Wikström, M.; Verkhovsky, M. I. *Biochim. Biophys. Acta* **2002**, *1555*, 128.
(69) Wikström, M. *Biochim. Biophys. Acta* **2000**, *1458*, 188.
(70) Zaslavsky, D.; Gennis, R. B. *Biochim. Biophys. Acta* **2000**, *1458*, 164.
(71) Han, S.; Ching, Y. C.; Rousseau, D. L. *J. Biol. Chem* **1989**, *264*, 6604.
(72) Han, S.; Ching, Y. C.; Rousseau, D. L. *Nature* **1990**, *348*, 89.
(73) Ogura, T.; Hirota, S.; Proshlyakov, D. A.; Shinzawa-Itoh, K.; Yoshikawa, S.; Kitagawa, T. *J. Am. Chem. Soc.* **1996**, *118*, 5443.
(74) Hill, B. C. *J. Biol. Chem.* **1994**, *269*, 2419.
(75) Aedelroth, P.; Gennis, R. B.; Brzezinski, P. *Biochemistry* **1998**, *37*, 2470.
(76) MacMillan, F.; Kannt, A.; Behr, J.; Prisner, T.; Michel, H. *Biochemistry* **1999**, *38*, 9179.
(77) Blomberg, M. R. A.; Siegbahn, P. E. M.; Babcock, G. T.; Wikström, M. *J. Am Chem. Soc.* **2000**, *122*, 12848.
(78) Blomberg, M. R. A.; Siegbahn, P. E. M.; Babcock, G. T.; Wikström, M. *J. Inorg. Biochem.* **2000**, *80*, 261.
(79) Blomberg, M. R. A.; Siegbahn, P. E. M. *J. Phys. Chem. B* **2001**, *105*, 9375.
(80) Ghiladi, R. A.; Hatwell, K. R.; Karlin, K. D.; Huang, H.-W.; Moeenne-Loccoz, P.; Krebs, C.; Huynh, B. H.; Marzilli, L. A.; Cotter, R. J.; Kaderli, S.; Zuberbuehler, A. D. *J. Am. Chem. Soc.* **2001**, *123*, 6183.
(81) Ghiladi, R. A.; Ju, T. D.; Lee, D.-H.; Moënne-Loccoz, P.; Kaderli, S.; Neuhold, Y.-M.; Zuberbühler, A. D.; Woods, A. S.; Cotter, R. J.; Karlin, K. D. *J. Am. Chem. Soc.* **1999**, *121*, 9885.
(82) Sasaki, T.; Nakamura, N.; Naruta, Y. *Chem. Lett.* **1998**, 351.
(83) Naruta, Y.; Sasaki, T.; Tani, F.; Tachi, Y.; Kawato, N.; Nakamura, N. *J. Inorg. Biochem.* **2001**, *83*, 239.
(84) Chishiro, T.; Shimazaki, Y.; Tani, F.; Tachi, Y.; Naruta, Y.; Karasawa, S.; Hayami, S.; Maeda, Y. *Angew. Chem., Int. Ed.* **2003**, *42*, 2788.
(85) Collman, J. P.; Herrmann, P. C.; Boitrel, B.; Zhang, X.; Eberspacher, T. A.; Fu, L.; Wang, J.; Rousseau, D. L.; Williams, E. R. *J. Am. Chem. Soc.* **1994**, *116*, 9783.
(86) Collman, J. P.; Sunderland, C. J.; Berg, K. E.; Vance, M. A.; Solomon, E. I. *J. Am Chem. Soc.* **2003**, *125*, 6648.
(87) Kim, E.; Helton, M. E.; Wasser, I. M.; Karlin, K. D.; Lu, S.; Huang, H.-W.; Moënne-Loccoz, P.; Incarvito, C. D.; Rheingold, A. L.; Honecker, M.; Kaderli, S.; Zuberbühler, A. D. *Proc. Natl. Acad. Sci. U.S.A.* **2003**, *100*, 3623.
(88) Gunter, M. J.; Mander, L. N.; Murray, K. S. *J. Chem. Soc., Chem. Commun.* **1981**, 799.
(89) Collman, J. P. *Acc. Chem. Res.* **1977**, *10*, 265.
(90) Collman, J. P.; Boulatov, R.; Sunderland, C. J.; Fu, L. *Chem. Rev.* **2004**, *104*, 561.
(91) Nanthakumar, A.; Fox, S.; Murthy, N. N.; Karlin, K. D.; Ravi, N.; Huynh, B. H.; Orosz, R. D.; Day, E. P.; Hagen, K. S.; Blackburn, N. J. *J. Am. Chem. Soc.* **1993**, *115*, 8513.
(92) Karlin, K. D.; Nanthakumar, A.; Fox, S.; Murthy, N. N.; Ravi, N.; Huynh, B. H.; Orosz, R. D.; Day, E. P. *J. Am. Chem. Soc.* **1994**, *116*, 4753.
(93) Du Bois, J.; Mizoguchi, T. J.; Lippard, S. J. *Coord. Chem. Rev.* **2000**, *200−202*, 443.
(94) Chufán, E. E.; Karlin, K. D. *J. Am Chem. Soc.* **2003**, *125*, 16160.
(95) McCandlish, E.; Miksztal, A. R.; Nappa, M.; Sprenger, A. Q.; Valentine, J. S.; Stong, J. D.; Spiro, T. G. *J. Am. Chem. Soc.* **1980**, *102*, 4268.

(96) Ju, T. D.; Ghiladi, R. A.; Lee, D.-H.; van Strijdonck, G. P. F.; Woods, A. S.; Cotter, R. J.; Young, J., V. G.; Karlin, K. D. *Inorg. Chem.* **1999**, *38*, 2244.
(97) Obias, H. V.; van Strijdonck, G. P. F.; Lee, D.-H.; Ralle, M.; Blackburn, N. J.; Karlin, K. D. *J. Am. Chem. Soc.* **1998**, *120*, 9696.
(98) Lee, D.-H.; Wei, N.; Murthy, N. N.; Tyeklár, Z.; Karlin, K. D.; Kaderli, S.; Jung, B.; Zuberbühler, A. D. *J. Am. Chem. Soc.* **1995**, *117*, 12498.
(99) Jacobson, R. R.; Tyeklár, Z.; Karlin, K. D.; Liu, S.; Zubieta, J. *J. Am. Chem. Soc.* **1988**, *110*, 3690.
(100) Tyeklár, Z.; Jacobson, R. R.; Wei, N.; Murthy, N. N.; Zubieta, J.; Karlin, K. D. *J. Am. Chem. Soc.* **1993**, *115*, 2677.
(101) Kim, K.; Lippard, S. J. *J. Am. Chem. Soc.* **1996**, *118*, 4914.
(102) Wilmot, C. M.; Hajdu, J.; McPherson, M. J.; Knowles, P. F.; Phillips, S. E. V. *Science* **1999**, *286*, 1724.
(103) Wilmot, C. M. *Biochem. Soc. Trans.* **2003**, *31*, 493.
(104) Collman, J. P. *Inorg. Chem.* **1997**, *36*, 5145.
(105) Collman, J. P.; Fu, L.; Herrmann, P. C.; Zhang, X. *Science* **1997**, *275*, 949.
(106) Collman, J. P.; Fu, L.; Herrmann, P. C.; Wang, Z.; Rapta, M.; Bröring, M.; Schwenninger, R.; Boitrel, B. *Angew. Chem., Int. Ed. Engl.* **1998**, *37*, 3397.
(107) Collman, J. P.; Schwenninger, R.; Rapta, M.; Bröring, M.; Fu, L. *Chem. Commun.* **1999**, 137.
(108) Collman, J. P.; Rapta, M.; Bröring, M.; Raptova, L.; Schwenninger, R.; Boitrel, B.; Fu, L.; L'Her, M. *J. Am. Chem. Soc.* **1999**, *121*, 1387.
(109) Collman, J. P.; Sunderland, C. J.; Boulatov, R. *Inorg. Chem.* **2002**, *41*, 2282.
(110) Karlin, K. D.; Kaderli, S.; Zuberbühler, A. D. *Acc. Chem. Res.* **1997**, *30*, 139.
(111) Blackman, A. G.; Tolman, W. B. *Struct. Bonding (Berlin)* **2000**, *97*, 179.
(112) Kopf, M.-A.; Neuhold, Y.-M.; Zuberbühler, A. D.; Karlin, K. D. *Inorg. Chem.* **1999**, *38*, 3093.
(113) Kopf, M. A.; Karlin, K. D. *Inorg. Chem.* **1999**, *38*, 4922.
(114) Ghiladi, R. A.; Kretzer, R. M.; Guzei, I.; Rheingold, A. L.; Neuhold, Y.-M.; Hatwell, K. R.; Zuberbühler, A. D.; Karlin, K. D. *Inorg. Chem.* **2001**, *40*, 5754.
(115) Hansson, O.; Karlsson, B.; Aasa, R.; Vanngard, T.; Malmstrom, B. G. *EMBO J.* **1982**, *1*, 1295.
(116) Baldwin, M. J.; Ross, P. K.; Pate, J. E.; Tyeklár, Z.; Karlin, K. D.; Solomon, E. I. *J. Am. Chem. Soc.* **1991**, *113*, 8671.
(117) Pidcock, E.; Obias, H. V.; Abe, M.; Liang, H.-C.; Karlin, K. D.; Solomon, E. I. *J. Am. Chem. Soc.* **1999**, *121*, 1299.
(118) Casella, L.; Monzani, E.; Gullotti, M.; Cavagnino, D.; Cerina, G.; Santagostini, L.; Ugo, R. *Inorg. Chem.* **1996**, *35*, 7516.
(119) Franceschi, F.; Gullotti, M.; Monzani, E.; Casella, L.; Papaefthymiou, V. *Chem. Commun.* **1996**, 1645.
(120) Monzani, E.; Casella, L.; Gullotti, M.; Panigada, N.; Franceschi, F.; Papaefthymiou, V. *J. Mol. Catal. A: Chem.* **1997**, *117*, 199.
(121) Casella, L.; Monzani, E.; Gullotti, M.; Gliubich, F.; De Gioia, L. *J. Chem. Soc., Dalton Trans.* **1994**, 3203.
(122) Sigman, J. A.; Kwok, B. C.; Gengenbach, A.; Lu, Y. *J. Am. Chem. Soc.* **1999**, *121*, 8949.
(123) Sigman, J. A.; Kwok, B. C.; Lu, Y. *J. Am. Chem. Soc.* **2000**, *122*, 8192.
(124) Sigman, J. A.; Kim, H. K.; Zhao, X.; Carey, J. R.; Lu, Y. *Proc. Natl. Acad. Sci. U.S.A.* **2003**, *100*, 3629.
(125) Argade, P. V.; Ching, Y. C.; Rousseau, D. L. *Science* **1984**, *225*, 329.
(126) Wang, J.; Takahashi, S.; Hosler, J. P.; Mitchell, D. M.; Ferguson-Miller, S.; Gennis, R. B.; Rousseau, D. L. *Biochemistry* **1995**, *34*, 9819.
(127) Wang, J.; Takahashi, S.; Rousseau, D. L. *Proc. Natl. Acad. Sci. U.S.A.* **1995**, *92*, 9402.
(128) Varotsis, C.; Vamvouka, M. *J. Phys. Chem. B* **1998**, *102*, 7670.
(129) Das, T. K.; Tomson, F. L.; Gennis, R. B.; Gordon, M.; Rousseau, D. L. *Biophys. J.* **2001**, *80*, 2039.
(130) Park, S.; Pan, L. P.; Chan, S. I.; Alben, J. O. *Biophys. J.* **1996**, *71*, 1036.
(131) Iwase, T.; Varotsis, C.; Shinzawa-Itoh, K.; Yoshikawa, S.; Kitagawa, T. *J. Am. Chem. Soc.* **1999**, *121*, 1415.
(132) Rost, B.; Behr, J.; Hellwig, P.; Richter, O.-M. H.; Ludwig, B.; Michel, H.; Maentele, W. *Biochemistry* **1999**, *38*, 7565.
(133) Dyer, R. B.; Einarsdottir, O.; Killough, P. M.; Lopez-Garriga, J. J.; Woodruff, W. H. *J. Am. Chem. Soc.* **1989**, *111*, 7657.
(134) Woodruff, W. H. *J. Bioenerg. Biomembr.* **1993**, *25*, 177.
(135) Dyer, R. B.; Peterson, K. A.; Stoutland, P. O.; Woodruff, W. H. *Biochemistry* **1994**, *33*, 500.
(136) Varotsis, C.; Kreszowski, D. H.; Babcock, G. T. *Biospectroscopy* **1996**, *2*, 331.
(137) Pinakoulaki, E.; Pfitzner, U.; Ludwig, B.; Varotsis, C. *J. Biol. Chem.* **2002**, *277*, 13563.
(138) Heitbrink, D.; Sigurdson, H.; Bolwien, C.; Brzezinski, P.; Heberle, J. *Biophys. J.* **2002**, *82*, 1.
(139) Stavrakis, S.; Koutsoupakis, K.; Pinakoulaki, E.; Urbani, A.; Saraste, M.; Varotsis, C. *J. Am. Chem. Soc.* **2002**, *124*, 3814.
(140) Ching, E.; Gennis, R. B.; Larsen, R. W. *Biophys. J.* **2003**, *84*, 2728.
(141) Farver, O.; Einarsdottir, O.; Pecht, I. *Eur. J. Biochem.* **2000**, *267*, 950.
(142) Namslauer, A.; Braenden, M.; Brzezinski, P. *Biochemistry* **2002**, *41*, 10369.
(143) Pinakoulaki, E.; Soulimane, T.; Varotsis, C. *J. Biol. Chem.* **2002**, *277*, 32867.
(144) Spiro, T. G.; Kozlowski, P. M. *Acc. Chem. Res* **2001**, *34*, 137.
(145) Collman, J. P.; Fu, L. *Acc. Chem. Res.* **1999**, *32*, 455.
(146) Collman, J. P.; Boulatov, R.; Shiryaeva, I. M.; Sunderland, C. J. *Angew. Chem., Int. Ed.* **2002**, *41*, 4139.
(147) Kretzer, R. M.; Ghiladi, R. A.; Lebeau, E. L.; Liang, H.-C.; Karlin, K. D. *Inorg. Chem.* **2003**, *42*, 3016.
(148) Einarsdottir, O.; Dyer, R. B.; Lemon, D. D.; Killough, P. M.; Hubig, S. M.; Atherton, S. J.; Lopez-Garriga, J. J.; Palmer, G.; Woodruff, W. H. *Biochemistry* **1993**, *32*, 12013.
(149) Kitajima, N.; Fujisawa, K.; Fujimoto, C.; Moro-oka, Y.; Hashimoto, S.; Kitagawa, T.; Toriumi, K.; Tasumi, K.; Nakamura, A. *J. Am. Chem. Soc.* **1992**, *114*, 1277.
(150) Imai, S.; Fujisawa, K.; Kobayashi, T.; Shirasawa, N.; Fujii, H.; Yoshimura, T.; Kitajima, N.; Moro-oka, Y. *Inorg. Chem.* **1998**, *37*, 3066.
(151) Sorrell, T. N.; Borovik, A. S. *J. Am. Chem. Soc.* **1987**, *109*, 4255.
(152) Sorrell, T. N.; Allen, W. E.; White, P. S. *Inorg. Chem.* **1995**, *34*, 952.
(153) Sorrell, T. N.; Jameson, D. L. *J. Am. Chem. Soc.* **1983**, *105*, 6013.
(154) Hellwig, P.; Pfitzner, U.; Behr, J.; Rost, B.; Pesavento, R. P.; von Donk, W.; Gennis, R. B.; Michel, H.; Ludwig, B.; Maentele, W. *Biochemistry* **2002**, *41*, 9116.
(155) Lambry, J.-C.; Vos, M. H.; Martin, J.-L. *J. Phys. Chem. A* **1999**, *103*, 10132.
(156) Das, T. K.; Pecoraro, C.; Tomson, F. L.; Gennis, R. B.; Rousseau, D. L. *Biochemistry* **1998**, *37*, 14471.
(157) Einarsdottir, O.; Killough, P. M.; Fee, J. A.; Woodruff, W. H. *J. Biol. Chem.* **1989**, *264*, 2405.
(158) Bailey, J. A.; Tomson, F. L.; Mecklenburg, S. L.; MacDonald, G. M.; Katsonouri, A.; Puustinen, A.; Gennis, R. B.; Woodruff, W. H.; Dyer, R. B. *Biochemistry* **2002**, *41*, 2675.
(159) Koutsoupakis, K.; Stafrakis, S.; Pinakoulaki, E.; Soulimane, T.; Varotsis, C. *J. Biol. Chem.* **2002**, *277*, 32860.
(160) Oertling, W. A.; Surerus, K. K.; Einarsdottir, O.; Fee, J. A.; Dyer, R. B.; Woodruff, W. H. *Biochemistry* **1994**, *33*, 3128.
(161) Tsubaki, M.; Mogi, T.; Hori, H.; Hirota, S.; Ogura, T.; Kitagawa, T.; Anraku, Y. *J. Biol. Chem.* **1994**, *269*, 30861.
(162) Lauraeus, M.; Wikstrom, M.; Varotsis, C.; Tecklenburg, M. M.; Babcock, G. T. *Biochemistry* **1992**, *31*, 10054.
(163) Gray, K. A.; Grooms, M.; Myllykallio, H.; Moomaw, C.; Slaughter, C.; Daldal, F. *Biochemistry* **1994**, *33*, 3120.
(164) Das, T. K.; Gomes, C. M.; Teixeira, M.; Rousseau, D. L. *Proc. Natl. Acad. Sci. U.S.A.* **1999**, *96*, 9591.
(165) Wang, J.; Gray, K. A.; Daldal, F.; Rousseau, D. L. *J. Am. Chem. Soc.* **1995**, *117*, 9363.
(166) Okuno, D.; Iwase, T.; Shinzawa-Itoh, K.; Yoshikawa, S.; Kitagawa, T. *J. Am. Chem. Soc.* **2003**, *125*, 7209.
(167) Woodruff, W. H.; Einarsdottir, O.; Dyer, R. B.; Bagley, K. A.; Palmer, G.; Atherton, S. J.; Goldbeck, R. A.; Dawes, T. D.; Kliger, D. S. *Proc. Natl. Acad. Sci. U.S.A.* **1991**, *88*, 2588.
(168) Collman, J. P.; Boulatov, R.; Shiryaeva, I. M.; Sunderland, C. J. *Angew. Chem., Int. Ed.* **2002**, *41*, 4139.
(169) Sorrell, T. N.; Borovik, A. S. *Inorg. Chem.* **1987**, *26*, 1957.
(170) Conry, R. R.; Ji, G.; Tipton, A. A. *Inorg. Chem.* **1999**, *38*, 906.
(171) Calhoun, M. W.; Hill, J. J.; Lemieux, L. J.; Ingledew, W. J.; Alben, J. O.; Gennis, R. B. *Biochemistry* **1993**, *32*, 11524.
(172) Fager, L. Y.; Alben, J. O. *Biochemistry* **1972**, *11*, 4786.
(173) Hirota, S.; Iwamoto, T.; Tanizawa, K.; Aduchi, O.; Yamauchi, O. *Biochemistry* **1999**, *38*, 14256.
(174) Jaron, S.; Blackburn, N. J. *Biochemistry* **1999**, *38*, 15086.
(175) Kraulis, P. J. *J. Appl. Crystallogr.* **1991**, *24*, 945.
(176) Pettingill, T. M.; Strange, R. W.; Blackburn, N. J. *J. Biol. Chem.* **1991**, *266*, 16996.
(177) Zhang, H.; Boulanger, M. J.; Mauk, A. G.; Murphy, M. E. P. *J. Phys. Chem. B* **2000**, *104*, 10738.
(178) Jonas, R. T.; Stack, T. D. P. *Inorg. Chem.* **1998**, *37*, 6615.
(179) Rondelez, Y.; Séneque, O.; Rager, M.-N.; Duprat, A. F.; Reinaud, O. *Chem. Eur. J.* **2000**, *6*, 4218.
(180) Baker, G. M.; Palmer, G. *Biochemistry* **1987**, *26*, 3038.
(181) Moody, A. J.; Cooper, C. E.; Rich, P. R. *Biochim. Biophys. Acta* **1991**, *1059*, 189.
(182) Brudvig, G. W.; Morse, R. H.; Chan, S. I. *J. Magn. Reson.* **1986**, *67*, 189.
(183) Barnes, Z. K.; Babcock, G. T.; Dye, J. L. *Biochemistry* **1991**, *30*, 7597.
(184) Kent, T. A.; Young, L. J.; Palmer, G.; Fee, J. A.; Munck, E. *J. Biol. Chem.* **1983**, *258*, 8543.
(185) Kent, T. A.; Muenck, E.; Dunham, W. R.; Filter, W. F.; Findling, K. L.; Yoshida, T.; Fee, J. A. *J. Biol. Chem.* **1982**, *257*, 12489.
(186) Tweedle, M. F.; Wilson, L. J.; Garcia-Iniguez, L.; Babcock, G. T.; Palmer, G. *J. Biol. Chem.* **1978**, *253*, 8065.

(187) Day, E. P.; Peterson, J.; Sendova, M. S.; Schoonover, J.; Palmer, G. *Biochemistry* **1993**, *32*, 7855.
(188) Hagen, W. R. *Biochim. Biophys. Acta* **1982**, *708*, 82.
(189) Watmough, N. J.; Cheesman, M. R.; Gennis, R. B.; Greenwood, C.; Thomson, A. J. *FEBS Lett.* **1993**, *319*, 151.
(190) Oganesyan, V. S.; Butler, C. S.; Watmough, N. J.; Greenwood, C.; Thomson, A. J.; Cheesman, M. R. *J. Am. Chem. Soc.* **1998**, *120*, 4232.
(191) Henkel, G.; Mueller, A.; Weissgraeber, S.; Buse, G.; Soulimane, T.; Steffens, G. C. M.; Nolting, H.-F. *Angew. Chem., Int. Ed.* **1995**, *34*, 1488.
(192) Powers, L.; Lauraeus, M.; Reddy, K. S.; Chance, B.; Wikstroem, M. *Biochim. Biophys. Acta* **1994**, *1183*, 504.
(193) Powers, L.; Chance, B.; Ching, Y.; Angiolillo, P. *Biophys. J.* **1981**, *34*, 465.
(194) Li, P. M.; Gelles, J.; Chan, S. I.; Sullivan, R. J.; Scott, R. A. *Biochemistry* **1987**, *26*, 2091.
(195) Scott, R. A.; Li, P. M.; Chan, S. I. *Ann. N. Y. Acad. Sci.* **1988**, *550*, 53.
(196) Fann, Y. C.; Ahmed, I.; Blackburn, N. J.; Boswell, J. S.; Verkhovskaya, M. L.; Hoffman, B. M.; Wikström, M. *Biochemistry* **1995**, *34*, 10245.
(197) Michel, H. *Proc. Natl. Acad. Sci. U.S.A.* **1998**, *95*, 12819.
(198) Saxton, R. J.; Olson, L. W.; Wilson, L. J. *J. Chem. Soc., Chem. Commun.* **1982**, 984.
(199) Lee, S. C.; Holm, R. H. *J. Am. Chem. Soc.* **1993**, *115*, 11789.
(200) Chang, C. K.; Koo, M. S.; Ward, B. *Chem. Commun.* **1982**, 716.
(201) Scott, M. J.; Zhang, H. H.; Lee, S. C.; Hedman, B.; Hodgson, K. O.; Holm, R. H. *J. Am. Chem. Soc.* **1995**, *117*, 568.
(202) Fox, S.; Nanthakumar, A.; Wikström, M.; Karlin, K. D.; Blackburn, N. J. *J. Am. Chem. Soc.* **1996**, *118*, 24.
(203) Corsi, D. M.; Murthy, N. N.; Young, V. G.; Karlin, K. D. *Inorg. Chem.* **1999**, *38*, 848.
(204) Lim, B. S.; Holm, R. H. *Inorg. Chem.* **1998**, *37*, 4898.
(205) Gunter, M. J.; Berry, K. J.; Murray, K. S. *J. Am. Chem. Soc.* **1984**, *106*, 4227.
(206) Scott, M. J.; Holm, R. H. *J. Am. Chem. Soc.* **1994**, *116*, 11357.
(207) Scott, M. J.; Lee, S. C.; Holm, R. H. *Inorg. Chem* **1994**, *33*, 4651.
(208) Scott, M. J.; Goddard, C. A.; Holm, R. H. *Inorg. Chem.* **1996**, *35*, 2558.
(209) Elliott, C. M.; Jain, N. C.; Cranmer, B. K.; Hamburg, A. W. *Inorg. Chem.* **1987**, *26*, 3655.
(210) Lee, S. C.; Holm, R. H. *Inorg. Chem.* **1993**, *32*, 4745.
(211) Gunter, M. J.; Mander, L. N.; McLaughlin, G. M.; Murray, K. S.; Berry, K. J.; Clark, P. E.; Buckingham, D. A. *J. Am. Chem. Soc.* **1980**, *102*, 1470.
(212) Serr, B. R.; Headford, C. E. L.; Elliott, C. M.; Anderson, O. P. *J. Chem. Soc., Chem. Commun.* **1988**, 92.
(213) Serr, B. R.; Headford, C. E. L.; Anderson, O. P.; Elliott, C. M.; Spartalian, K.; Fainzilberg, V. E.; Hatfield, W. E.; Rohrs, B. R.; Eaton, S. S.; Eaton, G. R. *Inorg. Chem.* **1992**, *31*, 5450.
(214) Dessens, S. E.; Merrill, C. L.; Saxton, R. J.; Ilaria, R. L., Jr.; Lindsey, J. W.; Wilson, L. J. *J. Am. Chem. Soc.* **1982**, *104*, 4357.
(215) Saxton, R. J.; Wilson, L. J. *J. Chem. Soc., Chem. Commun.* **1984**, 359.
(216) Cutler, A. C.; Brittain, T.; Boyd, P. D. W. *J. Inorg. Biochem.* **1985**, *24*, 199.
(217) Andrioletti, B.; Ricard, D.; Boitrel, B. *New J. Chem.* **1999**, *23*, 1143.
(218) Caughey, W. S. *Adv. Chem. Ser.* **1971**, *No. 100*, 248.
(219) Reed, C. A.; Landrum, J. T. *FEBS Lett.* **1979**, *106*, 265.
(220) Scheidt, W. R.; Cheng, B.; Safo, M. K.; Cukiernik, F.; Marchon, J.-C.; Debrunner, P. G. *J. Am. Chem. Soc.* **1992**, *114*, 4420.
(221) Scheidt, W. R.; Reed, C. A. *Chem. Rev.* **1981**, *81*, 543.
(222) Harding, C. J.; McKee, V.; Nelson, J.; Qin, L. *J. Chem. Soc., Chem. Commun.* **1993**, 1768.
(223) Haddad, M. S.; Wilson, S. R.; Hodgson, D. J.; Hendrickson, D. N. *J. Am. Chem. Soc.* **1981**, *103*, 384.
(224) Burk, P. L.; Osborn, J. A.; Youinou, M.-T.; Agnus, Y.; Louis, R.; Weiss, R. *J. Am. Chem. Soc.* **1981**, *103*, 1273.
(225) Spodine, E.; Manzur, J.; Garland, M. T.; Kiwi, M.; Pena, O.; Grandjean, D.; Toupet, L. *J. Chem. Soc., Dalton Trans.* **1991**, 365.
(226) Coughlin, P. K.; Lippard, S. J. *J. Am. Chem. Soc.* **1981**, *103*, 3228.
(227) Drew, M. G. B.; McCann, M.; Nelson, S. M. *Dalton Trans.* **1981**, 1868.
(228) Fang, Y. C.; Ahmad, I.; Blackburn, N. J.; Boswell, J. S.; Verkhovskaya, M. L.; Hoffman, B. M.; Wikström, M. *Biochemistry* **1995**, *34*, 10245.
(229) Zhang, H. H.; Filipponi, A.; Di Cicco, A.; Lee, S. C.; Scott, M. J.; Holm, R. H.; Hedman, B.; Hodgson, K. O. *Inorg. Chem.* **1996**, *35*, 4819.
(230) Bag, N.; Chern, S.-S.; Peng, S.-M.; Chang, C. K. *Inorg. Chem.* **1995**, *34*, 753.
(231) Serr, B. R.; Headford, C. E. L.; Anderson, O. P.; Elliott, C. M.; Schauer, C. K.; Akabori, K.; Spartalian, K.; Hatfield, W. E.; Rohrs, B. R. *Inorg. Chem.* **1990**, *29*, 2663.
(232) Koch, C. A.; Reed, C. A.; Brewer, G. A.; Rath, N. P.; Scheidt, W. R.; Gupta, G.; Lang, G. *J. Am. Chem. Soc.* **1989**, *111*, 7645.
(233) Kauffmann, K. E.; Goddard, C. A.; Zang, Y.; Holm, R. H.; Münck, E. *Inorg. Chem.* **1997**, *36*, 985.
(234) Unpublished observations.
(235) Goff, H. M. In *Iron Porphyrins*; Lever, A. B. P., Gray, H. B., Eds.; Addison-Wesley: Reading, MA, 1983; Vol. Part 1.
(236) Nanthakumar, A.; Fox, S.; Murthy, N. N.; Karlin, K. D. *J. Am. Chem. Soc.* **1997**, *119*, 3898.
(237) Walker, F. A. In *The Porphyrin Handbook*; Kadish, K. M., Smith, K. M., Guilard, R., Eds.; Academic Press: San Diego, CA, 2000; Vol. 5, NMR and EPR.
(238) Walker, F. A.; Simonis, U. In *Biological Magnetic Resonance*; Berliner, L. J., Reuben, J., Eds.; Plenum Press: New York, 1993; Vol. 12, NMR of Paramagnetic Molecules.
(239) Kopf, M. A.; Neuhold, Y. M.; Zuberbühler, A. D.; Karlin, K. D. *Inorg. Chem.* **1999**, *38*, 3093.
(240) Luchinat, C.; Ciurli, S. In *Biological Magnetic Resonance*; Berliner, J., Reuben, J., Eds.; Plenum: New York, 1993; Vol. 12.
(241) Baldwin, M. J.; Gelasco, A.; Pecoraro, V. L. *Photosynth. Res.* **1993**, *38*, 303 and references cited therein.
(242) Turowski, P. N.; Armstrong, W. H.; Liu, S.; Brown, S. N.; Lippard, S. J. *Inorg. Chem.* **1994**, *33*, 636 and references cited therein.
(243) Hage, R.; Krijnen, B.; Warnaar, J. B.; Hartl, F.; Stufkens, D. J.; Snoeck, T. L. *Inorg. Chem.* **1995**, *34*, 4973.
(244) Kramarz, K. W.; Norton, J. R. *Prog. Inorg. Chem.* **1994**, *42*, 1.
(245) Carroll, J. M.; Norton, J. R. *J. Am. Chem. Soc.* **1992**, *114*, 8744.
(246) Labianca, D. A. *J. Chem. Educ.* **1979**, *56*, 788.
(247) Jones, M. G.; Bickar, D.; Wilson, M. T.; Brunori, M.; Colosimo, A.; Sarti, P. *Biochem. J.* **1984**, *220*, 57.
(248) Jensen, P.; Wilson, M. T.; Aasa, R.; Malmstrom, B. G. *Biochem. J.* **1984**, *224*, 829.
(249) Mitchell, R.; Brown, S.; Mitchell, P.; Rich, P. R. *Biochim. Biophys. Acta* **1992**, *1100*, 40.
(250) Wilson, M. T.; Antonini, G.; Malatesta, F.; Sarti, P.; Brunori, M. *J. Biol. Chem.* **1994**, *269*, 24114.
(251) Palmer, G. *J. Bioenerg. Biomembr.* **1993**, *25*, 145.
(252) Yoshikawa, S.; Mochizuki, M.; Zhao, X.-J.; Caughey, W. S. *J. Biol. Chem.* **1995**, *270*, 4270.
(253) Yoshikawa, S.; Caughey, W. S. *J. Biol. Chem.* **1990**, *265*, 7945.
(254) Lee, S. C.; Scott, M. J.; Kauffmann, K.; Muenck, E.; Holm, R. H. *J. Am. Chem. Soc.* **1994**, *116*, 401.
(255) Scheidt, W. R.; Hatano, K. *Acta Crystallogr., Sect. C: Cryst. Struct. Commun.* **1991**, *47*, 2201.
(256) Zhang, H. H.; Filipponi, A.; Di Cicco, A.; Scott, M. J.; Holm, R. H.; Hedman, B.; Hodgson, K. O. *J. Am. Chem. Soc.* **1997**, *119*, 2470.
(257) Hirota, S.; Ogura, T.; Shinzawa-Itoh, K.; Yoshikawa, S.; Kitagawa, T. *J. Phys. Chem.* **1996**, *100*, 15274.
(258) Kim, Y.; Babcock, G. T.; Surerus, K. K.; Fee, J. A.; Dyer, R. B.; Woodruff, W. H.; Oertling, W. A. *Biospectroscopy* **1998**, *4*, 1.
(259) Caughey, W. S.; Dong, A.; Sampath, V.; Yoshikawa, S.; Zhao, X. J. *J. Bioenerg. Biomembr.* **1993**, *25*, 81.
(260) Tsubaki, M.; Mogi, T.; Anraku, Y.; Hori, H. *Biochemistry* **1993**, *32*, 6065.
(261) Tsubaki, M.; Mogi, T.; Hori, H.; Sato-Watanabe, M.; Anraku, Y. *J. Biol. Chem.* **1996**, *271*, 4017.
(262) Tsubaki, M.; Matsushita, K.; Adachi, O.; Hirota, S.; Kitagawa, T.; Hori, H. *Biochemistry* **1997**, *36*, 13034.
(263) Nakamoto, K. *Infrared and Raman Spectra of Inorganic and Coordination Compounds*, 5th ed.; Wiley-Interscience: New York, 1997.
(264) Schoonover, J. R.; Palmer, G. *Biochemistry* **1991**, *30*, 7541.
(265) Baker, G. M.; Gullo, S. M. *Biochemistry* **1994**, *33*, 8058.
(266) Baker, G. M.; Noguchi, M.; Palmer, G. *J. Biol. Chem.* **1987**, *262*, 595.
(267) Cooper, C. E.; Junemann, S.; Ioannidis, N.; Wrigglesworth, J. M. *Biochim. Biophys. Acta* **1993**, *1144*, 149.
(268) Brown, S.; Moody, A. J.; Mitchell, R.; Rich, P. R. *FEBS Lett.* **1993**, *316*, 216.
(269) Rardin, R. L.; Tolman, W. B.; Lippard, S. J. *New J. Chem.* **1991**, *15*, 417.
(270) Turner, P.; Gunter, M. J.; Hambley, T. W.; White, A. H.; Skelton, B. W. *Inorg. Chem.* **1992**, *31*, 2295.
(271) Debrunner, P. G. In *Iron Porphyrins*; VCH: New York, 1989; Vol. III.
(272) Cooper, C. E.; Salerno, J. C. *J. Biol. Chem.* **1992**, *267*, 280.
(273) Palmer, G.; Babcock, G. T.; Vickery, L. E. *Proc. Natl. Acad. Sci. U.S.A.* **1976**, *73*, 2206.
(274) Schauer, C. K.; Akabori, K.; Elliott, C. M.; Anderson, O. P. *J. Am. Chem. Soc.* **1984**, *106*, 1127.
(275) Elliott, C. M.; Akabori, K. *J. Am. Chem. Soc.* **1982**, *104*, 2671.
(276) Chunplang, V.; Wilson, L. J. *J. Chem. Soc., Chem. Commun.* **1985**, 1761.
(277) Koch, C. A.; Wang, B.; Brewer, G.; Reed, C. A. *J. Chem. Soc., Chem. Commun.* **1989**, 1754.
(278) Rogers, M. S.; Dooley, D. M. *Adv. Protein Chem.* **2001**, *58*, 387.

(279) Halcrow, M. A. *Angew. Chem., Int. Ed.* **2001**, *40*, 346.
(280) Rogers, M. S.; Dooley, D. M. *Curr. Opin. Chem. Biol.* **2003**, *7*, 189.
(281) Stubbe, J.; van der Donk, W. A. *Chem. Rev.* **1998**, *98*, 705.
(282) Okeley, N. M.; Van der Donk, W. A. *Chem. Biol.* **2000**, *7*, R159.
(283) Yoshikawa, S. *Adv. Protein Chem.* **2002**, *60*, 341.
(284) Lerch, K. *J. Biol. Chem.* **1982**, *257*, 6414.
(285) Gielens, C.; De Geest, N.; Xin, X. Q.; Devreese, B.; Van Beeumen, J.; Preaux, G. *Eur. J. Biochem.* **1997**, *248*, 879.
(286) Klabunde, T.; Eicken, C.; Sacchettini, J. C.; Krebs, B. *Nat. Struct. Biol.* **1998**, *5*, 1084.
(287) Ito, N.; Phillips, S. E. V.; Stevens, C.; Ogel, Z. B.; McPherson, M. J.; Keen, J. N.; Yadav, K. D. S.; Knowles, P. F. *Nature* **1991**, *350*, 87.
(288) McCauley, K. M.; Vrtis, J. M.; Dupont, J.; Van der Donk, W. A. *J. Am. Chem. Soc.* **2000**, *122*, 2403.
(289) Cappuccio, J. A.; Ayala, I.; Elliott, G. I.; Szundi, I.; Lewis, J.; Konopelski, J. P.; Barry, B. A.; Einarsdottir, O. *J. Am Chem. Soc.* **2002**, *124*, 1750.
(290) Aki, M.; Ogura, T.; Naruta, Y.; Le, T. H.; Sato, T.; Kitagawa, T. *J. Phys. Chem A* **2002**, *106*, 3436.
(291) Collman, J. P.; Wang, Z.; Zhong, M.; Zeng, L. *J. Chem. Soc., Perkin Trans. 1* **2000**, 1217.
(292) Buse, G.; Soulimane, T.; Dewor, M.; Meyer, H. E.; Blüggel, M. *Protein Sci.* **1999**, *8*, 985.
(293) Gennis, R. B. *Biochim. Biophys. Acta* **1998**, *1365*, 241.
(294) Kitagawa, T. *J. Inorg. Biochem.* **2000**, *82*, 9.
(295) He, Z.; Colbran, S. B.; Craig, D. C. *Chem. Eur. J.* **2003**, *9*, 116.
(296) Adelroth, P.; Ek, M. S.; Mitchell, D. M.; Gennis, R. B.; Brzezinski, P. *Biochemistry* **1997**, *36*, 13824.
(297) Adelroth, P.; Gennis, R. B.; Brzezinski, P. *Biochemistry* **1998**, *37*, 2470.
(298) Kamaraj, K.; Kim, E.; Galliker, B.; Zakharov, L. N.; Rheingold, A. L.; Zuberbuehler, A. D.; Karlin, K. D. *J. Am. Chem. Soc.* **2003**, *125*, 6028.
(299) Tomson, F.; Bailey, J. A.; Gennis, R. B.; Unkefer, C. J.; Li, Z.; Silks, L. A.; Martinez, R. A.; Donohoe, R. J.; Dyer, R. B.; Woodruff, W. H. *Biochemistry* **2002**, *41*, 14383.
(300) Pinakoulaki, E.; Pfitzner, U.; Ludwig, B.; Varotsis, C. *J. Biol. Chem.* **2003**, *278*, 18761.
(301) Kannt, A.; Lancaster, C. R. D.; Michel, H. *J. Bioenrg. Biomembr.* **1998**, *30*, 81.
(302) Nyquist, R. M.; Heitbrink, D.; Bolwien, C.; Gennis, R. B.; Heberle, J. *Proc. Natl. Acad. Sci., U.S.A.* **2003**, *100*, 8715.
(303) Yoshioka, Y.; Kawai, H.; Yamaguchi, K. *Chem. Phys. Lett* **2003**, *374*, 45.
(304) Poulos, T. L.; Fenna, R. E. *Met. Ions Biol. Syst.* **1994**, *30*, 25.
(305) Chuang, W. J.; Van Wart, H. E. *J. Biol. Chem.* **1992**, *267*, 13293.
(306) Benecky, M. J.; Frew, J. E.; Scowen, N.; Jones, P.; Hoffman, B. M. *Biochemistry* **1993**, *32*, 11929.
(307) Weng, L. C.; Baker, G. M. *Biochemistry* **1991**, *30*, 5727.
(308) Watmough, N. J.; Cheesman, M. R.; Greenwood, C.; Thomson, A. J. *Biochem. J.* **1994**, *300*, 469.
(309) Fabian, M.; Palmer, G. *Biochemistry* **1995**, *34*, 13802.
(310) Proshlyakov, D. A.; Ogura, T.; Shinzawa-Itoh, K.; Yoshikawa, S.; Kitagawa, T. *Biochemistry* **1996**, *35*, 76.
(311) Stack, T. D. P. *J. Chem. Soc., Dalton Trans.* **2003**, 1881.
(312) McDonald, M. R.; Scheper, W. M.; Lee, H. D.; Margerum, D. W. *Inorg. Chem.* **1995**, *34*, 229.
(313) McDonald, M. R.; Fredericks, F. C.; Margerum, D. W. *Inorg. Chem.* **1997**, *36*, 3119.
(314) Picot, D.; Loll, P. J.; Garavito, R. M. *Nature* **1994**, *367*, 243.
(315) Rich, P. R.; Rigby, S. E. J.; Heathcote, P. *Biochim. Biophys. Acta* **2002**, *1554*, 137.
(316) Iwaki, M.; Puustinen, A.; Wikstroem, M.; Rich, P. R. *Biochemistry* **2003**, *42*, 8809.
(317) Verkhovsky, M. I.; Jasaitis, A.; Verkhovskaya, M. L.; Morgan, J. E.; Wikstrom, M. *Nature* **1999**, *400*, 480.
(318) Rousseau, D. L. *Nature* **1999**, *400*, 412.
(319) Ralle, M.; Verkhovskaya, M. L.; Morgan, J. E.; Verkhovsky, M. I.; Wikstroem, M.; Blackburn, N. J. *Biochemistry* **1999**, *38*, 7185.
(320) Osborne, J. P.; Cosper, N. J.; Stalhandske, C. M.; Scott, R. A.; Alben, J. O.; Gennis, R. B. *Biochemistry* **1999**, *38*, 4526.
(321) Cozzi, P.; Carganico, G.; Fusar, D.; Grossoni, M.; Menichincheri, M.; Pinciroli, V.; Tonani, R.; Vaghi, F.; Salvati, P. *J. Med. Chem.* **1993**, *36*, 2964.
(322) Ohmori, J.; Shimizu-Sasamata, M.; Okada, M.; Sakamoto, S. *J. Med. Chem.* **1996**, *39*, 3971.
(323) Venuti, M. C.; Stephenson, R. A.; Alvarez, R.; Bruno, J. J.; Strosberg, A. M. *J. Med. Chem.* **1988**, *31*, 2136.
(324) Gungor, T.; Fouquet, A.; Teulon, J. M.; Provost, D.; Cazes, M.; Cloarec, A. *J. Med. Chem.* **1992**, *35*, 4455.
(325) Jacobs, C.; Frotscher, M.; Dannhardt, G.; Hartmann, R. W. *J. Med. Chem.* **2000**, *43*, 1841.
(326) Lo, Y. S.; Nolan, J. C.; Maren, T. H.; Welstead, W. J., Jr.; Gripshover, D. F.; Shamblee, D. A. *J. Med. Chem.* **1992**, *35*, 4790.
(327) Kiyomori, A.; Marcoux, J.-F.; Buchwald, S. L. *Tetrahedron Lett.* **1999**, *40*, 2657.
(328) Edmondson, S. D.; Mastracchio, A.; Parmee, E. R. *Org. Lett.* **2000**, *2*, 1109.
(329) Collman, J. P.; Zhong, M. *Org. Lett.* **2000**, *2*, 1233.
(330) Elliott, G. I.; Konopelski, J. P. *Org. Lett.* **2000**, *2*, 3055.
(331) Lam, P. Y. S.; Clark, C. G.; Saubern, S.; Adams, J.; Winters, M. P.; Chan, D. M. T.; Combs, A. *Tetrahedron Lett.* **1998**, *39*, 2941.
(332) Collman, J. P.; Zhong, M.; Zeng, L.; Costanzo, S. *J. Org. Chem.* **2001**, *66*, 152.
(333) Kozyrod, R. P.; Pinhey, J. T. *Org. Synth.* **1984**, *62*, 24.
(334) Kozyrod, R. P.; Morgan, J.; Pinhey, J. T. *Aust. J. Chem.* **1985**, *38*, 1147.
(335) Barker, R. *Organic Chemistry of Biological Compounds*; Prentice Hall: New York, 1971.
(336) *CRC Handbook of Chemistry and Physics*, 80th ed.; CRC Press: London, U.K., 1999.
(337) Naruta, Y.; Tachi, Y.; Chishiro, T.; Shimazaki, Y.; Tani, F. *Acta Crystallogr., Sect. E: Struct. Rep. Online* **2001**, *E57*, o550.
(338) Himo, F.; Eriksson, L. A.; Blomberg, M. R. A.; Siegbahn, P. E. M. *Int. J. Quantum Chem.* **2000**, *76*, 714.
(339) Himo, F.; Noodleman, L.; Blomberg, M. R. A.; Siegbahn, P. E. M. *J. Phys. Chem. A* **2002**, *106*, 8757.
(340) Ayala, I.; Range, K.; York, D.; Barry, B. A. *J. Am. Chem. Soc.* **2002**, *124*, 5496.
(341) Ramirez, B. E.; Malmstrom, B. G.; Winkler, J. R.; Gray, H. B. *Proc. Natl. Acad. Sci. U.S.A.* **1995**, *92*, 11949.
(342) Geren, L. M.; Beasley, J. R.; Fine, B. R.; Saunders: A. J.; Hibdon, S.; Pielak, G. J.; Durham, B.; Millett, F. *J. Biol. Chem.* **1995**, *270*, 2466.
(343) von Wachenfeldt, C.; de Vries, S.; der Oost, J. v. *FEBS Lett.* **1994**, *340*, 109.
(344) Lappalainen, P.; Aasa, R.; Malmstrom, B. G.; Saraste, M. *J. Biol. Chem.* **1993**, *268*, 26416.
(345) Slutter, C. E.; Sanders, D.; Wittung, P.; Malmstrom, B. G.; Aasa, R.; Richards, J. H.; Gray, H. B.; Fee, J. A. *Biochemistry* **1996**, *35*, 3387.
(346) van der Oost, J.; Lappalainen, P.; Musacchio, A.; Warne, A.; Lemieux, L.; Rumbley, J.; Gennis, R. B.; Aasa, R.; Pascher, T.; Malmstrom, B. G. *EMBO J.* **1992**, *11*, 3209.
(347) Kelly, M.; Lappalainen, P.; Talbo, G.; Haltia, T.; van der Oost, J.; Saraste, M. *J. Biol. Chem.* **1993**, *268*, 16781.
(348) Hay, M.; Richards, J. H.; Lu, Y. *Proc. Natl. Acad. Sci. U.S.A.* **1996**, *93*, 461.
(349) Dennison, C.; Vijgenboom, E.; de Vries, S.; van der Oost, J.; Canters, G. W. *FEBS Lett.* **1995**, *365*, 92.
(350) Antholine, W. E.; Kastrau, D. H. W.; Steffens, G. C. M.; Buse, G.; Zumft, W. G.; Kroneck, P. M. H. *Eur. J. Biochem.* **1992**, *209*, 875.
(351) Kroneck, P. M. H.; Antholine, W. A.; Riester, J.; Zumft, W. G. *FEBS Lett.* **1988**, *242*, 70.
(352) Haltia, T.; Brown, K.; Tegoni, M.; Cambillau, C.; Saraste, M.; Mattila, K.; Djinovic-Carugo, K. *Biochem. J.* **2003**, *369*, 77.
(353) Rosenzweig, A. C. *Nat. Struct. Biol.* **2000**, *7*, 169.
(354) Williams, P. A.; Blackburn, N. J.; Sanders, D.; Bellamy, H.; Stura, E. A.; Fee, J. A.; McRee, D. E. *Nat. Struct. Biol.* **1999**, *6*, 509.
(355) Robinson, H.; Ang, M. C.; Gao, Y.-G.; Hay, M. T.; Lu, Y.; Wang, A. H. J. *Biochemistry* **1999**, *38*, 5677.
(356) Wilmanns, M.; Lappalainen, P.; Kelly, M.; Sauer-Eriksson, E.; Saraste, M. *Proc. Natl. Acad. Sci. U.S.A.* **1995**, *92*, 11955.
(357) Blackburn, N. J.; Barr, M. E.; Woodruff, W. H.; van der Oost, J.; de Vries, S. *Biochemistry* **1994**, *33*, 10401.
(358) Blackburn, N. J.; de Vries, S.; Barr, M. E.; Houser, R. P.; Tolman, W. B.; Sanders, D.; Fee, J. A. *J. Am. Chem. Soc.* **1997**, *119*, 6135.
(359) Andrew, C. R.; Han, J.; de Vries, S.; van der Oost, J.; Averill, B. A.; Loehr, T. M.; Sanders-Loehr, J. *J. Am. Chem. Soc.* **1994**, *116*, 10805.
(360) Andrew, C. R.; Fraczkiewicz, R.; Czernuszewicz, R. S.; Lappalainen, P.; Saraste, M.; Sanders-Loehr, J. *J. Am. Chem. Soc.* **1996**, *118*, 10436.
(361) Gamelin, D. R.; Randall, D. W.; Hay, M. T.; Houser, R. P.; Mulder, T. C.; Canters, G. W.; de Vries, S.; Tolman, W. B.; Lu, Y.; Solomon, E. I. *J. Am. Chem. Soc.* **1998**, *120*, 5246.
(362) Gurbiel, R. J.; Fann, Y. C.; Surerus, K. K.; Werst, M. M.; Musser, S. M.; Doan, P. E.; Chan, S. I.; Fee, J. A.; Hoffman, B. M. *J. Am. Chem. Soc.* **1993**, *115*, 10888.
(363) Farrar, J. A.; Lappalainen, P.; Zumft, W. G.; Saraste, M.; Thomson, A. J. *Eur. J. Biochem.* **1995**, *232*, 294.
(364) Morgan, J. E.; Wikstrom, M. *Biochemistry* **1991**, *30*, 948.
(365) Williams, K. R.; Gamelin, D. R.; LaCroix, L. B.; Houser, R. P.; Tolman, W. B.; Mulder, T. C.; de Vries, S.; Hedman, B.; Hodgson, K. O.; Solomon, E. I. *J. Am. Chem. Soc.* **1997**, *119*, 613.
(366) George, S. D.; Metz, M.; Szilagyi, R. K.; Wang, H.; Cramer, S. P.; Lu, Y.; Tolman, W. B.; Hedman, B.; Hodgson, K. O.; Solomon, E. I. *J. Am. Chem. Soc.* **2001**, *123*, 5757.
(367) Farrar, J. A.; Neese, F.; Lappalainen, P.; Kroneck, P. M. H.; Saraste, M.; Zumft, W. G.; Thomson, A. J. *J. Am. Chem. Soc.* **1996**, *118*, 11501.
(368) Neese, F.; Zumft, W. G.; Antholine, W. E.; Kroneck, P. M. H. *J. Am. Chem. Soc.* **1996**, *118*, 8692.

(369) Olsson, M. H. M.; Ryde, U. *J. Am. Chem. Soc.* **2001**, *123*, 7866.
(370) Robin, M. B.; Day, P. *Adv. Inorg. Chem. Radiochem.* **1967**, *10*, 247.
(371) Harding, C. J.; McKee, V.; Nelson, J. *J. Am. Chem. Soc.* **1991**, *113*, 9684.
(372) Harding, C. J.; Nelson, J.; Symons, M. C. R.; Wyatt, J. *J. Chem. Soc., Chem. Commun.* **1994**, 2499.
(373) Al-Obaidi, A.; Baranovic, G.; Coyle, J.; Coates, C. G.; McGarvey, J. J.; McKee, V.; Nelson, J. *Inorg. Chem.* **1998**, *37*, 3567.
(374) Barr, M. E.; Smith, P. H.; Antholine, W. E.; Spencer, B. *J. Chem. Soc., Chem. Commun.* **1993**, 1649.
(375) Franzen, S.; Miskowski, V. M.; Shreve, A. P.; Wallace-Williams, S. E.; Woodruff, W. H.; Ondrias, M. R.; Barr, M. E.; Moore, L.; Boxer, S. G. *Inorg. Chem.* **2001**, *40*, 6375.
(376) LeCloux, D. D.; Davydov, R.; Lippard, S. J. *Inorg. Chem.* **1998**, *37*, 6814.
(377) He, C.; Lippard, S. J. *Inorg. Chem.* **2000**, *39*, 5225.
(378) Lo, S. M.-F.; Chui, S. S.-F.; Shek, L.-Y.; Lin, Z.; Xhang, X. X.; Wen, G.; Williams, I. D. *J. Am. Chem. Soc.* **2000**, *122*, 6293.
(379) Zhang, X.-M.; Tong, M.-I.; Lee, H.-K.; Luo, L.; Li, K.-F.; Tong, Y.-X.; Chen, Z.-M. *Chem. Eur. J.* **2002**, *14*, 3178.
(380) Hagadorn, J. R.; Zahn, T. I.; Que, L., Jr.; Tolman, W. B. *Dalton Trans.* **2003**, 1790.
(381) Gupta, R.; Zhang, Z. H.; Powell, D.; Hendrich, M. P.; Borovik, A. S. *Inorg. Chem.* **2002**, *41*, 5100.
(382) Farrar, J. A.; McKee, V.; Al-Obaidi, A. H. R.; McGarvey, J. J.; Nelson, J.; Thomson, A. J. *Inorg. Chem.* **1995**, *34*, 1302.
(383) Harding, C. J.; Nelson, J.; Wyatt, J.; Symons, M. C. R. *J. Chem. Soc., Chem. Commun.* **1991**, 2499.
(384) Farrar, J. A.; Grinter, R.; Neese, F.; Kroneck, P. M. H.; Nelson, J.; Thomson, A. J. *J. Chem. Soc., Dalton Trans.* **1997**, 4083.
(385) Zhang, X.-M.; Tong, M.-I.; Chen, Z.-M. *Angew. Chem., Int. Ed.* **2002**, *41*, 1029.
(386) Houser, R. P.; Young, V. G., Jr.; Tolman, W. B. *J. Am. Chem. Soc.* **1996**, *118*, 2101.
(387) Houser, R. P.; Halfen, J. A.; Young, V. G., Jr.; Blackburn, N. J.; Tolman, W. B. *J. Am. Chem. Soc.* **1995**, *117*, 10745.
(388) Branscombe, N. D. J.; Blake, A. J.; Marin-Becerra, A.; Li, W.-S.; Parsons, S.; Ruiz-Ramirez, L.; Schroeder, M. *J. Chem. Soc., Chem. Commun.* **1996**, 2573.

CR0206162